UNIVERSITÀ DEGLI STUDI DI NAPOLI

FEDERICO II

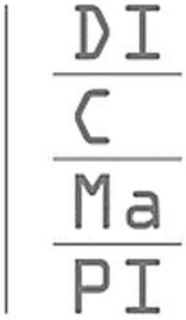

Dipartimento
di Ingegneria Chimica,
dei Materiali e della
Produzione Industriale
Università degli Studi
di Napoli Federico II

Scuola Politecnica e delle Scienze di Base

XXXII PHD PROGRAMME

IN

PRODUCTION TECHNOLOGIES AND SYSTEMS

Hole quality assessment and tool wear evaluation in drilling of CFRP/CFRP and Al/CFRP stack laminates for aeronautical applications

PHD TUTORS

Prof. Roberto Teti

Prof. Doriana M. D'Addona

Dr. Alessandra Caggiano

PHD CANDIDATE

Ing. Roberta Angelone

PHD PROGRAM COORDINATOR

Prof. Giuseppe Mensitieri

Table of content

Lists of figures

Lists of tables

Appendix - Lists of images

Appendix - Lists of tables

Summary

Composite material parts are typically produced in the near-net-shape, i.e. very close to the finished product. However, additional machining processes are often required to meet dimensional and tolerance requirements. Particularly drilling stands out as the most widespread machining process of carbon fibre reinforced plastic (CFRP) composite parts, primarily in the aerospace industry, due to the widespread use of mechanical joints, such as rivets, rather than welded or bonded joints. CFRP drilling is noticeably challenging due to material abrasiveness, inhomogeneity and anisotropic properties; tool wear rates are inherently high leading to superior cutting forces and detrimental effects on part surface quality and material integrity. Damages such as delamination, cracks or matrix thermal degradation are often observed as the result of uncontrolled tool wear or improper machining conditions. The development of effective non-destructive control techniques, such as optical inspection for drilled hole quality assessment for process, tool and pr oduct quality evaluation is dealt with in this PhD thesis with the aim to contribute to the reduction of scraps and tool costs as well as to the improvement of process productivity in the drilling of CFRP composite material parts for aeronautical assembly. In this thesis work, the most effective parameters for hole quality evaluation in drilling of CFRP/CFRP and Al/CFRP stacks for aeronautical assembly were studied and selected. An automatic technique based hole image processing was developed for the evaluation of these quality parameters for holes drilled with a traditional tool and an innovative tool purposely developed. Tool wear was finally evaluated to verify its relationship with the hole quality.

Introduction

Composite materials with a worldwide increase in technologies are progressively replacing traditional materials due to their versatility.

Composite materials can be defined as a combination of two or more constituent materials with significantly different physical or chemical, combined in order to obtain a product that has specific chemical and physical properties, different from the original elements. The two major elements are reinforcement (fibres) and matrix. The fibrous reinforcement represents the discontinuous phase used to enhance the strength, the toughness and the rigidity of the matrix, with which it must constitute a good chemical-physical bond. The main beneficial characteristics of composite materials includes high strength, stiffness and corrosion resistance (Campbell, 2010).

The classification of the composite materials can be made on the basis of several criteria. Since the field of possible applications is mostly influenced by the type of material used for the matrix is commonly used to classify the composite materials according to its characteristics. Therefore the composite materials can be distinguished into:

- metal matrix composites (MMC);
- ceramic matrix composites (CMC);
- polymer matrix composites (FRP).

The most commonly used reinforcing fibres are substantially three: Glass fibres (Fiberglass), Carbon fibres (Carbon fibre) and Aramid fibres (Kevlar).

The Carbon Fibre Reinforced Plastic (CFRP) materials are the widely used composite in the aerospace sector, mainly for their lightness and resistance (Wilhelm, 2001). The advantages of carbon fibres are:

- high elastic modulus;
- lightweight;
- high resistance to fatigue and compression;
- low thermal expansion coefficient;
- good electrical conductivity;
- good resistance to high temperatures (2000°C) in non-oxidizing atmosphere;
- good resistance to medium temperatures (400°C) in oxidizing atmosphere.

Therefore, the composite materials made up of resin and carbon reinforcements have an excellent combination of low weight, high mechanical strength and high rigidity.

In the last decades, there was an increasing percentage of composite materials employed in aeroplane realization. The aerospace industry is particularly interested in employing lightweight materials to reach the target in lowering costs by enhancing efficiency and reducing emissions to improve, i.e. decrease, global environmental impact.

Drilling is a cutting process which allows to obtain, through material removal, holes that normally act as housing for bolted or riveted junctions.

Drilling processing of composite materials is a challenge for manufacturing engineers (Zitoune et al., 2010) due to due to material fragmentation and delamination that occurs during the drilling operation which affects aesthetics and processed surface quality (Jain & Yang, 1994b).

As previously discussed, the use of CFRP composites is increasing in the aerospace and automotive industries thanks to their lightness which determines a lower vehicle weight and therefore a lower fuel consumption. Aluminum and its alloys offer high compressive and tensile strength at high temperatures, low density, excellent resistance to corrosion and erosion, superior fatigue resistance and low modulus of elasticity.

CFRPs are often more used in the form of stacks with metals such as aluminum to increase their weight/resistance ratio; despite the attractive and unique properties of composite materials, their processing, if the tolerances to defects are very close as in the aviation industry, is challenging and considerably different from metals. A large number of holes is required to allow mechanical assembly processes, for this reason, it would be desirable to drill the two materials simultaneously (one-shot drilling), therefore the optimization of the drilling process on the two dissimilar materials is necessary.

1. Use of composite materials and light alloys in the aeronautical field

The long term strategic objectives ‘‘Flightpath 2050’’(Darecki et al., 2011) have taken the Advisory Council for Aviation Research in Europe (ACARE) development targets beyond the year 2020. By the year 2050, the following goals for air traffic have to be achieved:

- 75% reduction in CO2 per passenger kilometre
- 90% reduction in NOx emissions
- 65% reduction in noise

These objectives will require improvement in all three areas Airframe, Engine and Air traffic management (ATM) & operations. This means:

- Lightweight designs and materials (e.g. composites) on airframes and engines.
- Advanced aerodynamic performance and lightweight designs
- Higher engine bypass ratio.
- Lean burn engine combustor technologies.
- Advanced turbine materials for aero-engines (discs and blades).

The need for enhanced aerodynamic performance requires improved accuracy and reduced part-to-part variation in manufacturing quality. 3D improved aerodynamics on integrally bladed rotors, blades and vanes lead to more complex free form geometries to be machined. Cost-effective and validated high-performance machining solutions and methods are required for advanced high-temperature alloys. In this context, the present paper is to provide an overview of machining characteristics of advanced aerospace alloys and composites for aerostructures and aero-engine applications. A critical assessment of machining behaviour, tool wear and surface integrity is presented. Further, advances in high-performance machining technologies are reviewed, and finally, industrial perspectives are provided in the context of machining specific aerospace components where future challenges are discussed.

Fuel economy is the main driving force in modern civil aircraft design. The strive for fuel-efficient aircraft is then translated into weight and aerodynamic challenges for aerospace engineers. The research and development in the last few decades into advanced lightweight metallic alloys and composites materials are addressing weight challenges while the design of advanced wing shapes and wingtips are contributing to aerodynamics challenges. Aluminium alloys are the most widely used alloys for mass-produced aerostructure parts due to its

convenience (most abundant metal in the Earth's crust), lightness, strength and manufacturability. Two most used advanced high strength aluminium alloys for aerostructure are:

- 7010 and 7050 alloys, which have high strength, stress corrosion cracking resistance and toughness properties, are suitable for heavy plate applications due to its lower quench sensitivity and retention of strength in thicker sections;
- 2024 alloys, which have high strength and excellent fatigue resistance.

Over the last two decades, there has been a strong interest in the use of advanced lightweight composites materials such as carbon fibre reinforced plastic (CFRP) for aerostructure components. The latest composite aircraft programmes, i.e. Bombardier CS300, Boeing B787, and Airbus A350XWB are using 46, 50 and 52% in weight, respectively (Tab. 1).

	Airbus A350 XWB	Boeing B787	Bombardier CS300
Composites	52	50	46
Aluminium	20	20	24
Titanium	14	15	8
Steel	7	10	1
Others	7	5	21

Tab. 1 Aircraft material composition by weight in percentage.

Composites are introduced in aircraft design and manufacturing for improved performance (lightweight and strength), reduced life cycle and maintenance cost and lower production cost, quality robustness and reduced lead time. Use of CFRP panels, stringers and frames in fuselage offers reduce operational costs and reduce global environmental impact. In contrast, use of CFRP spars, skins and panels in outer and centre wing box and offers aeroelastic tailoring as a passive adaptive structure in addition to weight reduction (operation costs and environmental impact) and fatigue and corrosion-free composites (maintenance costs).

Composite material parts are typically set out in the near-net-shape, i.e. very close to the finished product. However, additional machining processes are often required to meet dimensional and tolerance requirements. Drilling, edge trimming and slotting are the most widely employed cutting processes for FRP composite materials (Lopresto et al., 2016; Teti, 2002). Due to CFRP abrasiveness, inhomogeneity and anisotropic properties, tool wear rates

are inherently high, leading to high cutting forces and detrimental effects on workpiece surface quality. Damages such as delamination, cracks or matrix thermal degradation are observed as the result of tool wear or improper machining conditions (Brinksmeier et al., 2011; Lopresto et al., 2016; Teti, 2002).

Drilling is the most widespread machining process of FRP composite parts, due to the extensive use of mechanical joints such as rivets rather than welded or bonded joints. However, FRP drilling is challenging due to rapid tool wear and damage to material integrity and surface quality.

In the aeronautical industry, where mechanical fastening of joined components is a necessity, and the drilling of numerous thousands of holes per aeroplane is, therefore, unavoidable, stacking the parts in joint position and drilling them in a single operation (one-shot drilling) not only saves time, but also ensures proper hole alignment when rivets are inserted. So-called one-shot drilling would be preferable to avoid holes of low-quality result in out-of-tolerance assembly and long-standing weakening of structural properties, which are not adequate in the aeronautical sector. Tight geometrical/dimensional tolerances and surface integrity need to be met as they are a key prerequisite to guarantee the functionality of the assembled components. Drilling composite/metal stacks, deprived of using one-shot drilling techniques, has usually involved multistep operations to permit the use of drill bit optimized for each material. This could require either tool changes or the use of multiple drill motors. Despite these precautions, poor-quality holes are still common.

2. Drilling of composite materials and light alloys for aeronautical assembly

The use of new structural materials such as carbon fibre reinforced plastics (CFRP) allows for a substantial weight reduction on aircrafts, which positively affects emissions and management costs through a lower fuel consumption consistent with nowadays environmental requirements (M'Saoubi et al., 2015), so they are more and more replacing traditional materials, and their application is increasing in automotive and aerospace industries.

Due to the difficulties in realizing welding operations or adhesive joints for the assembly of CFRP components, mechanical joining techniques such as riveting are generally employed to realize strong and reliable joints; for this reason, drilling is the most widespread CFRP machining process in the aeronautical industry. However, the anisotropic nature of the material, the very rapid tool wear caused by the abrasive carbon fibres and the high concentrated efforts and vibrations that may cause damages affecting material integrity, processed surface quality and aspect, make the drilling of CFRP parts a great challenge for manufacturing engineers (A. Caggiano et al., 2017; Ho-Cheng & Dharan, 1990a; Jain & Yang, 1994b; Teti, 2002; Zitoune et al., 2010).

The drilling process involves two basic motions (El-Hoffy & Abdel-Gawad, 2013) (Fig. 1):

- The primary (or cutting) motion represents the rotation around the tool axis. The cutting speed is measurable by the following relation:

$$V_t = \frac{\pi * n * D}{1000}$$

  where:
  D is the bit diameter;
  n is the spindle rotation speed.
- The second motion is called the feed motion (V_a). It is obtained from the motion of the tool perpendicular to the work-piece. The feed of the main spindle is calculated as follows:

$$V_a = f_r * n$$

  where f_r is the feed per revolution.

The feed rate (f) or forward ratio is the ratio between forward speed Fs and spindle rotation speed:

$$f = \frac{V_a}{n}$$

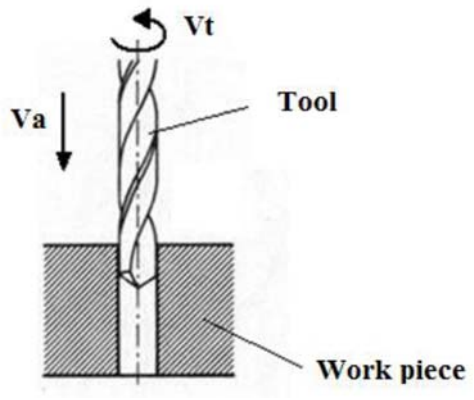

Fig. 1 Drilling basic motions.

Due to different orientations of fibres which constitute the laminates of composite materials, they acquire anisotropy and inhomogeneity properties, which make it, light and strong, but also hard to be machined (J. Sheikh-Ahmad & Davim, 2011).

Drilling is a particularly hostile operation for composite laminates, because high concentrated efforts and vibrations generated during such processing may cause widespread damages. Such damages cause problems from an aesthetical point of view, but it can also compromise finished part mechanical properties.

Although several applications of non-traditional machining operations to hole-making of composite laminates, such as laser machining (Herzog et al., 2008) and water-jet machining (Azmir & Ahsan, 2009), have been developed, mechanical drilling operations using conventional or special drill bits are primary applications for composite laminates.

With the aim to reduce the tool wear to improve the quality of the final product and cut off the costs related to frequent tool changes, some recent studies have been focused on the development of new drill bit geometries (Filiz & Burak Ozdoganlar, 2010a, 2010b; Hocheng & Tsao, 2003; Isbilir & Ghassemieh, 2013; Ko & Chang, 2003). Efforts have also been spent for modelling the thrust force during drilling operations, which was found to directly affect the quality of drilled holes (Iliescu et al., 2010; Karpat et al., 2014; López De Lacalle et al., 2009).

To reach high productivity, while preserving the integrity of the workpiece during drilling of CFRP components, in-process tool wear state monitoring is crucial; this goal can be performed by an on-line real-time multiple sensor monitoring procedure (Caggiano et al., 2016).

However, the entire replacement of the conventional metallic materials by CFRP laminates is not recommended. First of all, CFRP exhibits low bearing and shear strengths as well as high notch sensitivity. Additionally, the joint strength depends on the laminate configuration. Furthermore, the environmental conditions exert influence on the mechanical behaviour of the joint.

Hence, alternative advanced joining techniques such as bolted structures made of stacked composite laminates and metal alloy sheets have been developed to fulfil the material-specific requirements and take advantage of the favourable isotropic behaviour of metal alloys facing the complex stress state of bolt loaded holes (Fink et al., 2010). These stacks can be defined as composite/metal hybrid structures (Jelinek et al., 2015).

Multi-material components made of composite laminates overlaid on light-weight metal alloy sheets are becoming progressively employed in the aerospace sector. Aircraft industries are increasing the implementation of composite/metal alloy stacks due to their high strength to weight ratio to produce innovative structural configurations for key load-bearing components, favouring energy saving in the aerospace and automotive industries, and increasing fuel efficiency and cycle life. The use of such multi-material stacks is expanding for structural aerospace requests, especially where high mechanical loads exist such as for aircraft wing and tail-plane components (Castro, 2010; Ramulu & Spaulding, 2016). Conventional drilling processes using drill bits on CFRP laminates may damage the workpiece through chipping, cracking, delamination and high wear on the cutting tools (Karnik et al., 2008). Several critical defects such as entry/exit delamination, geometric/dimensional errors, internal delamination, fibre pullout, thermal damage have been reported (Dharan & Won, 2000). When stacked with metal alloy sheets, the drilling process becomes even more complex, due to the different properties of the stacked materials.

Industrial practice relating to hole production in multilayer composite/metal alloy stacks is often carried out by initially drilling each material element separately followed by temporary assembly of the workpiece laminates/sheets for subsequent deburring and finishing. Despite a reaming operation, difficulties still exist in meeting hole quality requirements as well as productivity issues. The application of one-shot drilling was proposed as a potential solution; however, the widely different mechanical/physical properties of the different materials involved and their associated machinability characteristics, pose significant challenges.

In general, relatively high cutting speed (150-200m/min) with feed rate < 0.05 mm/rev is recommended for drilling CFRP composites in order to minimise delamination, while low cutting speed (10–30m/min) with moderate feed rate (0.05–0.1mm/rev) is recommended for

machining Al alloys. Not surprisingly, there is a lack of knowledge/standards available in the literature concerning optimal process parameters, tool geometries/materials and cutting environment when machining dissimilar materials stacks (Shyha et al., 2011).

3. Research framework

3.1. Research project objectives

The activities of this thesis work have been developed in the context of a wider national project focused on the development of eco-compatible materials and technologies for drilling and assembly processes within the aeronautical sector. The project was carried out in collaboration with an industrial partner dedicated to the production of aircraft components for which weight reduction and optimization of cutting processes are an essential objective.

The overall aim of this project is the study of issues related to drilling and cutting techniques of advanced lightweight components, such as composite material parts, and their relative assembly, in view of potential process automation using cooperating anthropomorphic robots. The use of innovative materials and processes developed in this research project will lead to a reduction of weight and environmental impact in the construction and maintenance of primary aircraft structures. At least a 5% reduction in weight of the structures is foreseen without an increase in costs (the reduction of process costs compensates a possible rise in the cost of raw materials).

In the aeronautical industry, the reduction of aircraft weight is becoming an increasingly important aim both for environmental requirements (lower emissions) and contraction of the management costs (lower fuel consumption). Therefore, new structural architectures have been developed through the use of innovative materials and manufacturing technologies.

One of the innovative processes analysed in this project is the drilling aeronautical composite material stacks made of carbon fibre reinforced plastic (CFRP) as well as hybrid stacks combining light metal alloys and CFRP laminates, representing two industrial manufacturing applications of interest in the framework of the research projects.

In this context, particular attention is paid to the study of the coupling of hybrid metal-composite structures related issues. In particular, concerning the machining of hybrid aluminum/CFRP stacks and the related assembly processes, innovative drilling and cutting techniques based on laser employment on aluminum alloy parts and advanced automation technologies for one-shot mechanical drilling of the hybrid stacks in view of using cooperating anthropomorphic robots were investigated.

The research project included the following "Realization Objectives":

1. Definition of the design specifications of structural elements (definition of the reference platform, the conceptual layout definition of the technological demonstrator).
2. *Development of drilling and cutting processes using laser and automated mechanical drilling techniques implementing sensor monitoring procedures in view of process automation using anthropomorphic cooperating robots.*
3. “Green Objective” related to the introduction of innovative processes with low environmental impact for the protection of surfaces from degradation.
4. Mechanical and electrochemical characterization of "Cr free" systems and development of self-diagnostic organic systems
5. Development of reverse engineering techniques for surveying surfaces of the coupled parts in fuselages made of hybrid material composite/aluminum to make adjustments on detail components. Identification and demonstration of adjustment techniques.
6. Design, implementation and testing of sub-components
7. Design and implementation of the Technological Demonstrator
8. Cost reduction analysis and cost/benefit evaluation for the different aeronautics components made with the above mentioned innovative techniques.

The second "Realization Objective" was further divided into the following activities:

1. Laser cutting and drilling of aluminium alloys.
2. Realization of a prototype machine for drilling and cutting by laser processes, on aeronautical components of large dimensions in aluminium alloys.
3. Cooperating robotic systems for drilling with material removal.
4. *Study of geometries of tools for drilling of CFRP/CFRP and hybrid CFRP/aluminium alloy stacks.*
5. *Development of a sensor monitoring system for tool wear.*
6. *Development of an in-process survey system of delamination conditions.*
7. Study of orbital drilling techniques.

This thesis work has contributed to the second "Realization Objective" in activities 5 and 6, the innovative tool used in drilling CFRP/CFRP stacks comes from activity 2.4. For these innovative tools, the development of wear and hole quality has been analysed.

3.2. Background on the study of innovative tool geometries

In order to define the geometry of the innovative tool to be used for the experimental campaign, a bibliographic study was carried out to verify the state of the art with particular reference to the drilling of CFRP and hybrid stacks.

In the general context of composite material cutting, many authors have highlighted the differences in cutting mechanisms compared to metal alloys. (Caprino et al., 1996; König & Graß, 1989) Fig. 2 shows the force scheme in the case of orthogonal cutting of unidirectional composite.

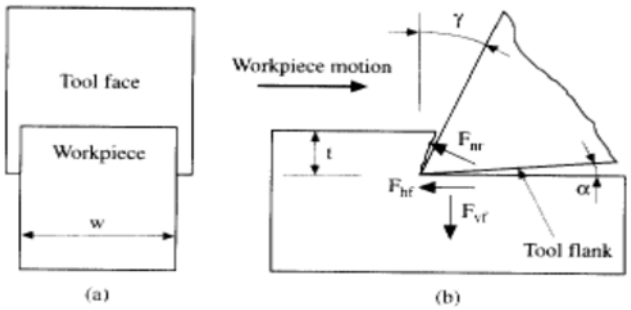

Fig. 2 Tool-material system a) front view; b) side view.

In particular, it has been pointed out that while for metal alloys there is a strong component of the force on the chest of the tool, due to the swarf sliding on it, in composite materials the sliding occurs on the side of the tool.

The nature of the different fibres and the discontinuity of the material make the cutting process in composite materials costly, especially concerning wear and defects induced in the processed material. With regard to drilling, many authors have pointed out that the main defect that occurs in drilling composite materials is delamination (Ho-Cheng & Dharan, 1990a, 1990b). Fig. 3 shows a diagram that clarifies the nature of delamination.

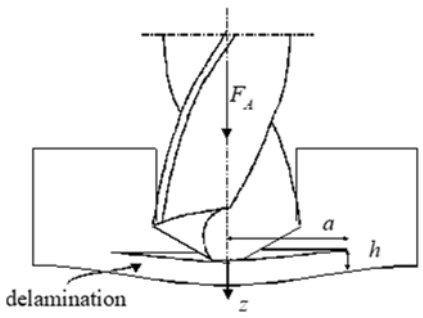

Fig. 3 Delamination.

Since composite materials are made up of a sequence of elementary laminas superimposed in the final phase of drilling, the edge of the tool exerts such a force that it induces delamination in the material.

Many authors have proposed models for the determination of forces and momentum in drilling composite materials (Khashaba, 2013; Langella et al., 2005).

Other authors have highlighted the dependence of the hole quality, e.g. on the presence of defects, i.e. tool wear, with the technological parameters. The most important factor influencing the performance of the drilling process is the tool geometry. About the feed force, thrust force, the most influential factor is the presence of the central edge of the tool (Galloway, 1957; Jain & Yang, 1994a).

Many authors have proposed special geometries for drilling tools for composite materials.

Jain and Yang (Jain & Yang, 1993, 1994b) have proposed and studied a tool the principle of which is based on the elimination of the central edge, called "core drill bit". The cutting action, abrasive in their proposal, is exerted by a circular crown, in order to carry out a sort of "core drilling".

Fig. 4 shows the proposed geometry.

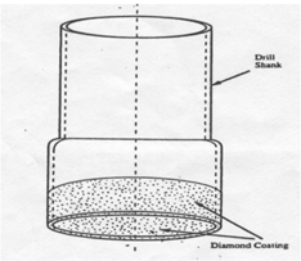

Fig. 4 Core drill bit geometry.

The core drill tool has also been studied by other authors, such as (Mathew et al., 1999; Tsao & Hocheng, 2007).

Their work shows a strong reduction in thrust force compared to a traditional tool, twist drill bit, and the absence of delamination (Fig. 5).

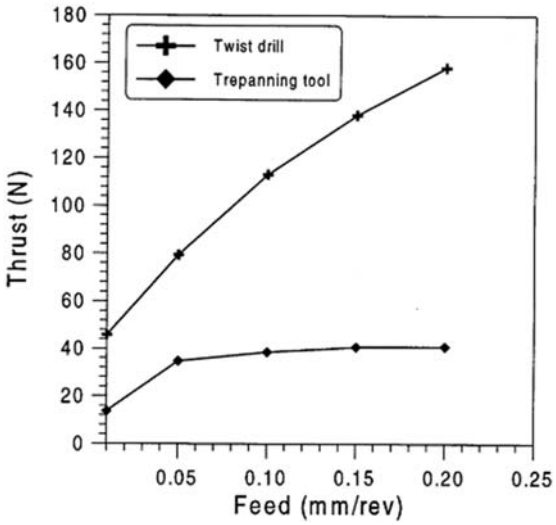

Fig. 5 "Core Drill Bit" feed force.

Another geometry proposed and studied by several authors is the so-called "multifacet drill bit" (Fig. 6).

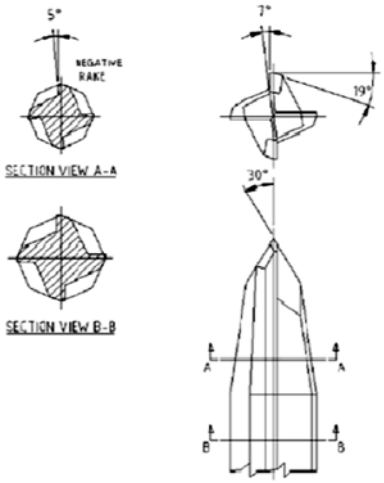

Fig. 6 Multifaced geometry.

Many authors have proposed work on this tool geometry (Faraz et al., 2009; Fernandes & Cook, 2006; Lazar & Xirouchakis, 2011; Lin & Chen, 1996; Murphy et al., 2002; Piquet et al., 2000). For example, Faraz and others (Faraz et al., 2009) proposed a study on four types of multifaceted tools (Fig. 7).

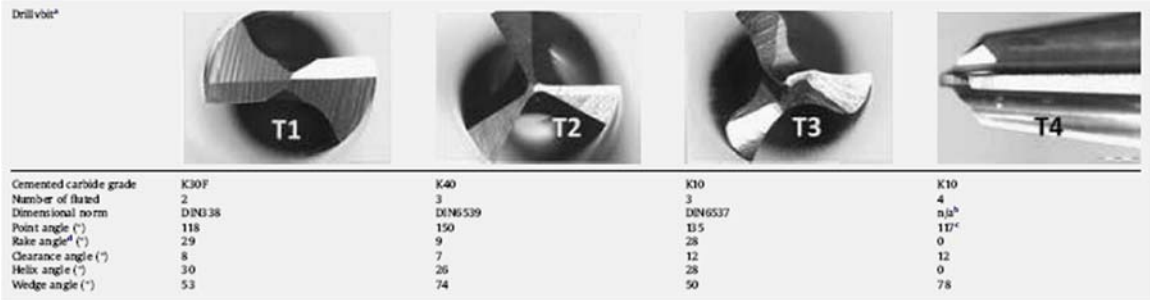

Cemented carbide grade	K30F	K40	K10	K10
Number of flutes	2	3	3	4
Dimensional norm	DIN338	DIN6539	DIN6537	n.a.[b]
Point angle (°)	118	150	135	117[c]
Rake angle[d] (°)	29	9	28	0
Clearance angle (°)	8	7	12	12
Helix angle (°)	30	26	28	0
Wedge angle (°)	53	74	50	78

Fig. 7 Tools geometry investigated by Faraz et al., 2009.

Fig. 8 states that the tool with four cutting edges is the one that exerts the lowest thrust force, but the highest moment.

As far as the delamination damage is concerned, the tool with the best behaviour is the tool with three cutting edges called T3.

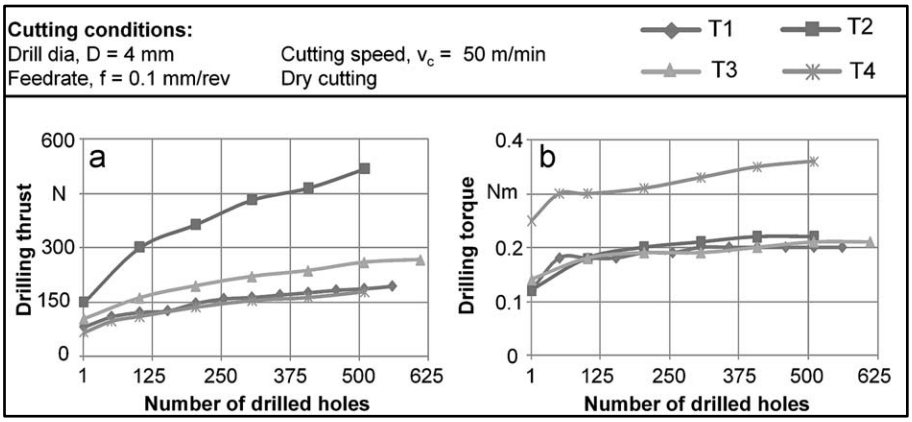

Fig. 8 Faraz et al., 2009 drilling tools thrust and torque.

Another geometry proposed is the one called "Brad & Spur drill", studied starting from the geometry of the tools used in the wood industry Fig. 9.

Fig. 9 Brad & Spur tool.

Many authors have also studied this geometry. It is a geometry that ensures reduced risk of delamination and low forward force(Abrão et al., 2008; Durão et al., 2010; Hocheng & Tsao, 2006; Tsao & Hocheng, 2004).

Step drill bit geometries (Fig. 10) have also been studied, still developed to eliminate the damage caused by the central cutting edge. They're two diameter geometries. The first part of the tool has a diameter smaller than the nominal diameter of the tool. The second part ends with the nominal diameter.

The drilling operation lasts longer than a "single step" tool, but in many cases, there is an improvement in delamination.

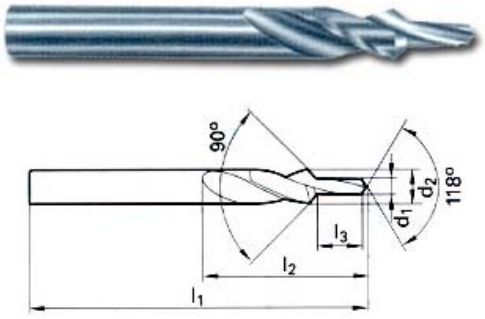

Fig. 10 Step drill tool.

The first and most important observation was the dependence of the thrust force on the chisel edge, so it was decided to develop a double diameter tool.

For thermosetting matrix composites, where no plastic behaviour occurs before breakage, it was decided to gradually cut the remaining part of the hole with a variable profile down to the final diameter.

Based on this bibliographic study, new drilling tool geometries were developed.

The principle on which the development was based was to eliminate, i.e. to reduce, as much as possible, the contribution of the "chisel edge" to the feed force.

Two geometries were designed, the first one has been called SEL (Step Elliptical Linear), Fig. 11, in which the cutting profile for the pilot hole is elliptical, and the side profile has linear development, while the other called SEE (Step Elliptical Elliptical) has both elliptical profiles, Fig. 12.

Fig. 11 SEL geometry.

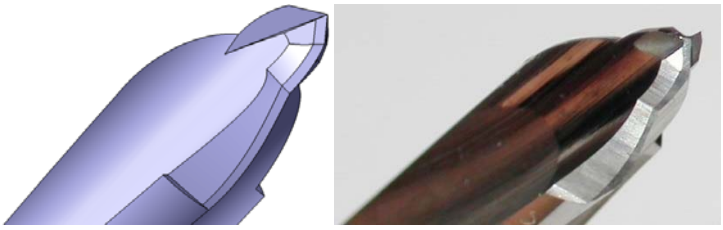

Fig. 12 SEE geometry.

Two tools with SEL and SEE geometries were then produced and tested; drilling tests were carried out with the cutting parameters showed in Tab. 2 and thrust force signal has been acquired and the values were compared with those of a tool traditionally used by the industrial partner called “traditional”.

Feed rate (mm/rev)	Spindle speed (rev/min)		
	5000	7500	10000
	Feed motion (m/min)		
0.10	0.500	0.750	1.000
0.25	1.250	1.875	2.500
0.50	2.500	3.750	5.000

Tab. 2 Cutting parameters.

By an analysis of the results, shown in Fig. 13, it is possible to verify that the SEE tool gives a lower thrust force than the other geometries, confirming the validity of the idea behind the development.

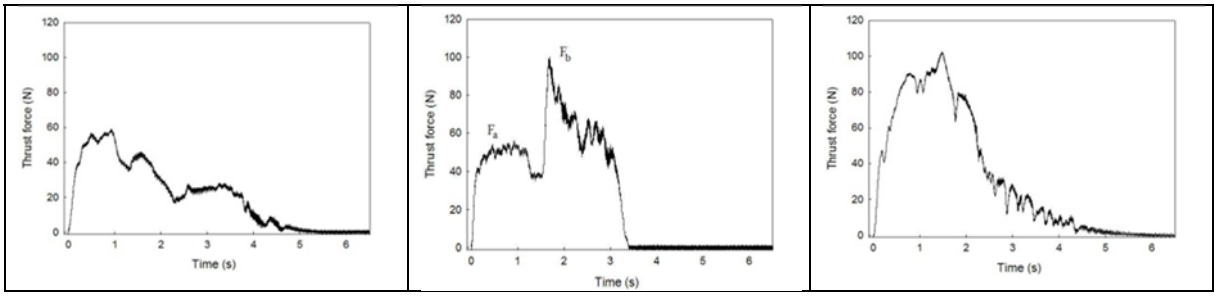

Fig. 13 Thrust force during drilling by a)SEE; b)SEL; c)traditional.

Several possible geometries of the SEE typology were then examined (Tab. 3); the analysis of the feed force made it possible to identify the innovative geometry with which to continue the experimentation (in bold in Tab. 3).

N. of cutting edge	Helix angle	Point angle
3	20°	110°
3	20°	120°
2	15°	110°
2	20°	110°
2	15°	120°
2	**30°**	**125°**

Tab. 3 SEE tested geometry

3.3. Sensor monitoring for drilling process automation

In order to achieve the objective set by activities 2.5 of the project, a multiple sensor monitoring system employed during the experimental drilling tests was configured; it is composed of the following sensors (Fig. 14):

- Force sensor;
- Torque sensor;
- Acoustic Emission (AE) sensor and Vibration Acceleration sensor.

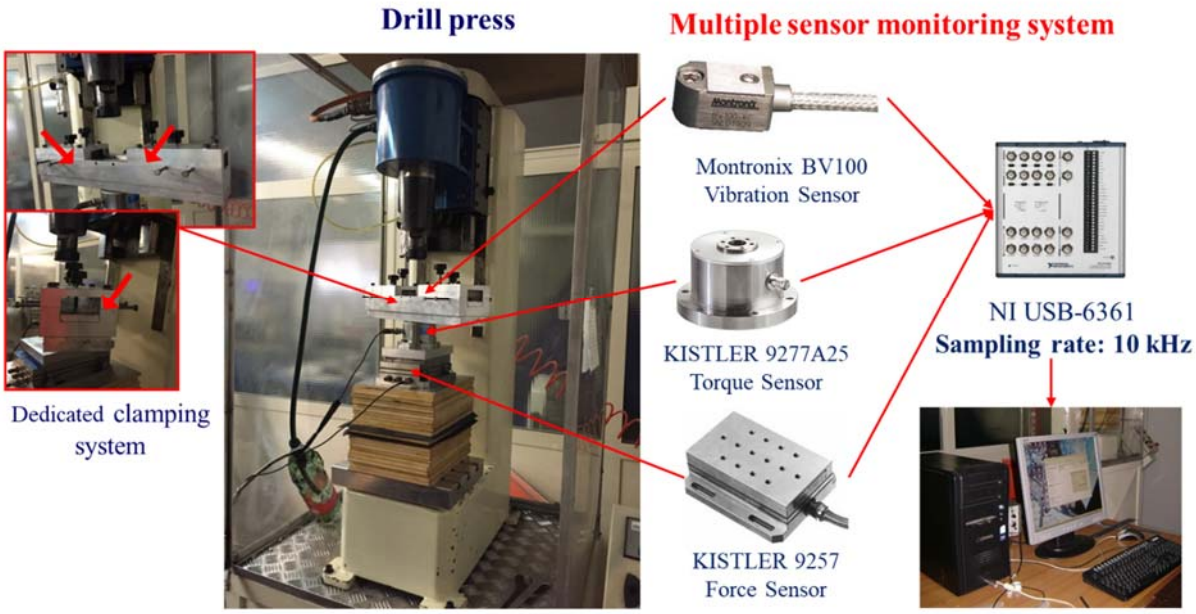

Fig. 14 Multiple sensors system for drilling process monitoring setup.

The characteristics of the sensor signals to be used for the detection of correlations with the tool wear have been identified using an extraction process, at the end of which the characteristics most related to tool wear have been selected. The extraction procedure of the characteristics has been carried out through a statistical analysis of the signals in the time domain for the extraction of mean, variance, asymmetry, kurtosis, energy. The correlation of these statistical characteristics with the tool wear will be evaluated by using a special index for the evaluation of the degree of correlation (Pearson correlation index), on the basis of which it will be possible to select the most relevant characteristics for monitoring the drilling process.

4. Drilling of CFRP/CFRP stacks

4.1. Work materials

The classification of the composite materials can be made on the basis of multiple criteria. One of the most common classification is according to the type of components used in the realization of the composite material, with particular reference to the type of matrix and the reinforcing fibre type. Since the field of possible applications is mostly influenced by the type of material used for the matrix is commonly used to classify the composite materials according to its characteristics. Due to the excellent physical properties of the final product, the polymer matrix composites, also known as FRP (Fibre Reinforced Plastic), have been widely used in different sectors including aerospace, automotive and civil engineering.

Composite materials can also be distinguished according to the type of reinforcement used. The fibres may be of carbon, glass, steel or aluminium and differ from each other for their mechanical properties (e.g. elastic modulus, breaking strength, specific weight) as well as chemical and electrical properties. It is important to highlight that, with constant Young's modulus, the carbon fibres have a lower density and a resistance six times higher than steel or aluminium.

The Carbon Fibre Reinforced Plastic (CFRP) materials are the widely used composite in the aerospace sector, mainly for their lightness and resistance (Wilhelm et al., 2001). The advantages of carbon fibres are high elastic modulus, lightweight, high resistance to fatigue and compression, low thermal expansion coefficient, good electrical conductivity, good resistance to high temperatures (2000°C) in non-oxidizing atmosphere and good resistance to medium temperatures (400°C) in oxidizing atmosphere. Therefore, the composite materials made up of resin and carbon reinforcements have an excellent combination of low weight, high mechanical strength and high rigidity.

In the last decades, there was an increasing percentage of composite materials employed in aeroplane realization. Generally, the application of CFRP reduces the overall weight of the aeroplane and increases efficiency and safety, also reducing fuel consumption.

Both the CFRP laminates and the Aluminium alloy, which were employed in different stack configurations, were provided from the industrial partner company and belonged to real production batches actually employed on the production lines. The setup of the workpiece has the objective to reproduce the real aeronautical industry operating conditions, in which these types of laminates are superimposed and then drilled together to allow the subsequent riveting.

The configuration CFRP/CFRP stack under study is composed of two overlaid symmetrical and balanced laminates. Each laminate has a thickness of 5 mm and is made up of 26 prepreg unidirectional plies arranged according to the following stacking sequence $[\pm 45_2/0/90_4/0/90/0_2]_s$. A very thin fibreglass/epoxy ply, reinforced with 0°/90° fabric (areal weight 80 g/m2) is laid on the top and bottom of each laminate. The prepreg plies are made of Toray T300 carbon fibres and CYCOM 977-2 epoxy matrix.
Laminates were fabricated by hand layup, vacuum bag moulding (Fig. 15a) and autoclave curing (180 min at 180 °C and 6 bar) (Fig. 15b).

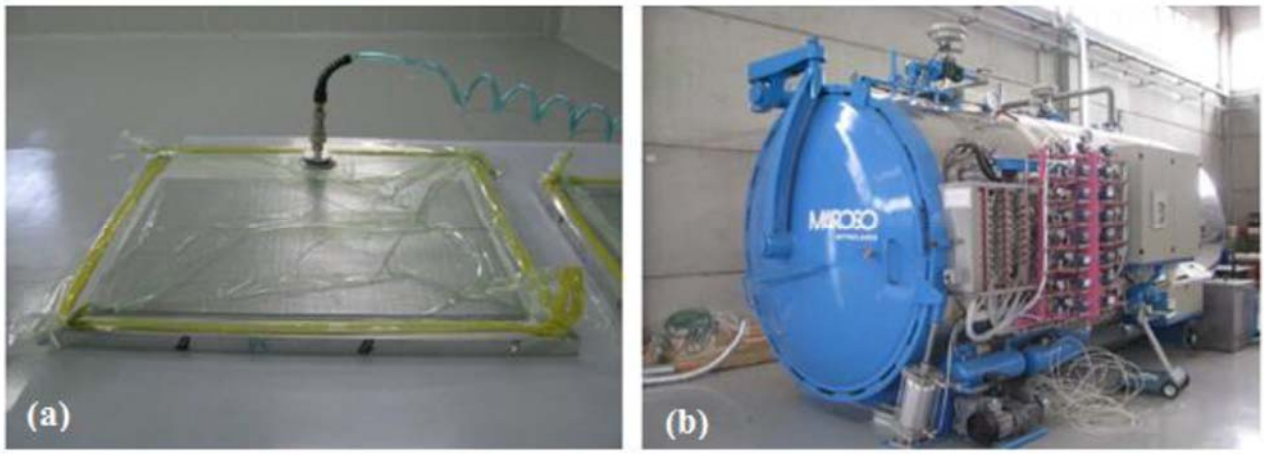

Fig. 15 a) Vacuum bag moulding; b) Autoclave.

The surface texture of the laminates on the bag side is very irregular and with a larger matrix thickness compared to the mould side, which is smooth and thinner (Fig. 16).

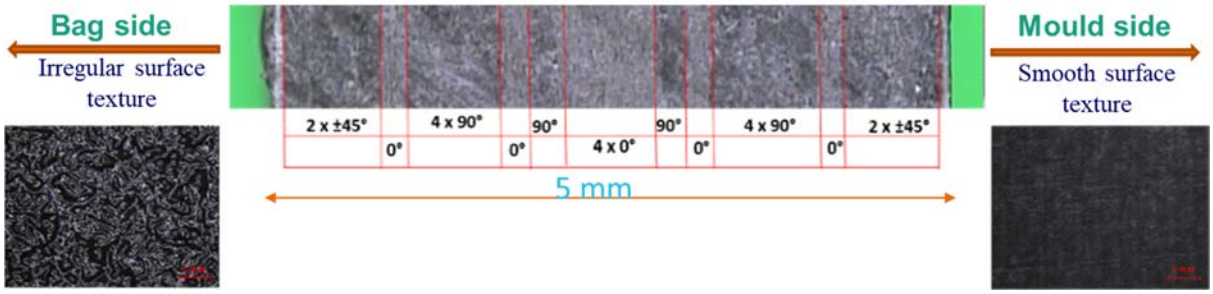

Fig. 16 The sequence of layers in the sectioned CFRP laminate and surface texture.

The experimental campaign was conducted on a stack made of two CFRP laminates. The CFRP laminate is composed of 26 CFRP prepreg plies made of CYCOM 977-2 epoxy matrix and Toray T300 carbon fibres with the following stacking sequence $[\pm 45_2/0/90_4/0/90/0_2]_s$.

Fig. 17 CFRP/CFRP stack

The total thickness of the CFRP/CFRP stack is about 10 mm; in order to reproduce as close as possible the drilling conditions in the aerospace industry, the two laminates have been clamped and drilled together. The two stacked CFRP laminates were placed with the bag side in contact to experiment with the severest possible drilling conditions.

4.2. Drilling tools

Drilling tools can be divided into different types depending on the processes for which they are designed, but the most widely used are the twist-drill bits (Fig. 18).

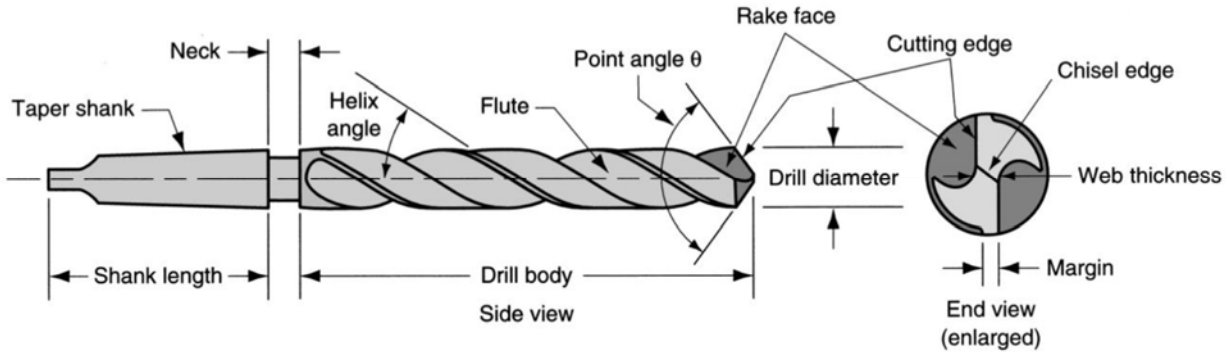

Fig. 18 Standard geometry of a twist drill (Mikell P. Groover, 2014).

The standard twist drill has two opposite helical grooves. The angle between the spiral flutes and the tool axis is called the helix angle, which usually varies between 30° and 35° degrees. The flutes are necessary for the extraction of chips from the hole. Although the flute openings should be large enough to provide all-out clearance for the chips, the body of the drill must be supported over its length. This support is provided by the web, which is the thickness of the drill between the flutes.

The last part of the body of the twist drill has a conical shape. A typical value for the point angle is 118°. Finally, there is the chisel edge. Connected to the chisel edge are two cutting edges (sometimes called lips). The portion of each flute adjacent to the cutting edge acts as the rake face of the tool.

The bit is also equipped with margins, which drive the tools into the hole and realizes the finishing of the cylindrical wall. The bit ends, on the other side, with a cylindrical or conical shank, which serves to fix it to the drill spindle.

In drilling CFRP/CFRP stacks, two different kinds of drilling tools were used (Fig. 19):

- one traditional twist drill, commercially available and already used by the industrial partner;

- an innovative twist step drill developed within our department.

Both tools are uncoated made of tungsten carbide and have the geometric parameters shown in the following table (Tab. 4); each drill bit produced 60 holes with the same cutting condition:

	traditional	innovative
Diameter	6.35	4.35 to 6.35
Geometry	twist	step/twist
Point angle	120°	125°
Helix angle	20°	30°

Tab. 4 geometric parameters.

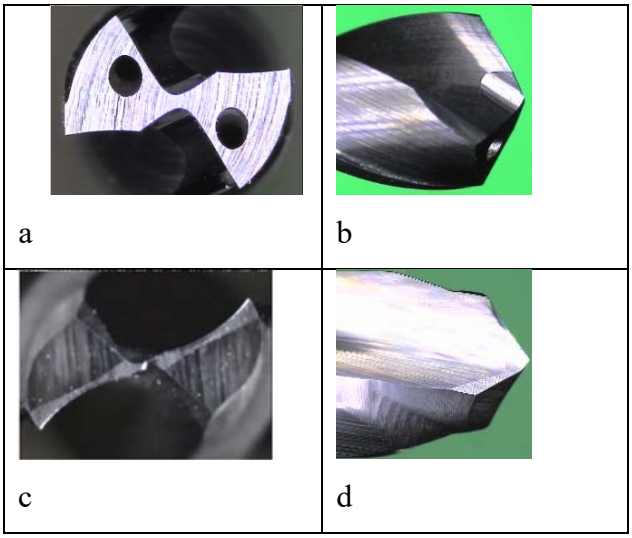

Fig. 19 a) Traditional tool front view; b) Traditional tool side view; c) Innovative tool front view; d) Innovative tool side view.

4.3. Process parameters

In order to recognise the influence of the cutting parameters on the machinability of the stacks under study in terms of tool wear and quality of the holes, different cutting conditions were adopted for the experimental drilling tests: three feed values and three different spindle speeds were employed, as shown in Tab. 1. Each drill bit realized 60 holes in CFRP/CFRP stacks with the same process parameters; every 10 holes drilled the drilling operation has been suspended in order to acquire images of the drill bit to assess its wear.

CFRP/CFRP Process parameters		Spindle speed (rpm)		
		2700	6000	9000
Feed (mm/rev)	0.11		B	E
	0.15	A	C	F
	0.20		D	

Tab. 5 Experimental testing conditions CFRP/CFRP

To facilitate reading, each processing condition has been assigned a letter; the prefixes "T" and "I" have been used to distinguish the traditional tool from the innovative one.

5. Drilling of Al/CFRP stacks

5.1. Work materials

As mentioned above also the Aluminium alloy sheet was provided from the industrial partner company and belonged to real production batches actually employed on the production lines. The second case of study is the Al/CFRP stack (Fig. 20); the configuration proposed is composed by an Aluminium sheet which has a thickness of 2.5 mm and is made of 2024 alloy and a CFRP laminates which is the same type mentioned above.

Fig. 20 Al/CFRP stack

Aluminium alloys have a strong corrosion resistance characteristics and are sensitive to high temperatures ranging between 200 and 250°C. An increase in strength takes place when these alloys are exposed at sub-zero temperatures and it is lost when these alloys are exposed to high temperatures, so they are useful low-temperature alloys. These alloys are commonly used in the manufacture of truck wheels, aircraft structures, and screw machine products, scientific instruments, veterinary and orthopaedic braces and equipment, and in rivets. The chemical composition of the Aluminium 2024 alloys and the principal physical, mechanical and thermal properties are outlined in the following tables (Tab. 6, Tab. 7).

Element	**Weight (%)**
Aluminium, Al	Balanced
Copper, Cu	3.80 - 4.90
Magnesium, Mg	1.20 - 1.80
Manganese, Mn	0.30 - 0.90
Silicon, Si	0.50
Iron, Fe	0.50
Zinc, Zn	0.25
Titanium, Ti	0.15
Chromium, Cr	0.10

Tab. 6 Chemical composition of the Aluminium 2024 alloy.

Property	Value
Density (g/cm^3)	2.78
Melting point (°C)	510
Tensile strength, ultimate (MPa)	220
Elastic modulus (GPa)	70 - 80
Poisson's ratio	0.33
Thermal expansion in the range 20 - 100 °C (µm/m °C)	22.8
Thermal conductivity at 25°C (W/mK)	193

Tab. 7 Physical, mechanical and thermal properties of the Aluminium 2024 alloy.

In tests conducted on Al/CFRP stacks, aluminum was drilled first to prevent aluminium chips from ruining the CFRP hole and the laminates were, as in CFRP/CFRP drilling, overlapped with the irregular part of the CFRP between them to test the severest condition.

5.2. Drilling tools

In drilling Al/CFRP stacks, experimental tests were carried out through the traditional tool. Each drill bit performed 30 holes with the same cutting condition.

5.3. Process parameters

In order to find the influence of the cutting parameters on the machinability of the stacks under study in terms of tool wear and quality of the holes, different cutting conditions were adopted for the experimental drilling tests: three feed values and three different spindle speeds were employed, as shown in Tab. 8. Each drill bit realized 30 holes in Al/CFRP stacks with the same process parameters

Al/CFRP **Process parameters**		**Spindle speed (rpm)**		
		3000	**4500**	**6000**
Feed (mm/rev)	**0.05**	1	4	7
	0.10	2	5	8
	0.15	3	6	9

Tab. 8 Experimental testing conditions Al/CFRP

To facilitate reading, each processing condition has been assigned a number for the Al/CFRP stacks.

In the case of too high parameters (8, 9), a catastrophic tool failure occurred. It was therefore chosen to eliminate the tests at 6000 rpm from this study.

6. Setup of drilling operations

With the final aim to develop a sensory monitoring system for tool wear, it was necessary to configure a multiple sensor monitoring system to employed during the experimental drilling tests.

The CNC drilling centre and the sensors monitoring system have been reported in Fig. 21.

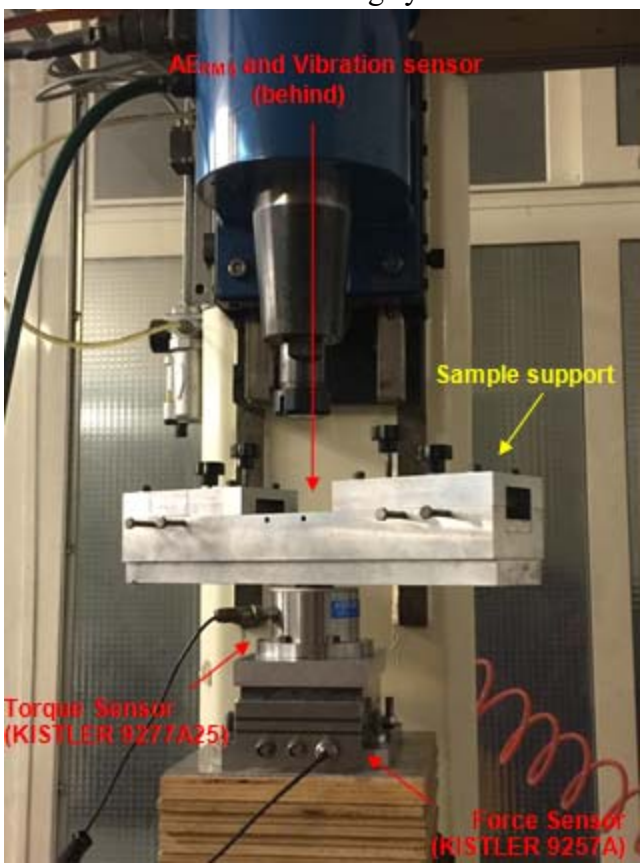

Fig. 21 Drilling centre used for the experimental campaign

The thrust force and cutting torque were measured using two Kistler piezoelectric dynamometers, respectively, the model 9257A and the model 9277A25. The Montronix® BV100-AX sensor has acquired the Acoustic Emission (AE) RMS and acceleration of vibrations.

The multiple sensor monitoring system employed during the experimental drilling tests comprised the following sensors:

- Force sensor;
- Torque sensor;
- Acoustic Emission (AE) sensor;

- Vibration Acceleration sensor.

Force and Torque sensor

A Kistler-9257A piezoelectric dynamometer was employed to acquire the thrust force along the z-direction, Fz (Fig. 22a). The cutting torque about the z-axis, Mz, was acquired using a Kistler-9277A25 piezoelectric dynamometer (Fig. 22b).

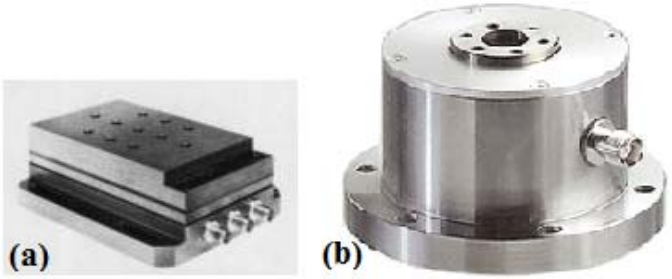

Fig. 22 (a) Kistler-9257A piezoelectric dynamometer; (b) Kistler-9277A25 piezoelectric dynamometer.

Two Kistler 5007 amplifiers (Fig. 23) were employed for the force and torque signals. The time constant setup was set to "long". The selected scale in the mechanical unit (M.U.) / V was 100. Calibration was necessary for both force and torque after each single drilling test. The transducer sensitivity values to be set are suggested by the technical datasheets of the two piezoelectric dynamometers. As regards force, the amounts are equal to -7.5 pC / N for the force components along the x and y axes, Fx and Fy, and -3.5 pC / N for the force component along the z-axis, Fz, which represents the thrust force of the drilling process. Conversely, the value to be set for the torque component about the z-axis, Mz, is - 2.5 pC / Ncm.

Fig. 23 Kistler 5007 amplifiers.

Acoustic Emission and Vibration acceleration sensor

The acoustic emission and vibration acceleration signals were acquired using the Montronix BV100™ broadband vibration sensor, provided with two channels to measure both the vibrations and the high-frequency acoustic emission (AE) signals. (Fig. 24a). The analogue acoustic emission and vibration acceleration sensor signals were then amplified by a Montronix TSVA4G amplifier (Fig. 24b). The AE amplifier specifications are reported in the following Tab. 9.

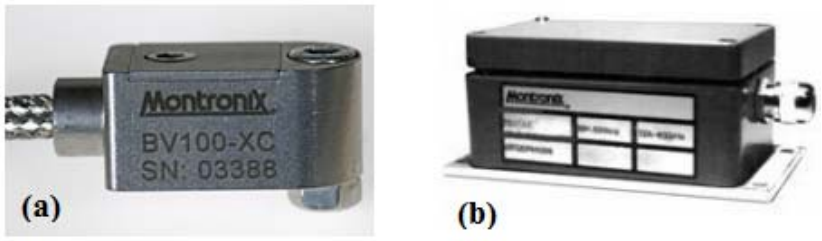

Fig. 24 (a) Vibration and high-frequency Acoustic Emission sensor - Montronix BV100™; (b) Montronix TSVA4G amplifier

Gain Settings:	1, 2, 5, 10, 20, 40, 80, 200, 400, 800
Gain Error	±2%
Output Voltage	0 to 10 V
Power provided to Sensor	+ 15 VDC @ 4mA constant current
Amplifier Power Requirements	+15 VDC @ 80mA -15 VDC @ -60 mA
Temperature Range	0° to 60° C
Connectors	PG9 threated fittings, sensor-specific
Weight	680 g

Tab. 9 AE Amplifier Specifications

The amplifier was configured with the settings reported in Fig. 25.

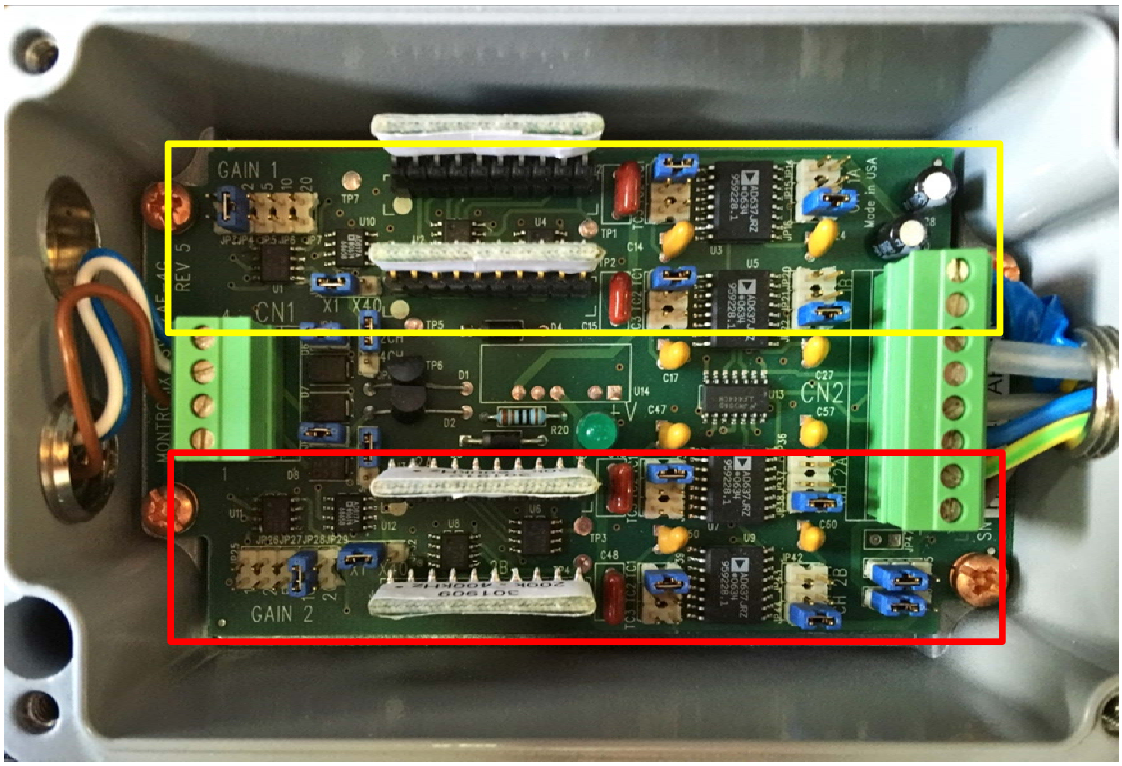

Fig. 25 Acoustic Emission and Vibration Acceleration amplifier settings

The amplifier has two channels:

- the yellow on the top (channel 1) is dedicated to the Acceleration signals amplification
- the red on the bottom (channel 2) is dedicated to the AE signals amplification

The gain set for Acceleration signals is equal to 2 while the one for the AE_{RMS} signals is equal to 10 in order to accurately visualize the signals without exceeding the maximum threshold of 10 V imposed by the data acquisition (DAQ) board.
Both the AE and Acceleration signals have been acquired as Root Mean Square (RMS) signals. RMS is a technique used to rectify a RAW signal and convert it to an amplitude envelope, which is easier to view. The rectification process converts all the numbers into positive values rather than positive and negative.
During the experimental tests, the RMS conversion time constant was set to TC1 = short, corresponding to a time constant of 0.12 ms.
The output low-pass filter cut-off frequency was set to F3 = high for both channels.

Signal Acquisition

The analogue signal from the Thrust Force, cutting Torque, Vibration Acceleration and AE_{RMS} sensors were digitalized by the National Instruments DAQ device NI USB-6361 (Fig. 26). The specifications of the device are reported in Tab. 10.

Fig. 26 Data acquisition device - NI USB-6361

Analog Inputs (AI)	16
Max AI Sampling Rate (1-Channel)	2MS/s
Max Total AI Throughput	2MS/s
Analog Outputs (AO)	2
Max AO Update Rate	2.86 MS/s
Digital I/O Lines	24
Max Digital I/O Rate	10 MHz
Triggering	Analog, Digital

Tab. 10 Data acquisition device NI USB-6361

According to the Nyquist-Shannon sampling theorem, the sampling rate was set equal to 10kHz. The sampling theorem provides a prescription for the nominal sampling interval required to avoid aliasing, i.e. the effect that causes different signals to become indistinguishable when sampled. The theory states that "the sampling frequency should be at least twice the highest frequency contained in the signal":

$$f_s \geq 2 * f_c$$

where:

f_s is the signal sampling frequency and f_c is the highest frequency observed in the signal.

The data acquisition software used is the NI SignalExpress 2014. The software allows to quickly acquire, analyse and visualize data using the software interface shown in Fig. 27.

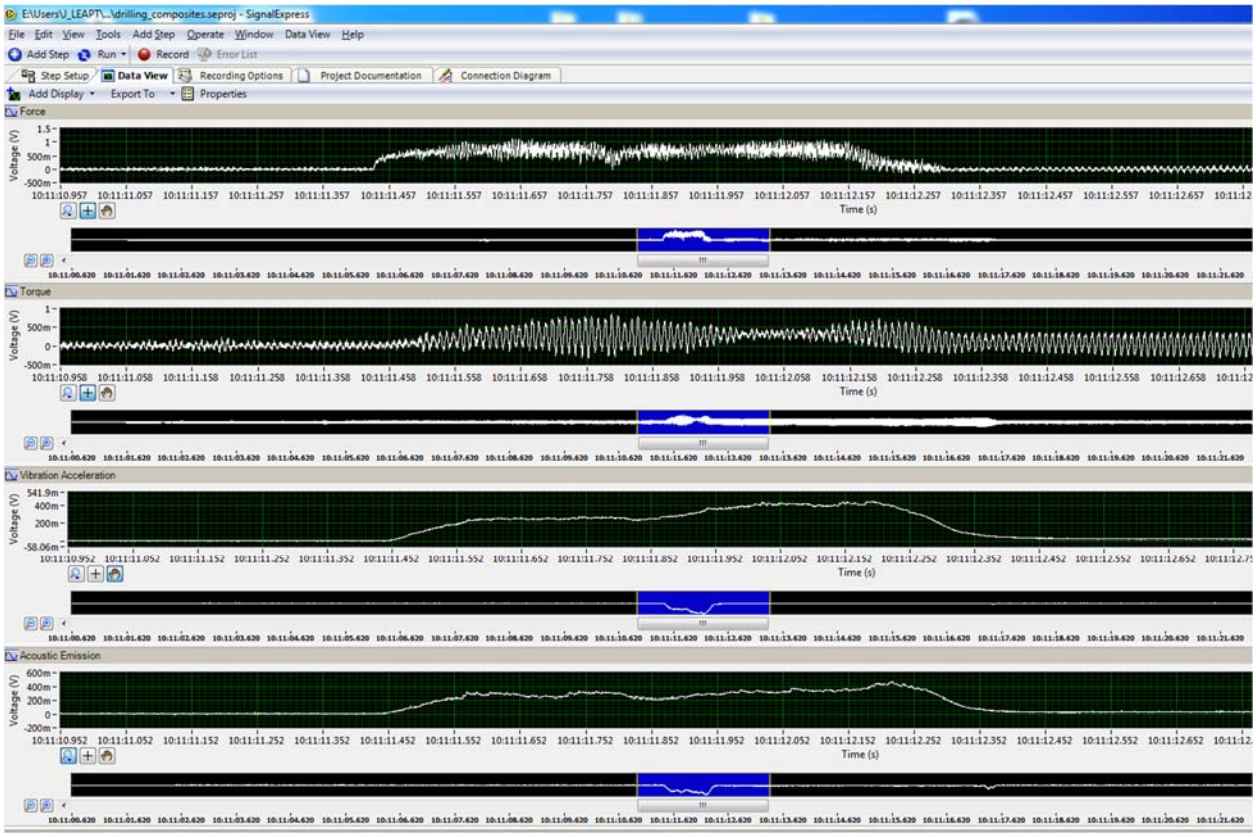

Fig. 27 NI SignalExpress software interface.

7. Instrumentation for image acquisition

This thesis work, as will be explained later, is based on an optical approach for the evaluation of the tool wear and the quality of the drilled holes. In order to evaluate the wear and quality parameters that will be illustrated in the following sections, the acquisition of images was therefore fundamental. All the images were acquired using a Tesa Visio V-200 optical measuring machine shown in Fig. 28.

Fig. 28 Tesa Visio V-200

8. Tool wear assessment

8.1. Tool wear evaluation

The use of a specific cutting tool influences both the quality and the cost of the machined parts. Tools must guarantee the following two properties:

- Material removal action.
- Adequate surface finishing achievement.

One of the primary limits in the drilling of polymer matrix composites with conventional twist drills, such as high-speed steel tools, is the excessive tool wear suffered by these tools.

In fact, while a drill bit made of high-speed steel can be used for drilling hundreds of holes in carbon steel before it wears out entirely, the same tool when drilling composite materials is able to drill less than ten holes.

The tool wear, i.e. the progressive removal of material from the tools surface, is linked to the combined effect of high temperature, chemical characteristics of the material, and high stresses to which the tool and workpiece are subjected during machining.

The wear mechanisms can be classified as:

- Wear by abrasion: produced by the sliding of a hard and rough surface on a softer one.
- Wear for bond: originated by the high contact pressures between chip and tool which causes welds between the surfaces in contact.
- Wear by diffusion: produced by the migration of atoms through the tool-chip interface.

The combined effect of mechanical and thermal stresses can cause both tool chipping, i.e. removal of metal particles near the cutting edge due to impacts or excessive pressures, and tool plastic deformation due to high temperatures in the cutting zone.

The mechanisms of tool wear can occur on both tool flank (flank wear) and tool rake (crater wear). Flank wear and crater wear are the two most widely used wear phenomena considered for tool wear characterisation (Fig. 29). However, flank wear is most commonly used for wear monitoring due to its trend during machining (J. Sheikh-Ahmad & Davim, 2011).

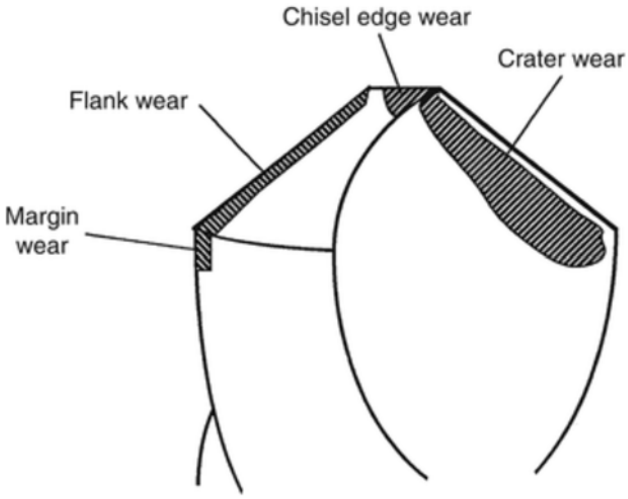

Fig. 29 Schematic representation of a twist drill (Stephenson & Agapiou, 2006).

Flank wear is the result of friction between the machined surface of the workpiece and the tool flank. Flank wear appears in the form of the so-called wear land and is measured by the width of this wear land, VB. Cutting forces increase significantly with flank wear. Crater wear is the consequence of the action of the chip sliding on the tool rake face. In Fig. 30, the tool flank wear as a function of cutting time is reported (tool wear curve). Crater wear follows almost the same curve trend.

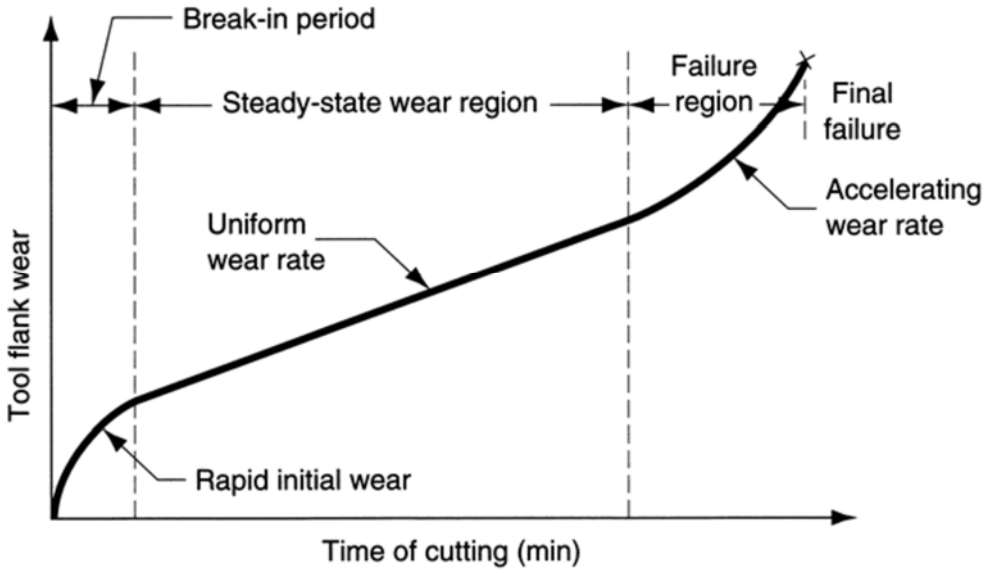

Fig. 30 Tool flank wear as a function of cutting time (Marinov, 2004).

As cutting proceeds, the amount of tool wear increases gradually. The tool wear must be lower than a specific limit in order to avoid tool failure; this value is known as tool life (generally in the steady-state wear region), and it depends on the operating conditions. The duration of the

life of the tool, T, is defined broadly by imposing a limit to the value VB. When this limit is exceeded, the tool must be changed.

Parameters, which affect the amount of tool wear are:

- cutting paramenters (cutting speed V, feed rate f, depth of cut d);
- cutting tool geometry (tool rake angle);
- properties of the work material.

Among these parameters, cutting speed is the most significant in terms of influence on tool wear. As cutting speed is increased, tool wear rate increases too; thus, the same wear is reached in less time, meaning that tool life T decreases with cutting speed (Fig. 31).

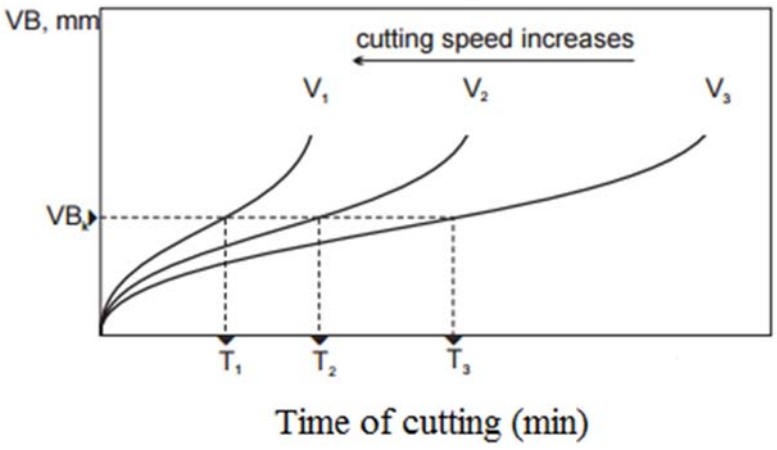

Fig. 31 Effect of cutting speed on tool wear and tool life for three cutting speeds: $V_1 > V_2 > V_3$.

In general, the tool life T can be expressed:

- as a function of the dimensional tolerances permitted on the workpiece;
- as a function of the tolerances of surface roughness of the workpiece;
- as a function of a given parameter for the quality of the holes;
- as a function of the limit fixed for the tool wear.

According to the literature, the most widely used parameter for tool wear monitoring during drilling operations is the flank wear (Park et al., 2011; Zitoune et al., 2013, 2010). Although it is not possible to make an exact comparison of the two drill bit types due to their different geometries, the flank wear was measured for both of them and used to assess the behaviour of the two different drill bit types during the drilling process.

Tool wear measurements were carried out during the drilling tests after every 10 holes for CFRP/CFRP stacks and after every 5 holes for Al/CFRP stacks. A magnified picture of the cutting lip was acquired through an optical measuring machine (Tesa Visio V-200) to optically measure the flank wear. Fig. 33 shows the TC tool (traditional tool: T; process condition C:

6000 rpm - 0.15 mm rev) before starting the drilling procedure (left) and after the realisation of 60 holes (right).

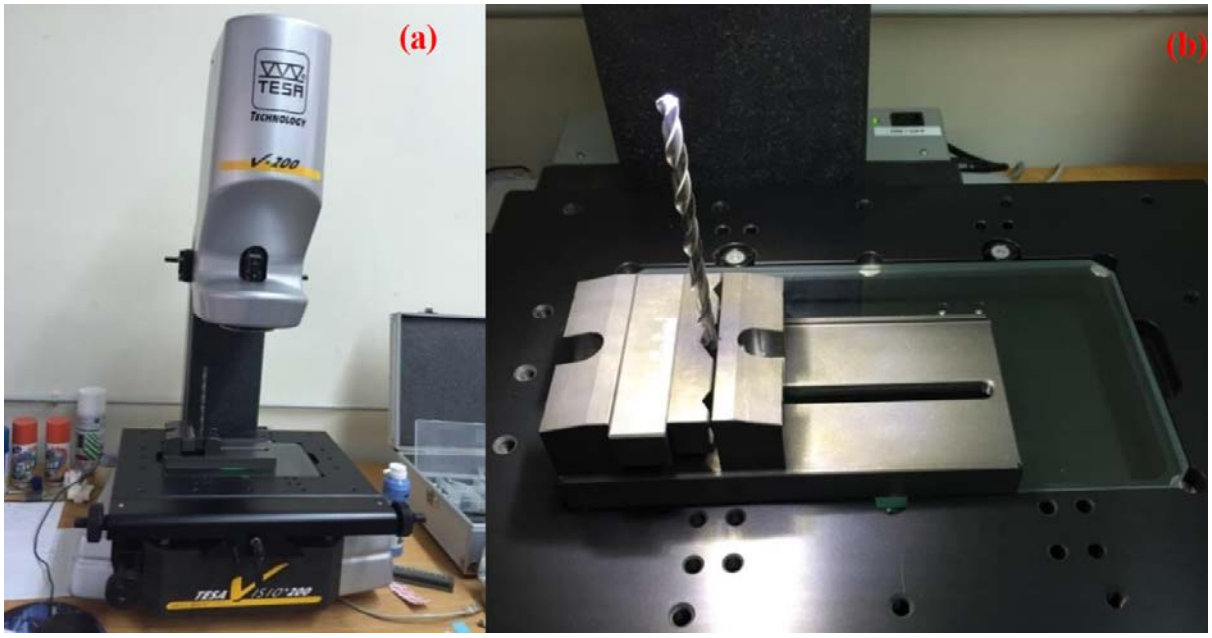

Fig. 32 (a) Tesa Visio V-200 optical microscope, (b) clamping system.

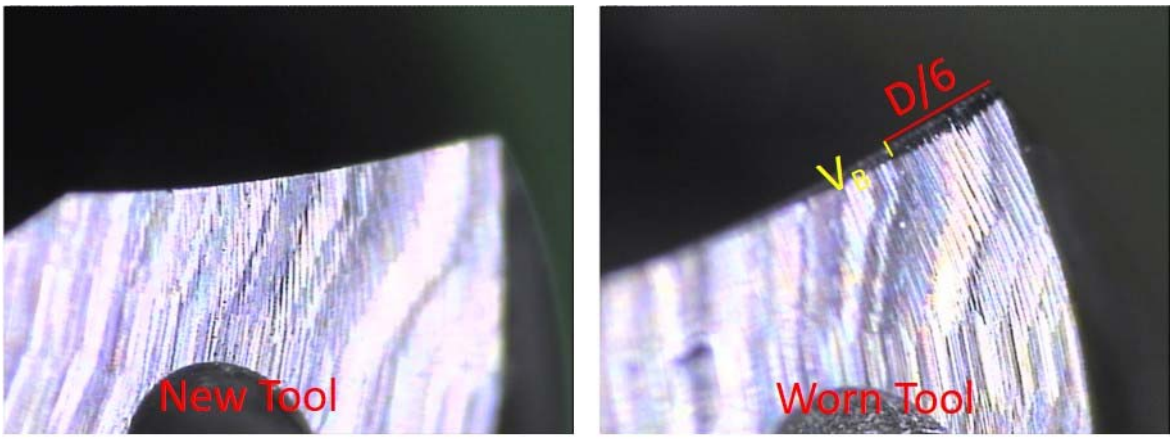

Fig. 33 Tool wear evaluation for a TC tool: a traditional tool, T, operating with process conditions C (6000 rpm – 0.15 mm/rev).

Flank wear measurements, VB (mm), were taken at 1/6 of the tool diameter following the procedure proposed in (A. Caggiano et al., 2017; Dolinšek et al., 2001; J. Y. Sheikh-Ahmad & Davim, 2012; Sousa et al., 2014) (Fig. 34): three VB measurements were carried out on each of the two cutting lips, obtaining six VB values for each tool. The average of the six VB values, measured after every 10 holes for the CFRP/CFRP stacks and after every 5 holes for the Al/CFRP stacks, were used to describe the tool wear development in Fig. 35 and Fig. 37.

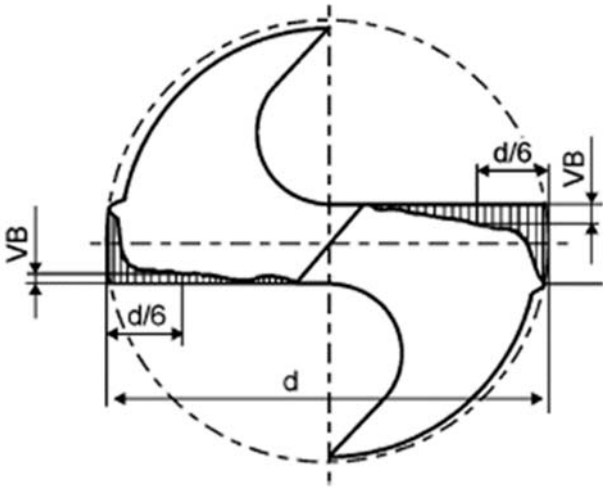

Fig. 34 Tool wear measurement scheme for drill bits (Dolinšek et al., 2001).

8.2. Results

The drilling process was interrupted every 10 holes for the CFRP/CFRP stacks and every 5 holes for the Al/CFRP stacks in order to evaluate the progress of tool wear.

For each drilling condition, 6 VB values (3 for each flank) were measured and averaged to describe the tool wear development. The average VB values were plotted with different colours corresponding to each process condition in Fig. 35.

CFRP/CFRP stacks

To make the results more readable, the information from Tab. 5 and Tab. 8 containing the process parameters are summarized in Tab. 11.

CFRP/CFRP Process parameters		**Spindle speed (rpm)**		
		2700	**6000**	**9000**
Feed (mm/rev)	**0.11**		B	E
	0.15	A	C	F
	0.20		D	

Al/CFRP Process parameters		**Spindle speed (rpm)**		
		3000	**4500**	**6000**
Feed (mm/rev)	**0.05**	1	4	7
	0.10	2	5	8
	0.15	3	6	9

Tab. 11 CFRP/CFRP and Al/CFRP process parameters

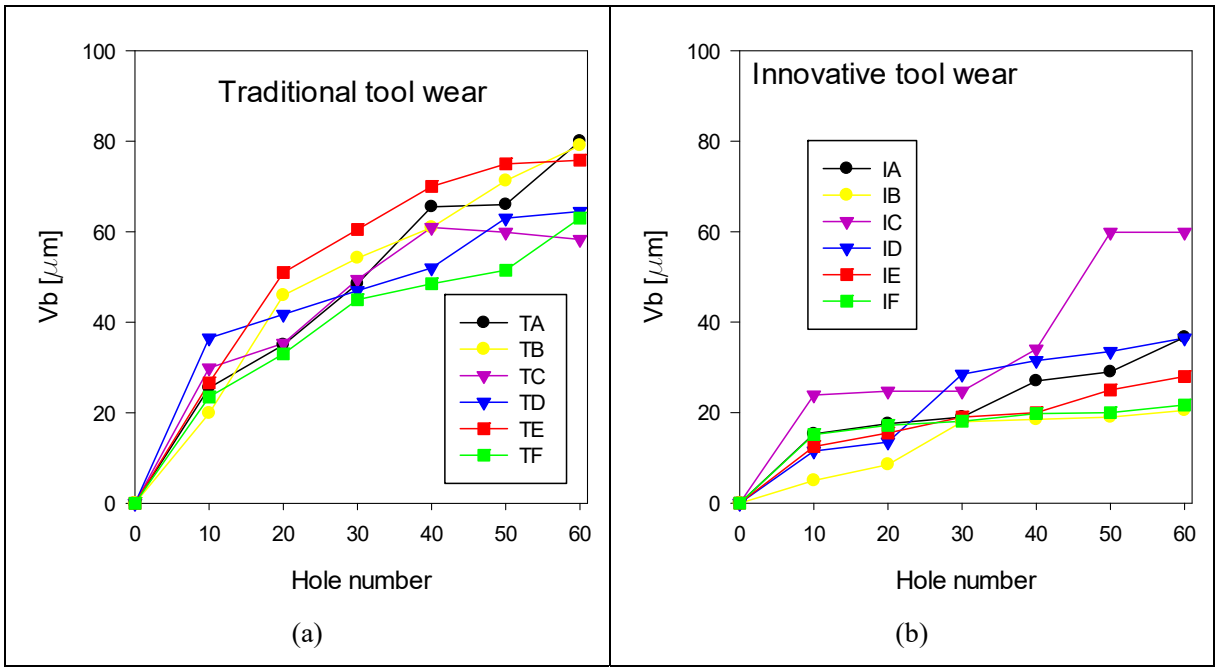

Fig. 35 Experimental tool wear curves for CFPR/CFRP stacks: (a) traditional tools T and (b) innovative tools I with process parameters A, B, C, D, E, F.

Tool wear appears to progress more rapidly for traditional tools than for innovative tools; this may depends on two factors:

- innovative tools also cut with margins and, therefore, a portion of the wear develops on them;
- VB is measured at D/6 which is 6.35/6 = 1.06 mm for the traditional tool, and 4.35/6 = 0.73 mm for the innovative tool.

These factors make the data not comparable.

For traditional tools, those that have shown lower wear progression are TC, TD and TF tools.

For innovative tools, IB, IE and IF tools had better behaviour.

Al/CFRP stacks

A catastrophic tool failure occurred for the T4 tool (Fig. 36) making it impossible to determine the wear level for this tool; for the other tools, the tool wear is reported in Fig. 37.

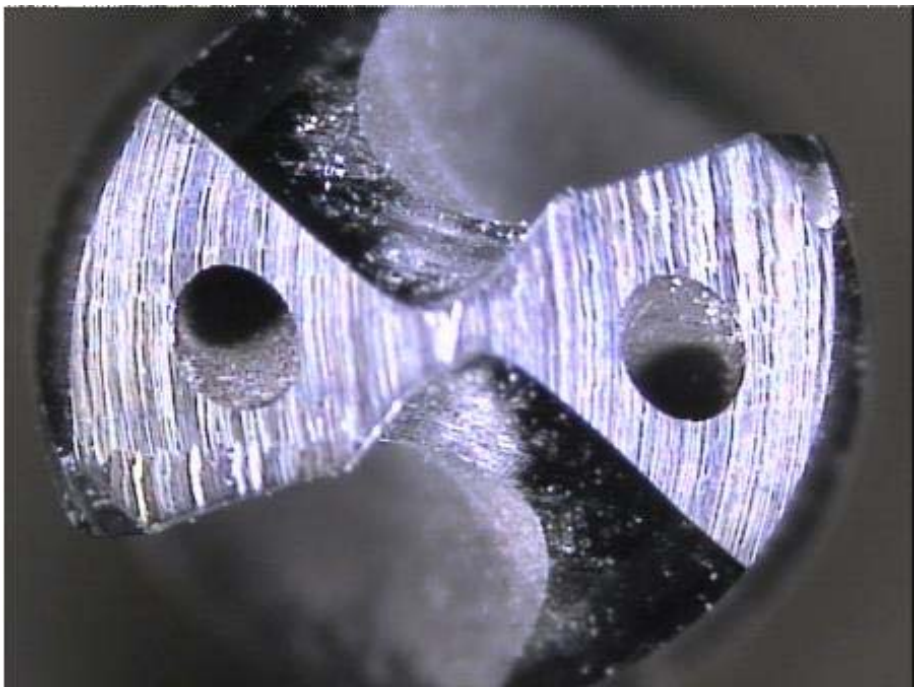

Fig. 36 Catastrophic tool failure for traditional tool, T, under process conditions 4 (4500 rpm – 0.05 mm/rev).

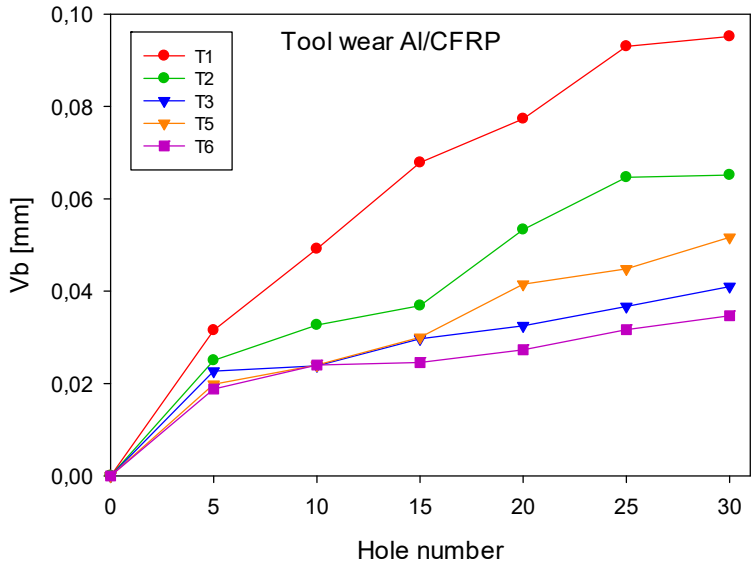

Fig. 37 Experimental tool wear curves for Al/CFRP stacks drilled with traditional tools T and process parameters 1, 2, 3, 5, 6.

Also in this case, 6 VB values for each drill bit were measured after every 5 drilled holes and their average values were plotted in Fig. 37 with 6 different colours, each corresponding to one experimental testing condition.

The less worn tools are traditional tools T3 and T6, working with process conditions 3 (3000 rpm – 0.15 mm/rev)) and 6 (4500 rpm – 0.15 mm/rev), respectively. Both these tools worked with the maximum feed rate value equal to 0.15 mm/rev.

From the tool wear curve, it can be noticed that there is a rising trend in the evolution of tool wear for all operating conditions. It is possible to apply a 3rd order polynomial interpolation of the VB values to construct the tool wear curves with the final aim of developing a sensor monitoring system for tool wear evaluation.

9. Hole quality assessment

9.1. Drilled hole quality parameters

Drilling of composite materials is a widespread machining process in the aerospace industry. Frequently, the parts realized in composite materials must be assembled to other parts using mechanical joints due to the difficulties to realize welding operations or adhesive joints.

The drilled holes reduce the laminate resistance to stress, so they are subjected to strict quality requirements. As far as geometric requirements, the holes must be in the right position, have the set diameter and the right shape (roundness).

The drilling process impacts the workpiece surface quality that has different acceptance levels depending on the aerospace industrial company. Nevertheless, workpiece quality can be affected by different non-compliance conditions. However, delamination damage is one of the most common parameters used for the evaluation of hole quality (Zhang, Wang, & Liu, 2001; Won & Dharan, 2002; Davim & Reis, 2003; Bhatnagar, Singh, & Nayak, 2004; Babu & Pradhan, 2007; Romoli & Dini, 2008). As a matter of fact, the main modality of composite failure is delamination, which happens in the drilling of composite laminates when the thrust force overcrosses a specific value, causing the layers of a multilayer material laminate such as CFRP to become separated. This failure causes a significant loss of material mechanical toughness and would remarkably diminish interlaminar strength. Avoiding delamination becomes one of the main objective in the drilling of CFRP materials since these composite materials continue to grow in applications for the aerospace and the automotive industries (Lenin, Ramkumar, & Senthilkumar, 2015).

Delamination can be defined as an inter-laminar failure occurring in the stacks at both the top and the bottom laminate surfaces around the drilled hole.

The exit delamination (or push-down delamination at hole exit) is generally more severe than the entry delamination (or peel-up delamination) (Dharan & Won, 2000). This two types of delamination damage mechanisms have different causes and effects. Peel-up delamination is produced by the cutting force pushing the abraded and cut materials to the flute surface. At the beginning of the interaction, the cutting edge of the drill abrades the laminate. As the drill moves forward, it pulls the abraded material along the flute and the material spirals up earlier than being effectively cut. Normally, a reduction in the feed rate can reduce this effect.

On the other hand, push-out delamination is a damage that occurs in interlaminar regions, so it depends on both fibre nature and resin type and their respective properties. This damage type

is a consequence of the thrust force applied by the drill bit on the uncut laminate plies of the workpiece. At a certain point, the loading exceeds the interlaminar bond strength and delamination occurs before the laminate is totally penetrated by the drill (Durão, et al., 2010). This damage can be reduced by using proper optimization of the process variables (cutting speed, feed rate and drill point geometry) (Singh & Bajpai, 2013).
In Fig. 38), the peel-up and push-down delamination phenomena are schematically shown:

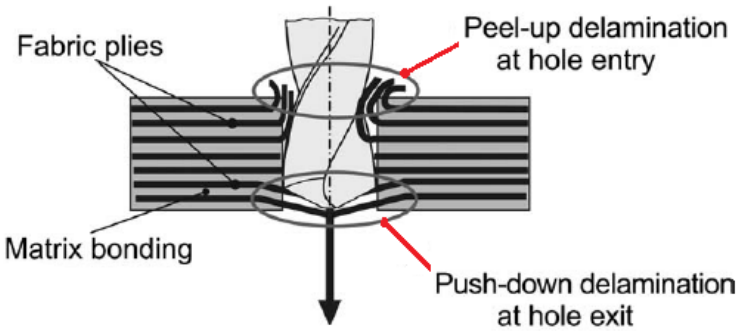

Fig. 38 Entry and exit delamination representation (Faraz, Biermann, & Weinert, 2009)

The delamination damage (entry and exit) was estimated in terms of delamination factor, F_d (Fig. 39), according to the following relationship proposed by (Chen, 1997):

$$F_d = \frac{D_{max}}{D_a}$$

where:
D_{max} is the diameter of the circumference including the damaged area
D_a is the actual measured hole diameter (Rawat & Attia, 2009)

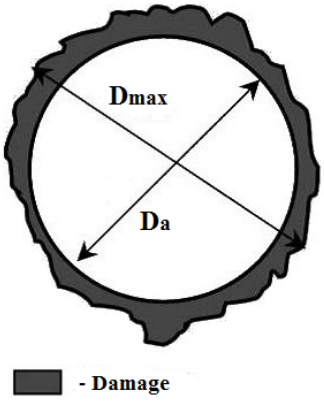

Fig. 39 Delamination factor Fd.

As some of these damages are not visible in a visual inspection, it is needed to establish non-destructive testing (NDT) procedures to be able to determine the existence of internal damages, like delamination, between the laminate plies. Carbon/epoxy laminates are opaque, so ultrasonic testing or radiography are desirable for laminate damage evaluation after drilling (Marques, Durão, Magalhães, & Tavar, 2007).

A relevant delamination parameter to be measured is the delamination area. The delaminated area around the hole is characterized by the amount of delamination at the hole exit A_d and not just by the maximum damaged diameter D_{max}. The damaged area A_d is more difficult to assess than the D_{max} and the delamination factor F_d (Davim, Rubio, & Abrao, 2007). Fig. 40 shows two holes with the same delamination factor F_d: it can be seem that the magnitudes of the damaged area are completely different. This example shows that delamination factor F_d alone is insufficient when the material generates irregular damages, especially in CFRP.

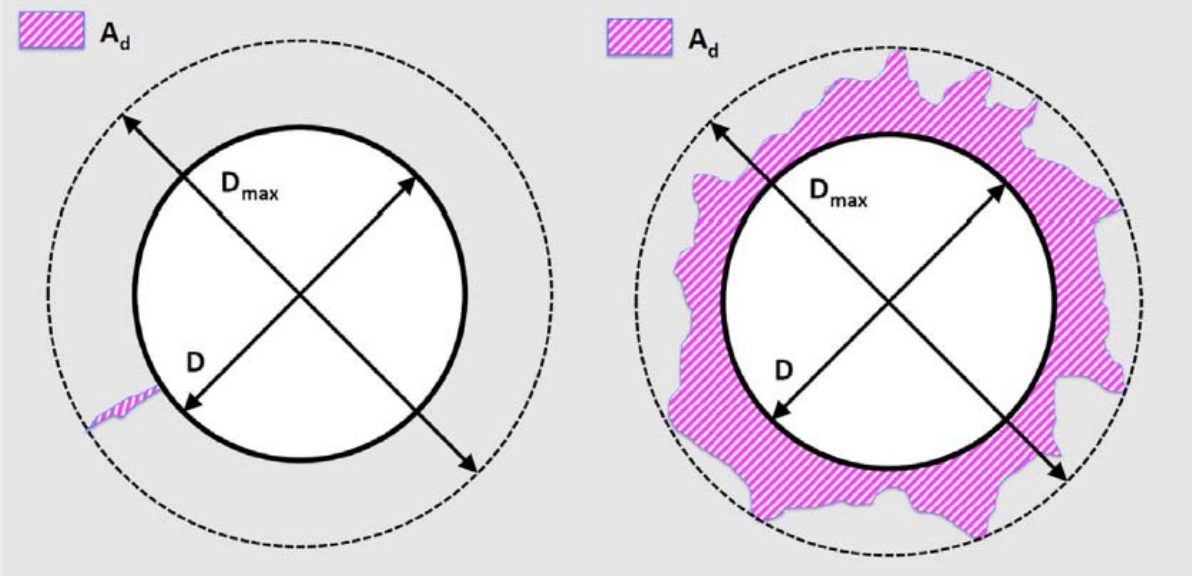

Fig. 40 Representation of hole delamination factor and delaminated area (Voß, Henerichs, Rupp, Kuster, & Wegener, 2016).

Based on the delamination factor F_d formula and the damaged area around the hole (A_d), (Davim, Rubio, & Abrao, 2007) developed an adjusted delamination factor measure in order to evaluate the percentage of the damaged area in the circular ring:

$$F_{da} = F_d + \frac{A_d}{(A_{max} - A_0)} \left({F_d}^2 - F_d\right), \qquad F_d \in [1; \infty]$$

where

A_{max} is the circular area of diameter D_{max}

A_0 is the area belonging to the hole diameter D

For each drilling condition, both entry and exit delamination damages were evaluated. In addition to the above mentioned surface integrity parameters, also geometrical and dimensional parameters were considered; in particular:

- Hole diameter
- Hole roundness
- Smoothness of the perimeter

As regards geometric problems, in the aeronautical sector the value of the hole diameter should remain within a very narrow tolerance range (often ≤ 0.076 mm). The roundness of the hole, according to the definition of ISO 1101: 2012, is evaluated as the ratio between the diameter of the maximum inscribed circle and the minimum circumscribed circle to the hole. Since the two situations described by the smooth blue line and the irregular red line in Fig. 41 are characterized by the same roundness value, the smoothness of the perimeter was introduced. Like for roundness, its value ranges between 0 and 1, being 1 for a mathematically perfect circumference and close to zero when it deviates very much from it.

$$\text{Smoothness of the perimeter} = 4\pi \times \left(\frac{A}{p^2}\right) \qquad (2)$$

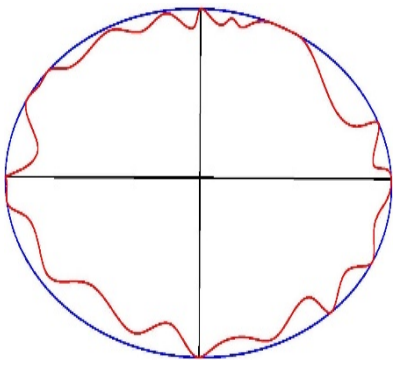

Fig. 41 Smoothness of the perimeter.

9.2. Image acquisition

All the images were acquired with the TESA Visio 200 optical machine. As regards the CFRP/CFRP stacks, 4 images of each hole were acquired (Fig. 42); for the Al/CFRP stacks, following the results obtained from the CFRP/CFRP stacks reported below, 3 images were acquired for each hole (Fig. 43).

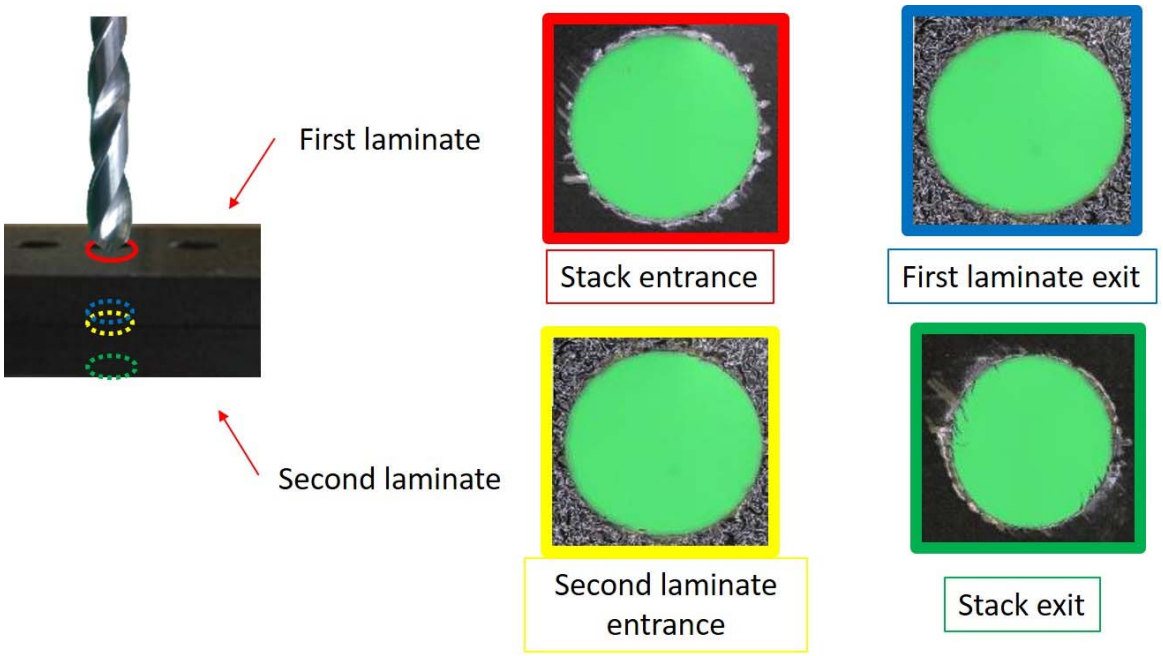

Fig. 42 CFRP/CFRP stack image acquisition.

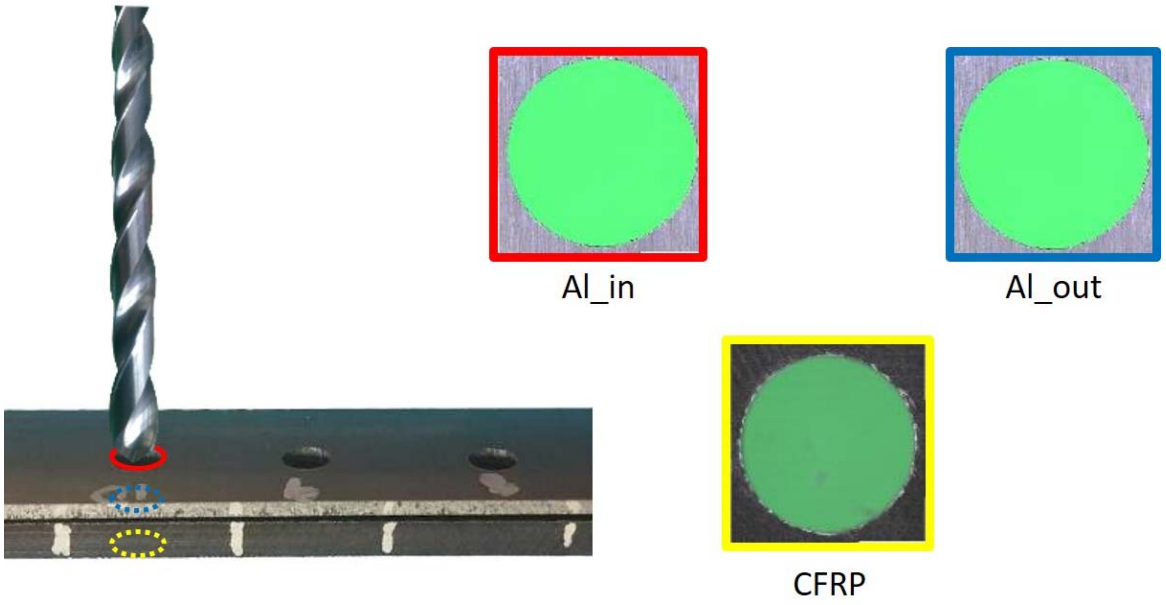

Fig. 43 Al/CFRP stack image acquisition.

9.3. Image processing for hole quality assessment

The developed procedure consists of the following steps. The first step is the conversion of the RGB image (Fig. 44a) to the HSV format. The HSV format consists of 3 levels named hue, saturation and value. Only the second level, i.e. the saturation level, highlights a remarkable contrast between the drilled hole (the green part of the RGB image) and the rest of the material,

and it is useful for the hole diameter measurement procedure; therefore, this level is extracted as shown in Fig. 44b.

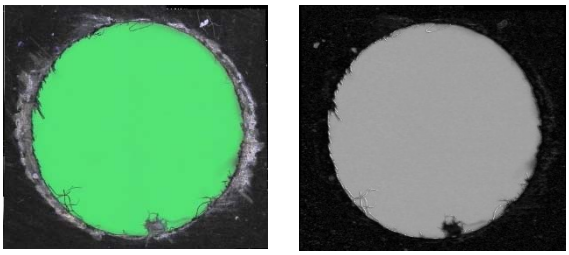

(a) (b)

Fig. 44 (a) Original RGB image; (b) second level of the HSV image.

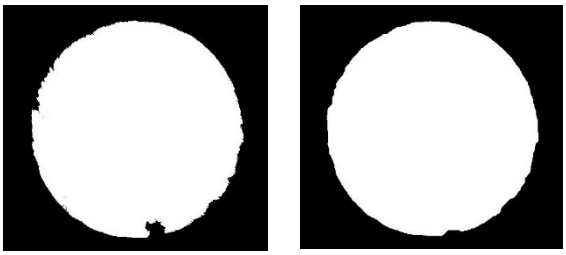

(a) (b)

Fig. 45 (a) Black and white picture before smoothing; (b) black and white picture after smoothing.

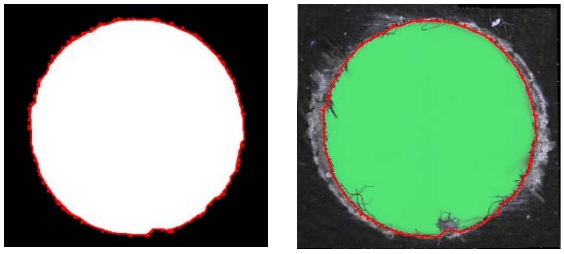

(a) (b)

Fig. 46 (a) Boundary pixels; (b) identified points for circle fitting.

A mask is then applied to the HSV second level (saturation > 0.3), with the aim to convert it to a binary black and white (BW) picture (Fig. 45a). This technique is applied with the aim to identify the edges of the hole, as this task can carried out more easily on BW pictures. On the BW image, smoothing is performed to exclude the uncut fibres from the diameter measurement (Fig. 45b).

The hole perimeter is then identified by the boundary pixels (Fig. 46a) between the black and white parts of the picture; the circumference that best fits the identified boundary pixels is then

calculated using the mean squared algorithm (Fig. 46b), thus obtaining the hole diameter dimension.

In order to measure the entry and exit delaminations of the drilled holes, it is necessary to identify the boundary of the visible delaminated area. To this aim, the third level of the HSV image is isolated and a mask (value > 0.25) is applied to obtain a binary BW image in which the damaged area is white while the undamaged area remains black (Fig. 47b). Then, the damaged area is merged with the hole and the image is cleaned from isolated white spots (< 1000 pixels) (Fig. 48a).

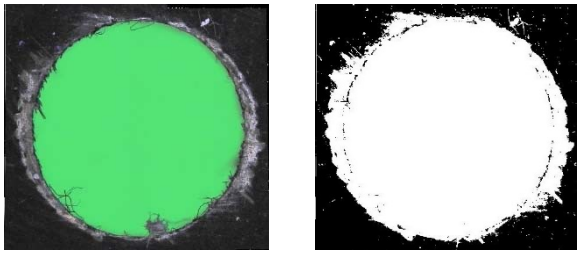

(a) (b)

Fig. 47 (a) Original RGB image; (b) value > 0.25.

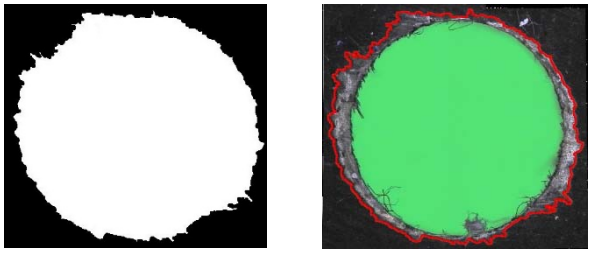

(a) (b)

Fig. 48 (a) Damaged area binary image; (b) outlined RGB image.

On the binary BW image, the boundary of the damaged area can be easily detected (red border in Fig. 48b) and it can be used to evaluate all the above mentioned delamination characteristic parameters.

9.4. Results and discussion on hole quality assessment

Fig. 49 shows the 2 bag sides related to the 60th hole produced by a traditional tool T with process condition C (6000 rpm – 0.15 mm/rev). The accumulation of the polymeric matrix on the bag side, due to the production process of the laminate, reduces the damage extention making it less evident than for the smooth side of the same hole (Tab. 12). For this reason,

together with the irregular geometry of the surface, the developed automatic procedure was not able to evaluate the hole quality indexes on the bag side laminate surfaces.

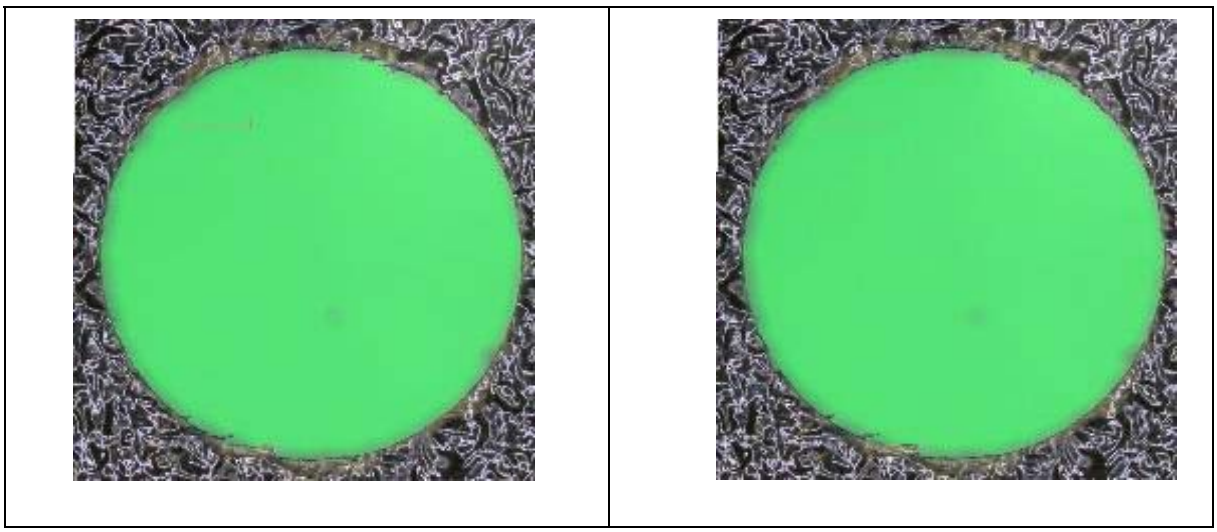

Fig. 49 Hole 60, bag side of the laminates: traditional tool T, process condition C (6000 rpm – 0.15 mm/rev).

For each drilling condition, the entry delamination (top laminate of the CFRP/CFRP stack) remained approximately constant or did not show a significant trend with increasing number of holes. In Fig. 50, the entry delamination indices (Fd and Fda) are plotted versus hole number, confirming this behaviour. This phenomenon is also evident from the images of the holes in Tab. 12 where entry and exit hole images are compared showing that exit hole delamination is more dependent on tool wear. The present study was therefore focused on the exit surface (bottom laminate of the CFRP/CFRP stack).

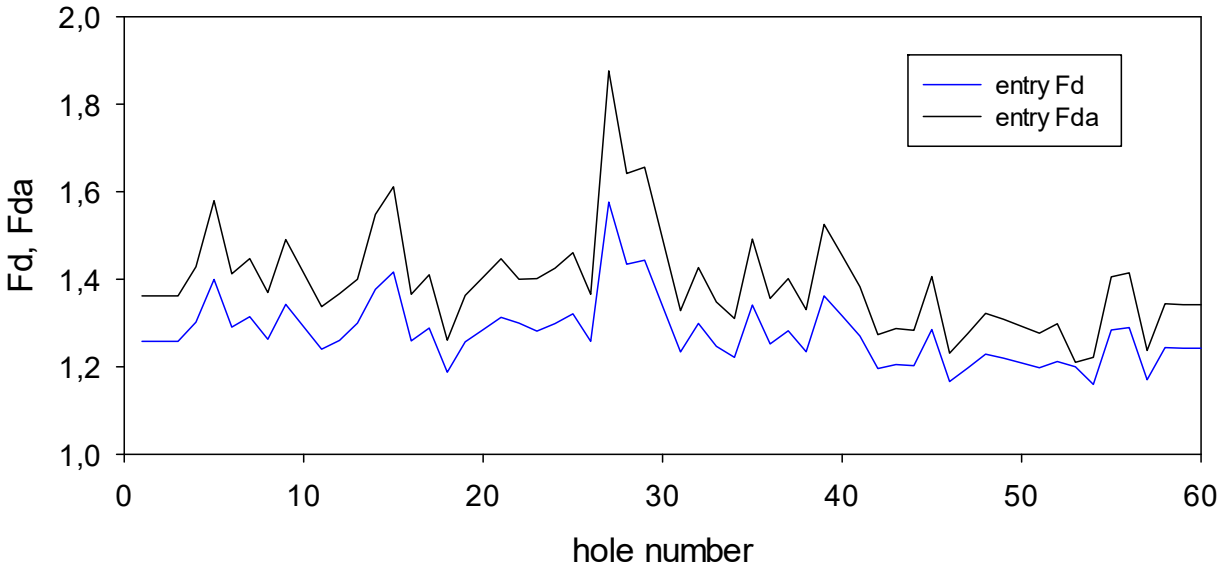

Fig. 50 Entry delamination vs hole number: traditional tool T, process condition C (6000 rpm – 0.15 mm/rev).

	Hole N. 10	Hole N. 20	Hole N. 30	Hole N. 40	Hole N. 50	Hole N. 60
Entry hole	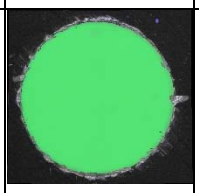	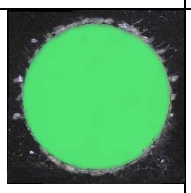	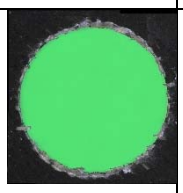	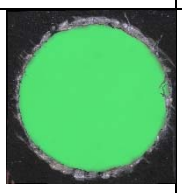	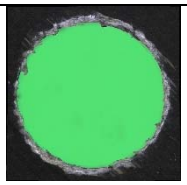	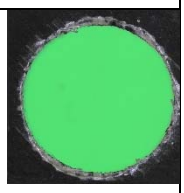
Exit hole	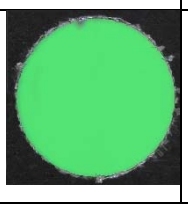	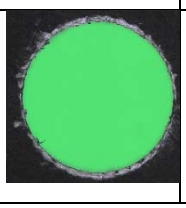	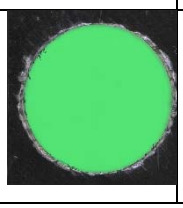	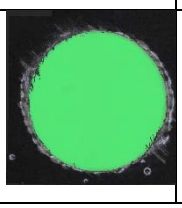	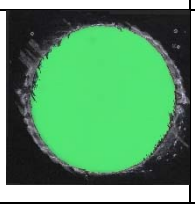	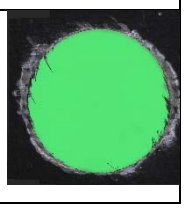

Tab. 12 Entry and exit hole images: traditional tool T, process condition C (6000 rpm – 0.15 mm/rev).

As regards the dimensional errors that affect CFRP drilled holes, it is known from literature that the hole diameter is generally reduced with increasing number of drilled holes; this behaviour is confirmed by the results obtained by the automatic image processing procedure, showing a decreasing trend of the evaluated hole diameter for 60 consecutive holes drilled with a traditional tool, T, and process conditions C (6000 rpm - 0.15 mm/rev) (Fig. 51). For all process conditions, though the hole entry diameter is generally higher than the hole exit diameter, the values are very similar and deviate from the nominal diameter by a maximum of ±0.1 mm.

Concerning the CFRP hole geometry, the hole roundness was evaluated as the ratio between the diameter of the maximum inscribed circle and the diameter of the minimum circumscribed circle. As expected, both at hole entry and hole exit, the hole roundness values evaluated for the 60 consecutive holes decrease with increasing number of holes (Fig. 52). For all drilling conditions, these values always remain in the range between 0.80 and 1.00.

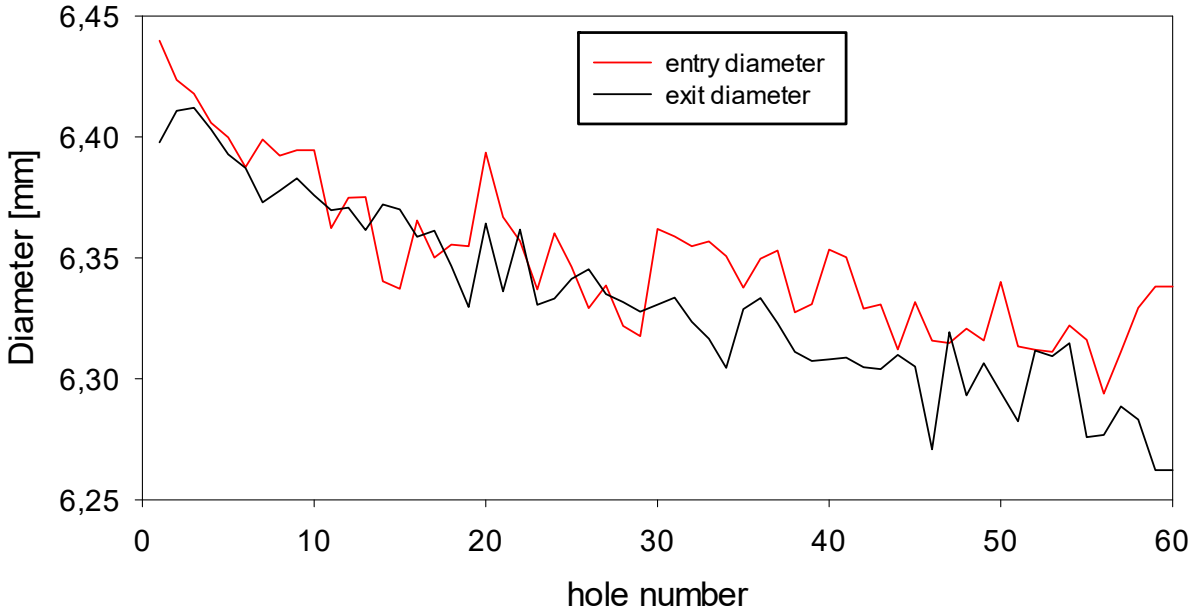

Fig. 51 Entry and exit hole diameter vs hole number: traditional tool T, process condition C (6000 rpm – 0.15 mm/rev).

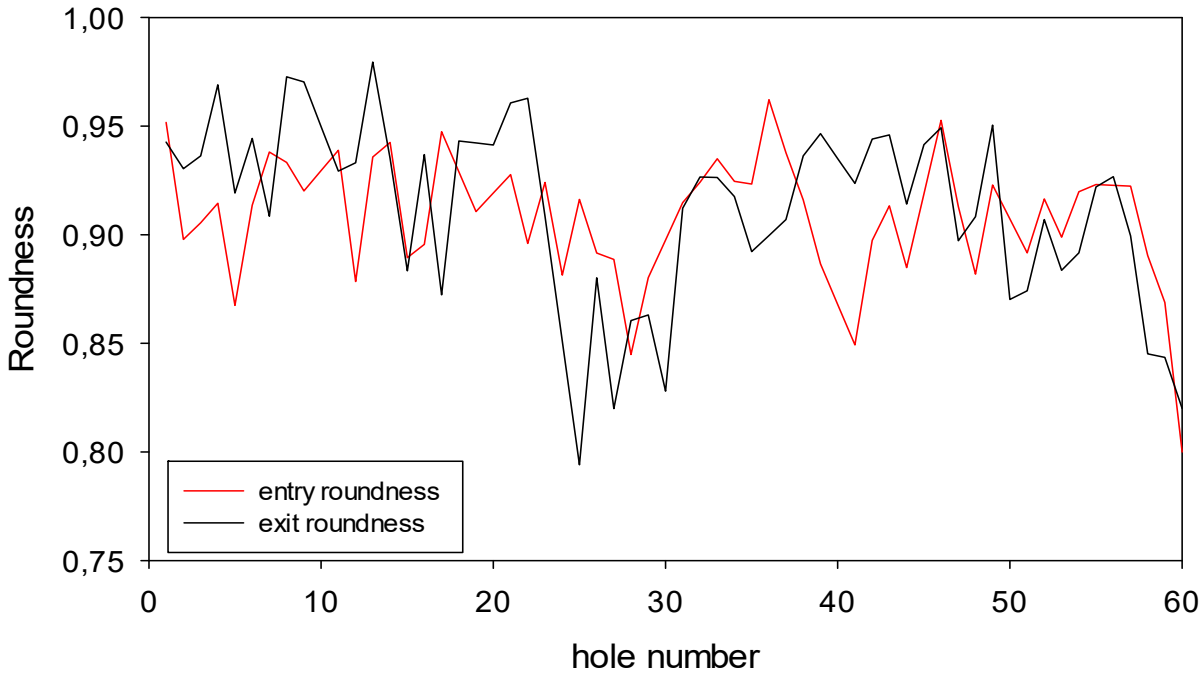

Fig. 52 Entry and exit hole roundness vs hole numer: traditional tool T, process condition C (6000 rpm – 0.15 mm/rev).

To compare the quality of the CFRP/CFRP stack holes produced by traditional and innovative tools, the following criteria were considered:

- Hole diameter: closeness to the nominal diameter of the hole (6.35 mm)
- Hole roundness: closeness to a perfect circumference (roundness = 1)
- Delamination factor (Fd), adjusted delamination factor (Fda): smallest value (as close to 1 as possible)

CFRP/CFRP stacks

In the following charts (Fig. 53-Fig. 58) traditional and innovative tools are compared in order to evaluate the best performing ones for each process conditions.

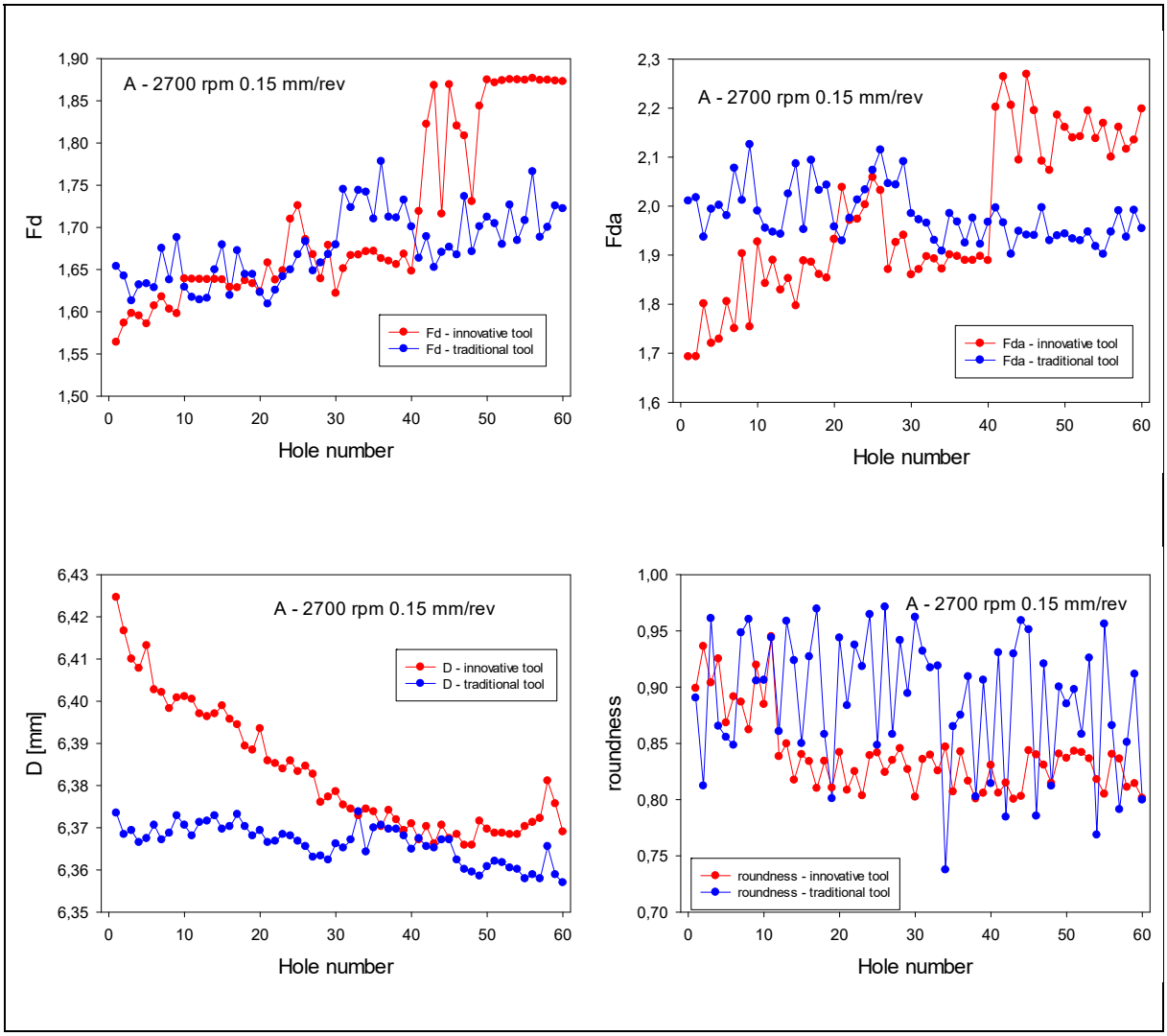

Fig. 53 Comparison of hole quality parameters for traditional and innovative tools: process condition A (2700 rpm – 0.15 mm/rev).

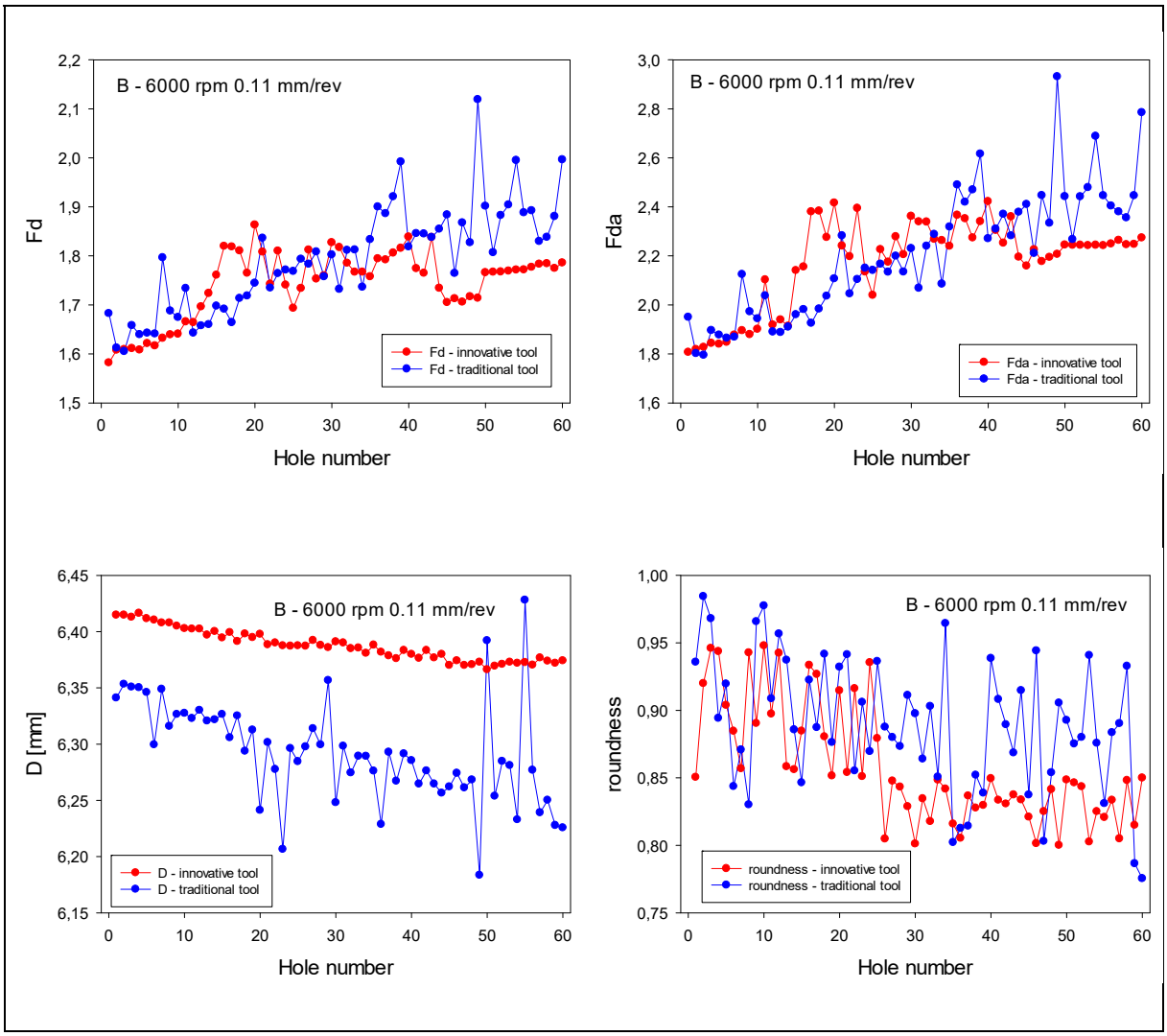

Fig. 54 Comparison of hole quality parameters for traditional and innovative tool: process condition B (6000 rpm – 0.11 mm/rev).

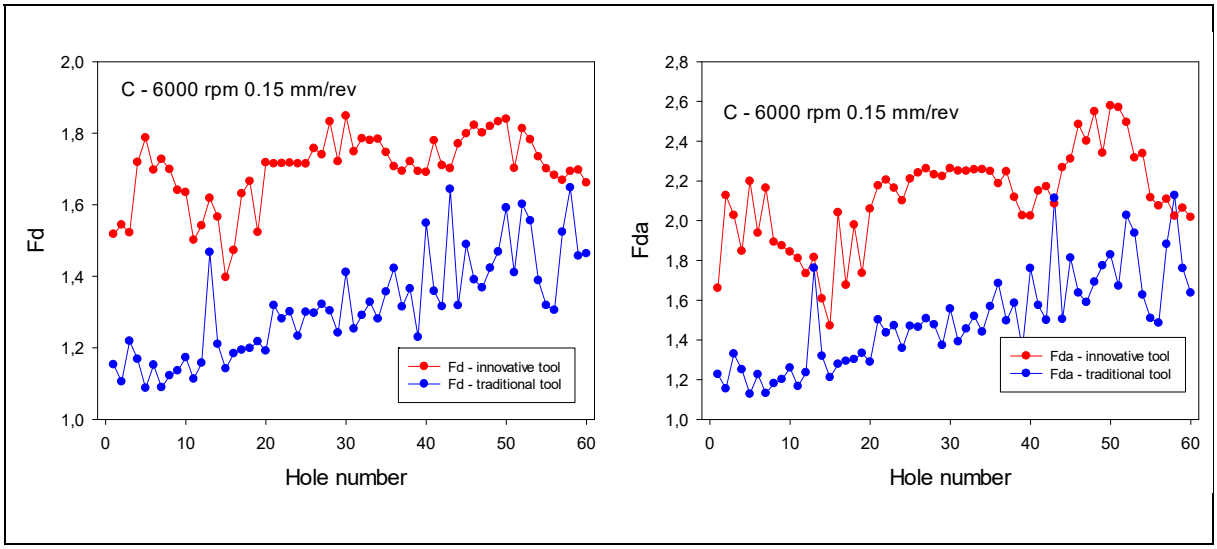

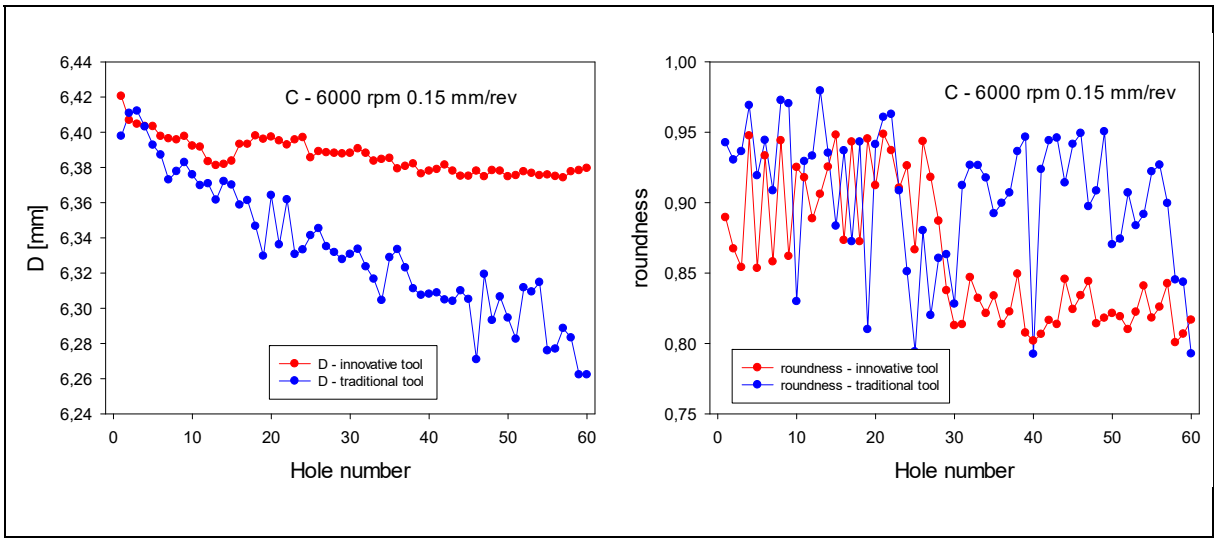

Fig. 55 Comparison of hole quality parameters for traditional and innovative tool: process condition C (6000 rpm – 0.15 mm/rev).

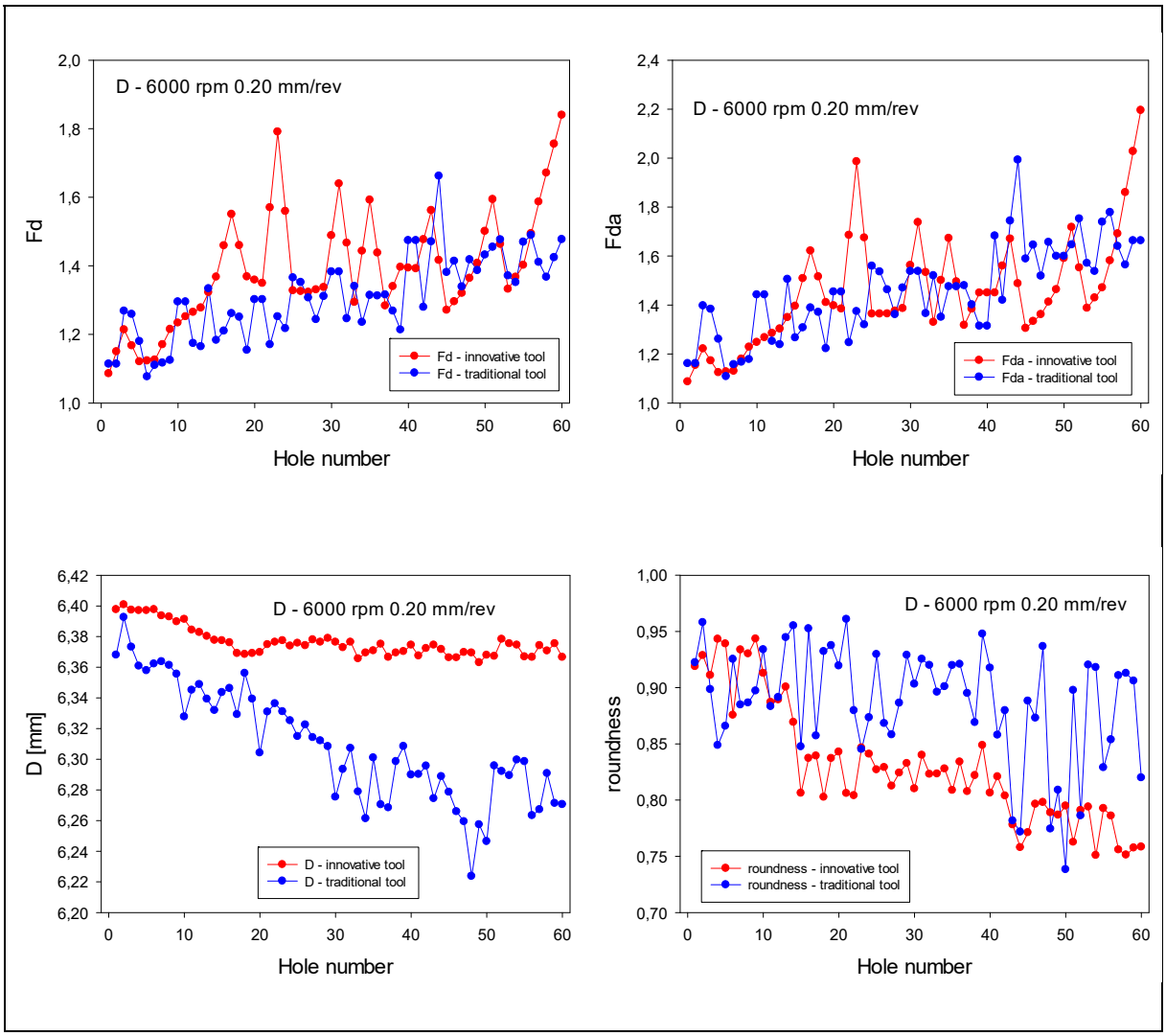

Fig. 56 Comparison of hole quality parameters for traditional and innovative tool: process condition D (6000 rpm – 0.20 mm/rev).

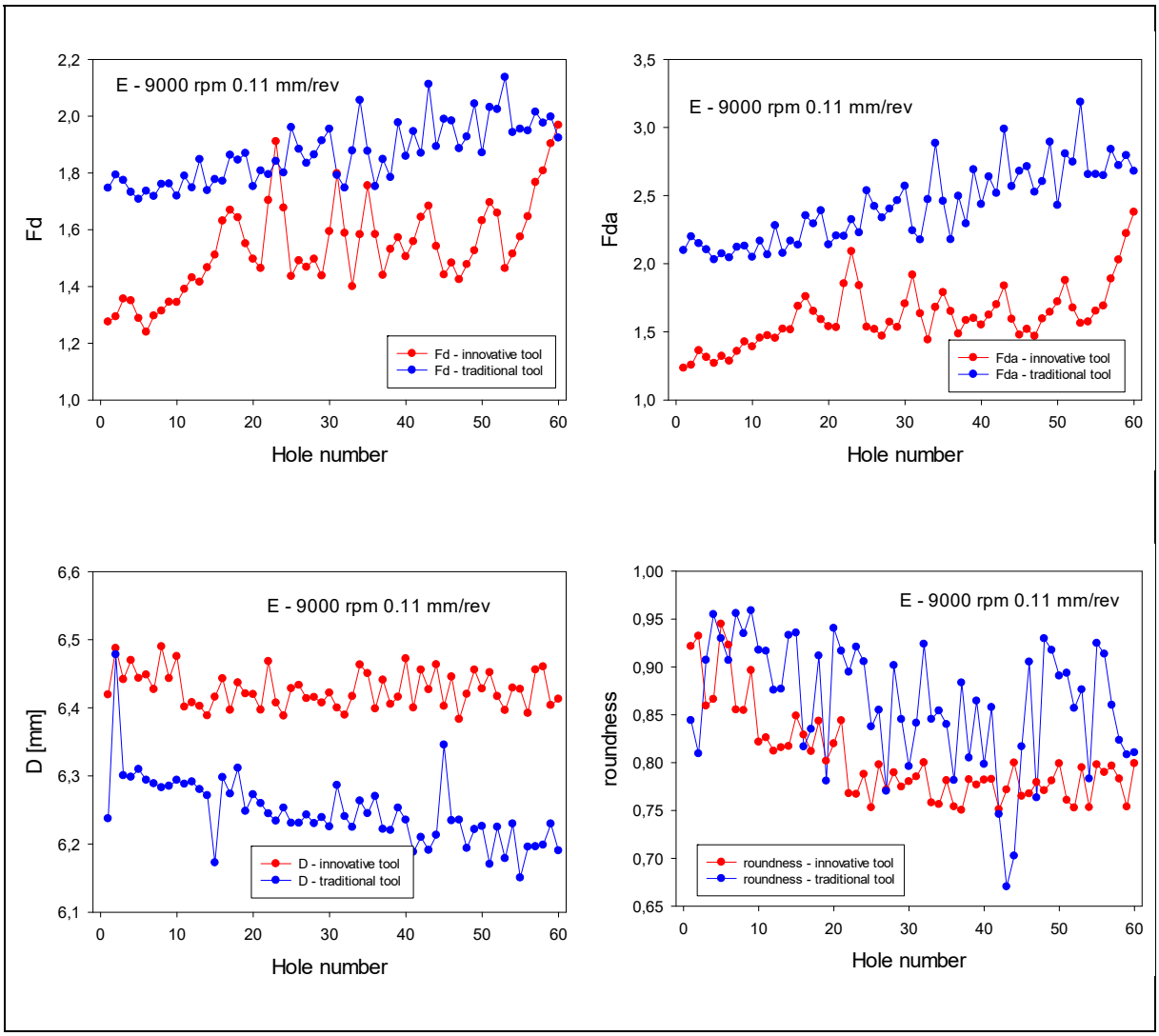

Fig. 57 Comparison of hole quality parameters for traditional and innovative tool: process condition E (9000 rpm – 0.11 mm/rev).

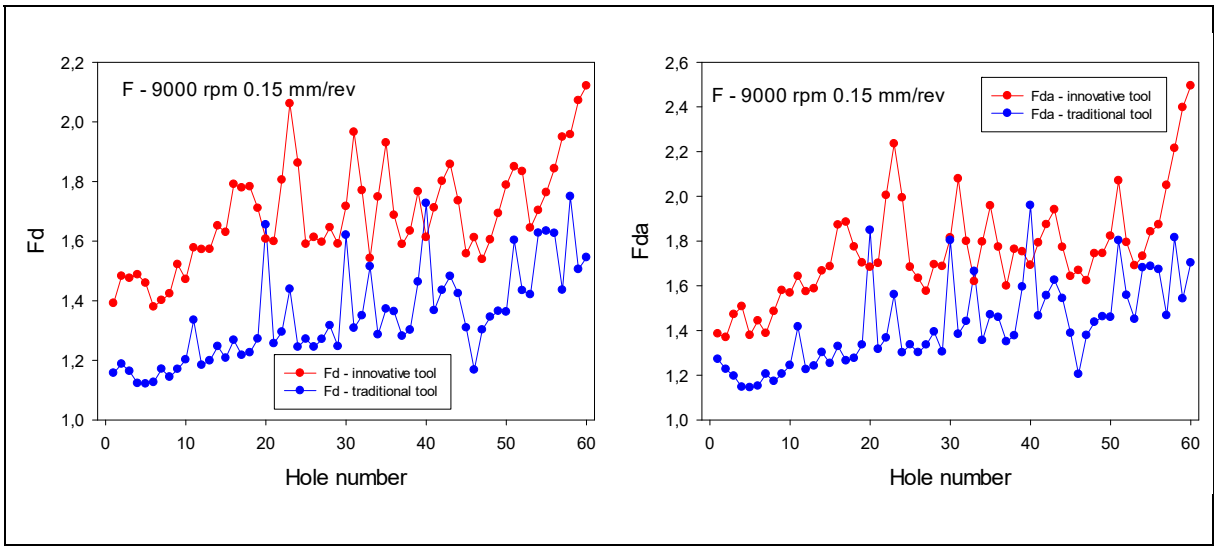

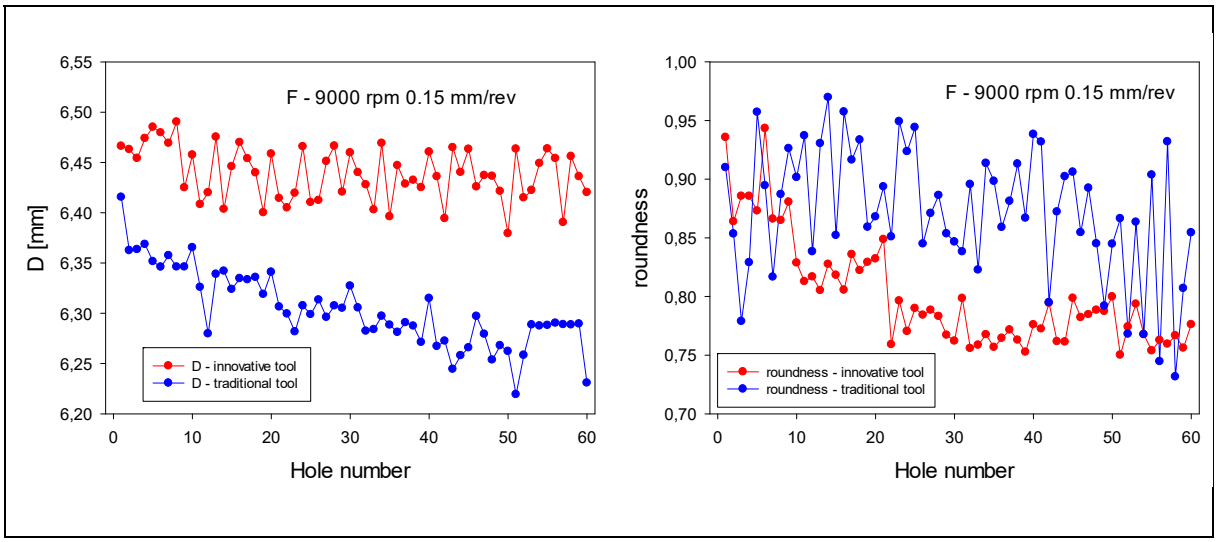

Fig. 58 Comparison of hole quality parameters for traditional and innovative tool: process condition F (9000 rpm – 0.15 mm/rev).

Using the quality criteria previously reported, the traditional or innovative tool producing the best results in terms of hole quality for each process condition was identified. The results in terms of best tool for each process condition are reported in **Errore. L'origine riferimento non è stata trovata.**.

To identify the process conditions that produced the best results, Fig. 59-Fig. 62 are reported, each composed of two charts. The first chart compares all the tools that gave the best results for each hole quality parameter whereas, to improve the readability of the results, the second chart shows only the best performing tools. In terms of roundness (Fig. 62), no best performing tools were highlighted, but all tools are in a range between 0.70 and 0.98.

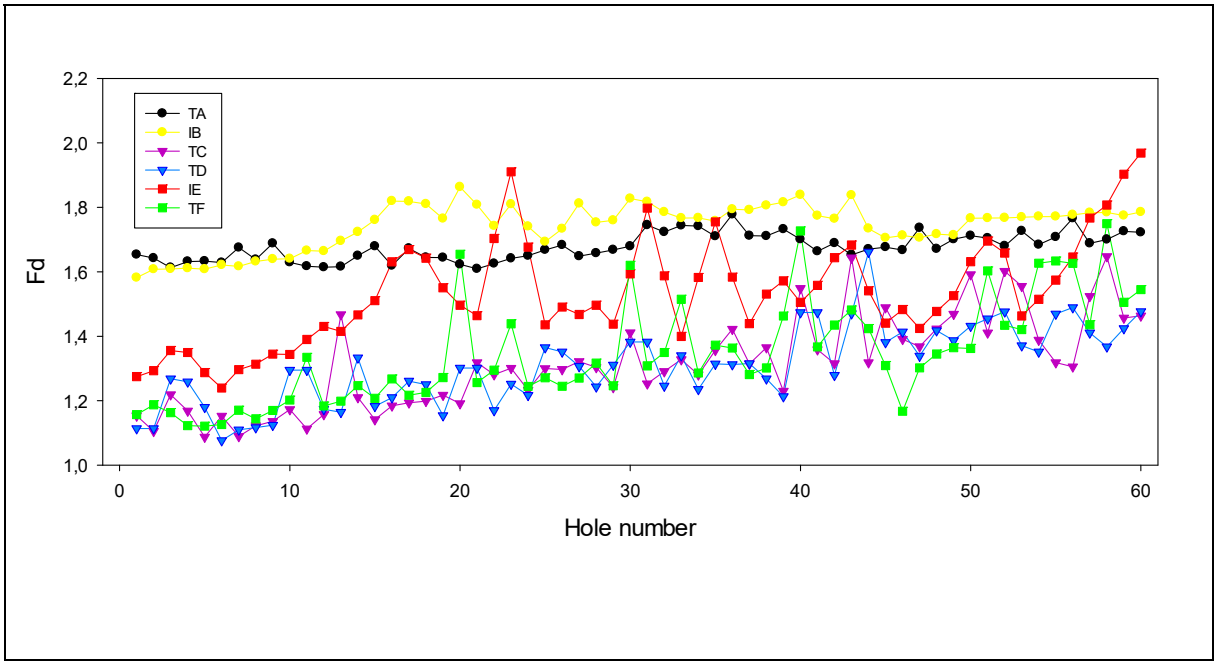

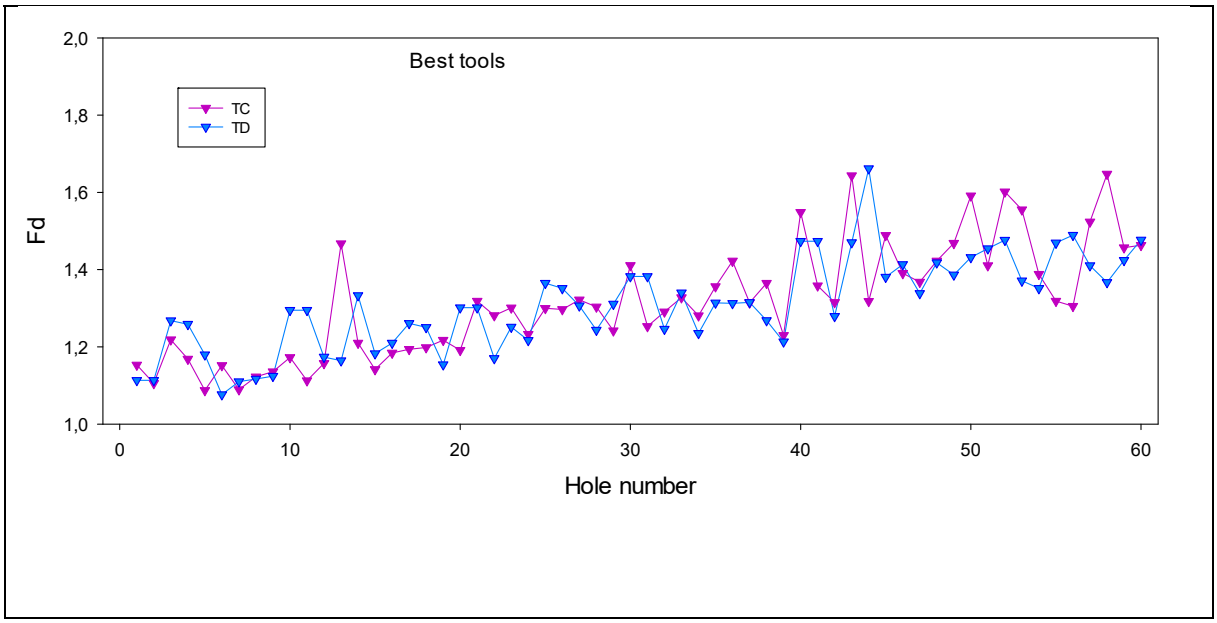

Fig. 59 Best performing tools in terms of delamination factor, Fd.

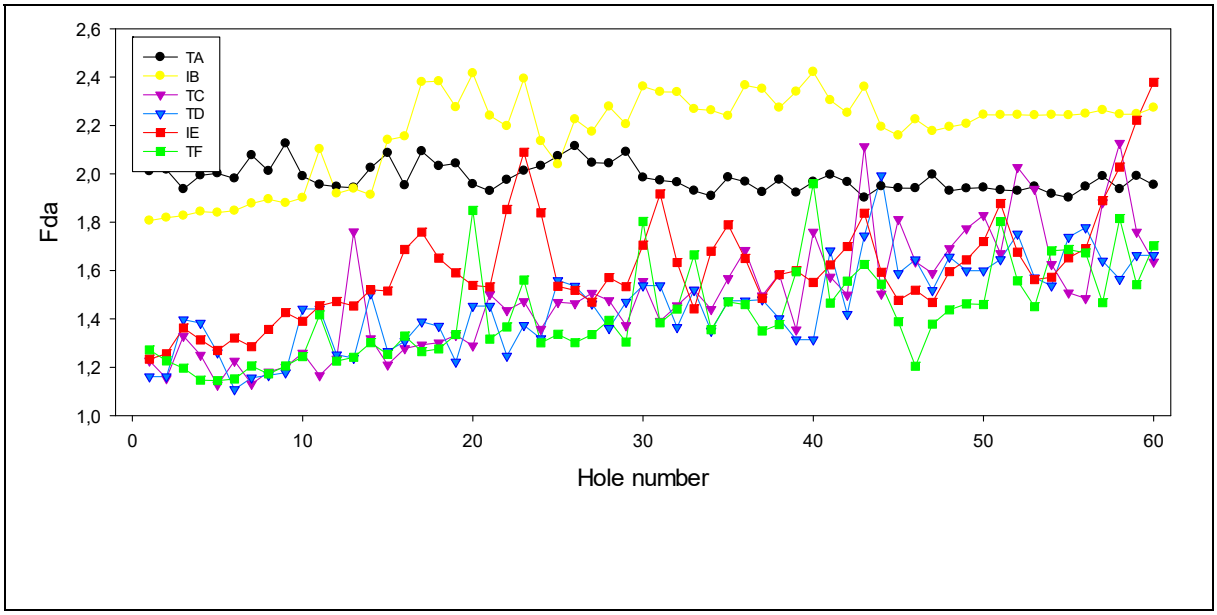

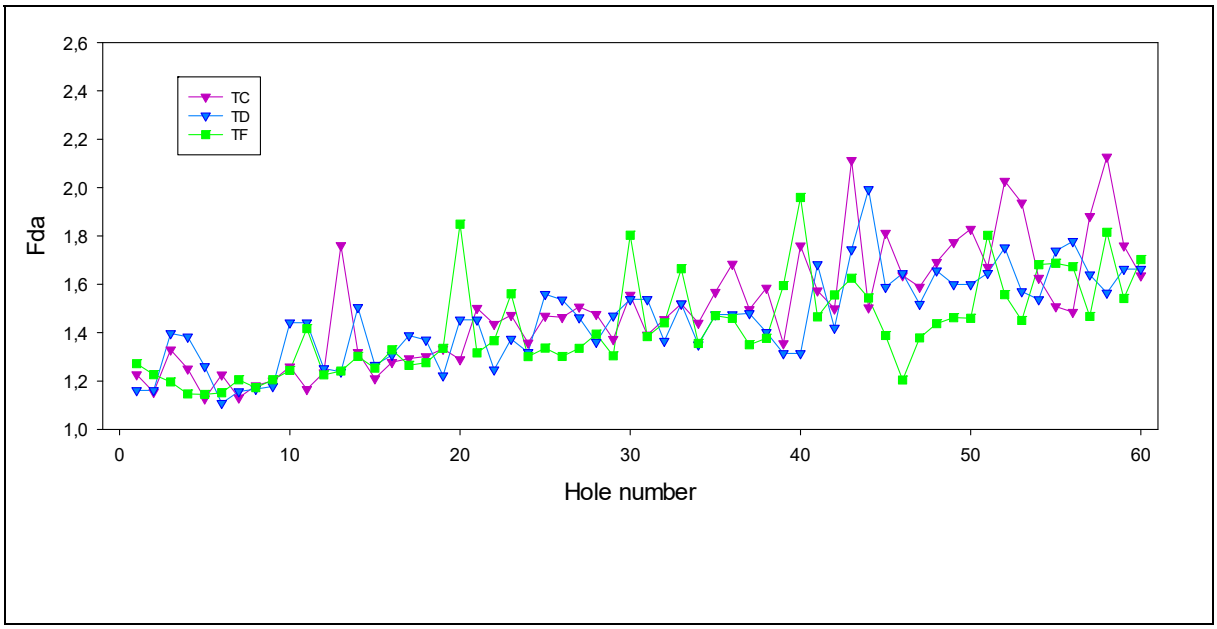

Fig. 60 Best performing tools in terms of adjusted delamination factor, Fda.

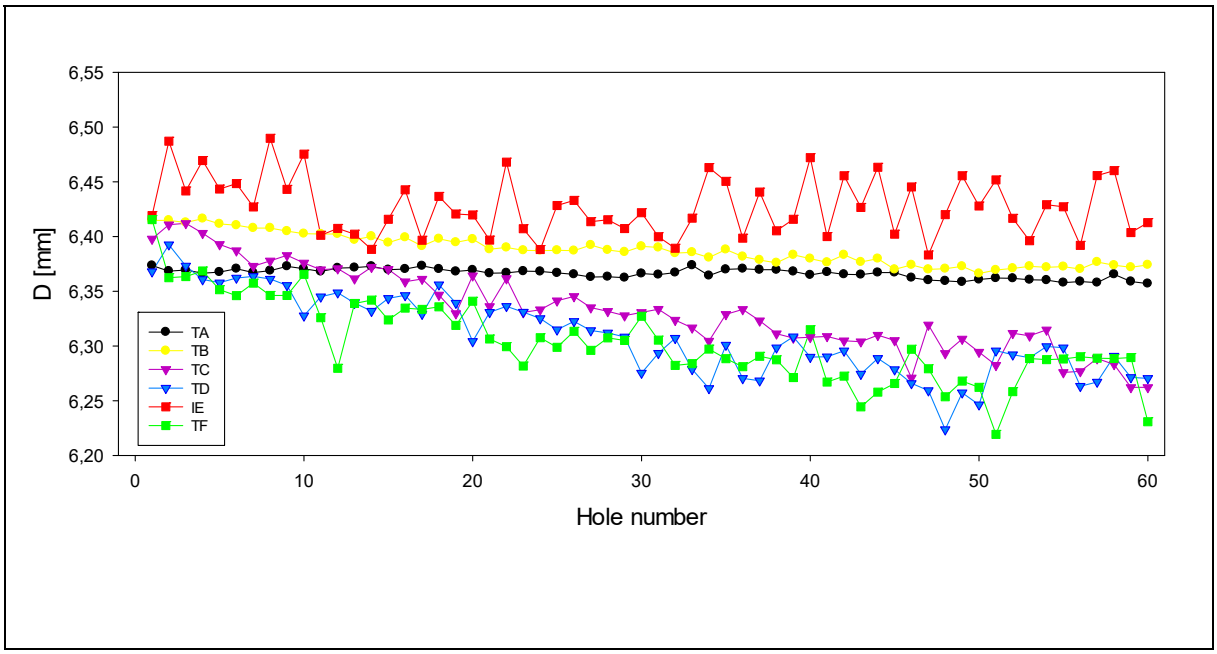

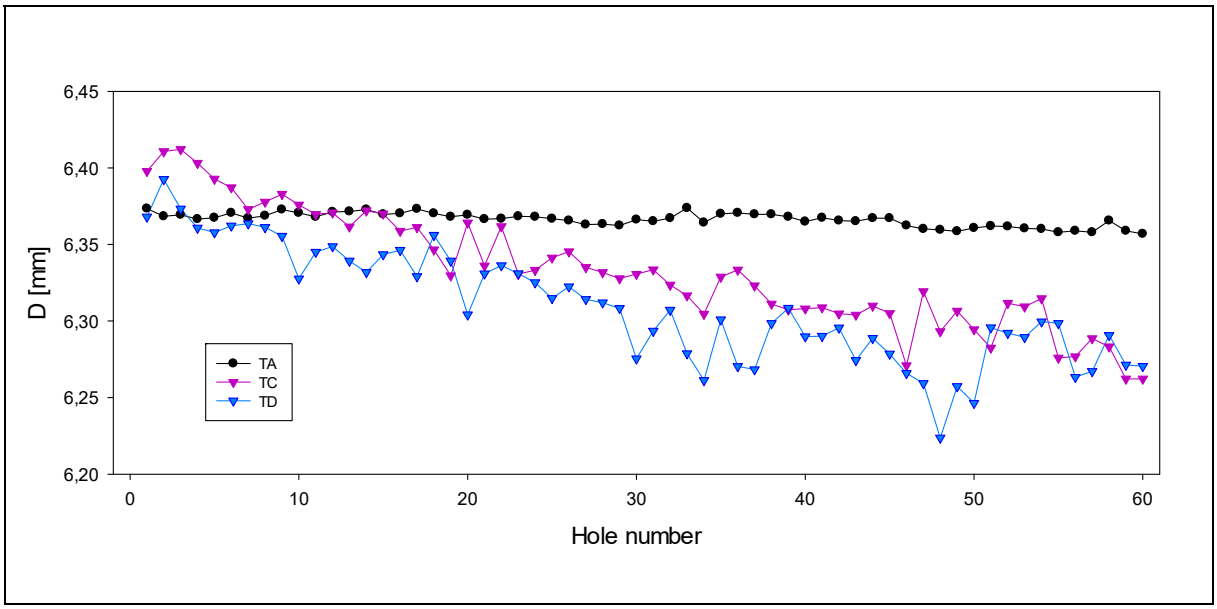

Fig. 61 Best performing tools in terms of hole diameter, D.

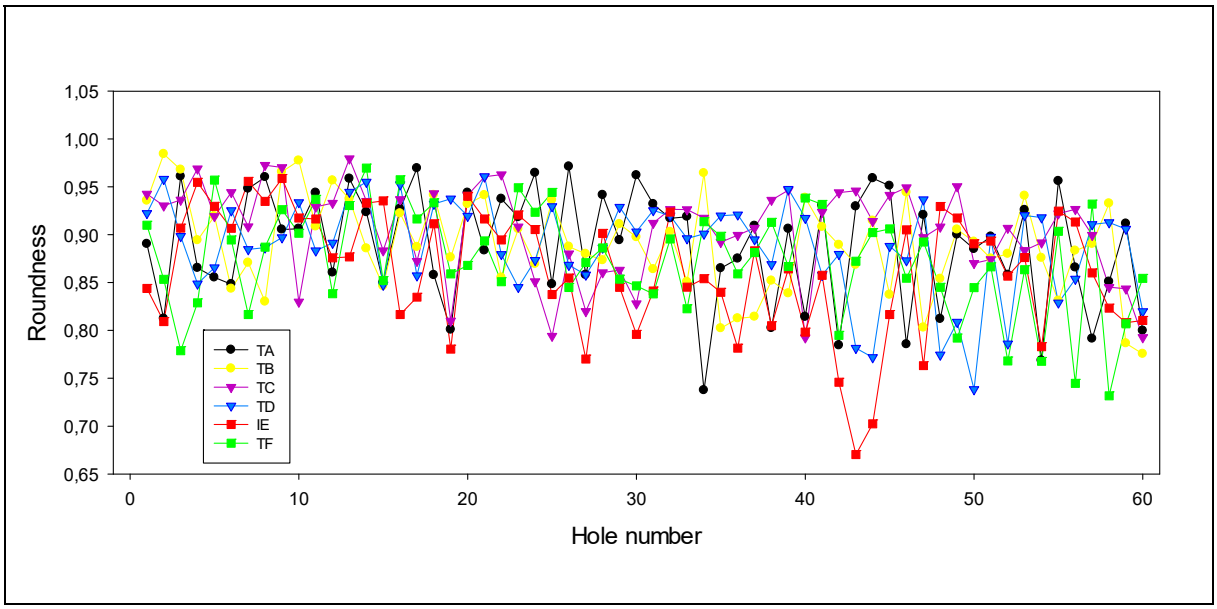

Fig. 62 Best performing tools in terms of hole roundness.

In this case, the obtained results are reported in Tab. 13.

	Best Tools
Delamination factor, Fd	**TC**/**TD**
Adjusted delamination factor, Fda	**TC**/**TD**/TF
Hole diameter, D	TA/**TC**/**TD**
Hole roundness	**TC**/**TD**

Tab. 13 Best CFRP/CFRP tools: T = traditional tools; A = 2700 rpm - 0.15 mm/rev; C = 6000 rpm - 0.15 mm/rev; D = 6000 rpm - 0.20 mm/rev; F = 9000 rpm - 0.15 mm/rev.

The tools that provided the most satisfactory results were the traditional tools T working respectively with process conditions C (6000 rpm – 0.15 mm/rev) and D (6000 rpm – 0.20 mm/rev). These results confirm those obtained by evaluating tool wear.

Al/CFRP stacks

The same optimum criterion was used for tools in the drilling of Al/CFRP stacks:

- Hole diameter: closeness to the nominal diameter of the hole (6.35 mm)
- Hole roundness: closeness to the perfect circumference (roundness = 1)
- Delamination factor (Fd), adjusted delamination factor (Fda): smallest value (as close to 1 as possible)
- Smoothness of the hole perimeter: like for roundness, it was rated with reference to the closeness to a perfect circumference (as close to 1 as possible).

All tools working with the same spindle speed were compared; the corresponding graphs can be find in appendix. Tab. 14 summarizes the results in terms of best performing feed rate for both spindle speeds.

		Best tools	
		3000 rpm	4500 rpm
Al_in	Hole roundness	T2	**T6**
	Smoothness of the perimeter	**T3**	**T6**
	Hole diameter	**T3**	**T6**
Al_out	Hole roundness	**T3**	T5
	Smoothness of the perimeter	T1	**T6**
	Hole diameter	T1	**T6**
CFRP	Hole roundness	**T3**	T5

	Smoothness of the perimeter	**T3**	**T6**
	Hole diameter	T1	**T6**
	Delamination factor, Fd	**T3**	**T6**
	Ajusted delamination factor, Fda	**T3**	**T6**

Tab. 14 Best performing Al/CFRP tools for each process condition: T = traditional tools; 1 = 3000 rpm - 0.05 mm/rev; 2 = 3000 rpm - 0.10 mm/rev; 3 = 3000 rpm - 0.15 mm/rev; 5 = 4500 rpm - 0.10 mm/rev; 6 = 4500 rpm - 0.15 mm/rev.

.

The best holes were obtained with traditional tools T3 and T6, working respectively with 3000 rpm – 0.15 mm/rev (process condition 3) and with 4500 rpm – 0.15 mm/rev (process condition 6). As both tools worked with the maximum feed rate (0.15 mm/rev), the two tools were directly compared. The results are shown in the charts of (Fig. 63-Fig. 73) and summarized in Tab. 15.

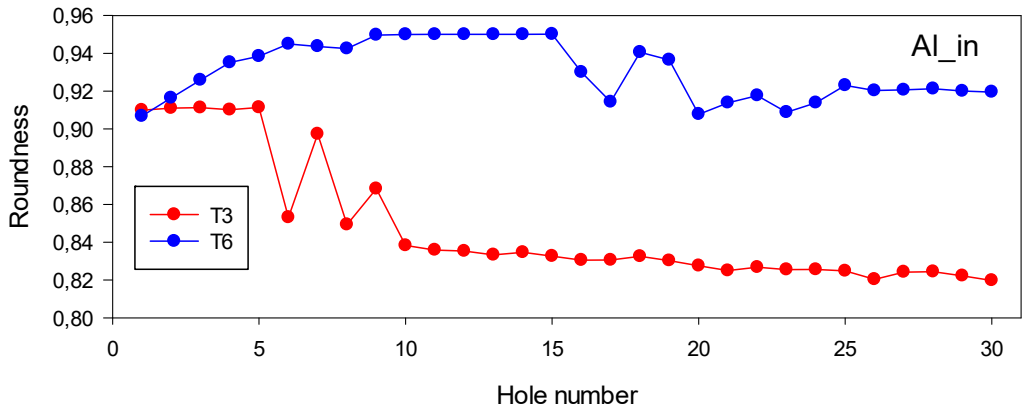

Fig. 63 T3 vs T6: Al_in roundness.

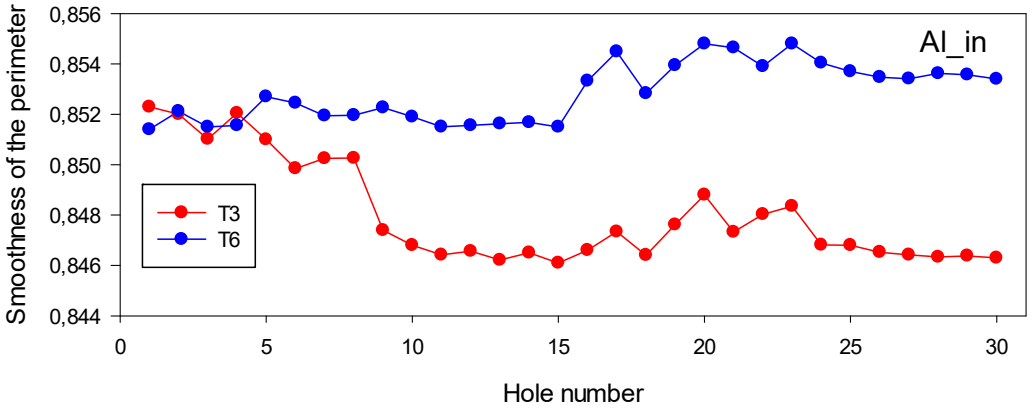

Fig. 64 T3 vs T6: Al_in smoothness of the perimeter.

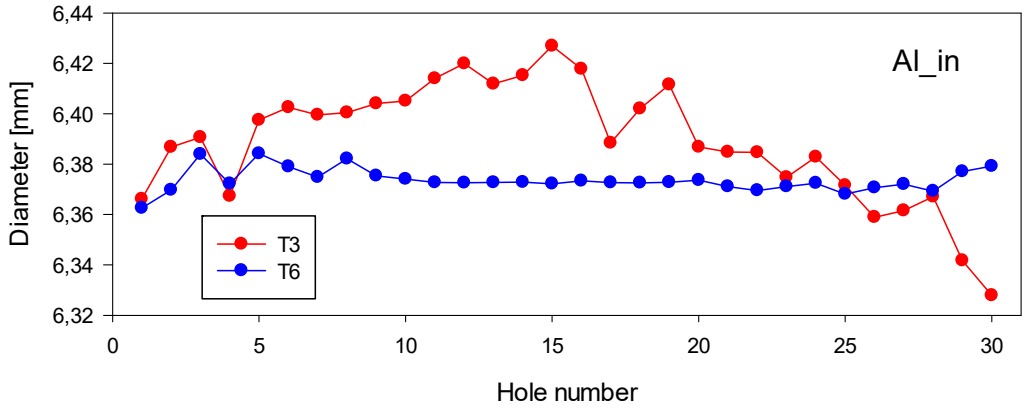

Fig. 65 T3 vs T6: Al_in diameter.

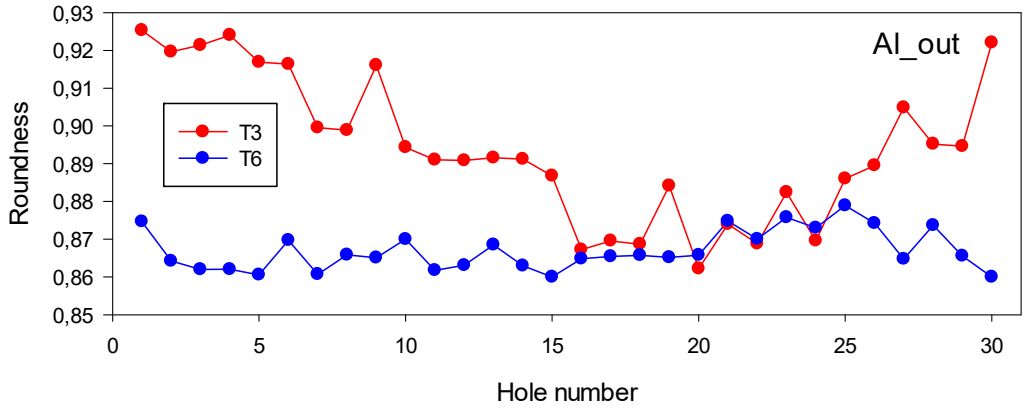

Fig. 66 T3 vs T6: Al_out hole roundness.

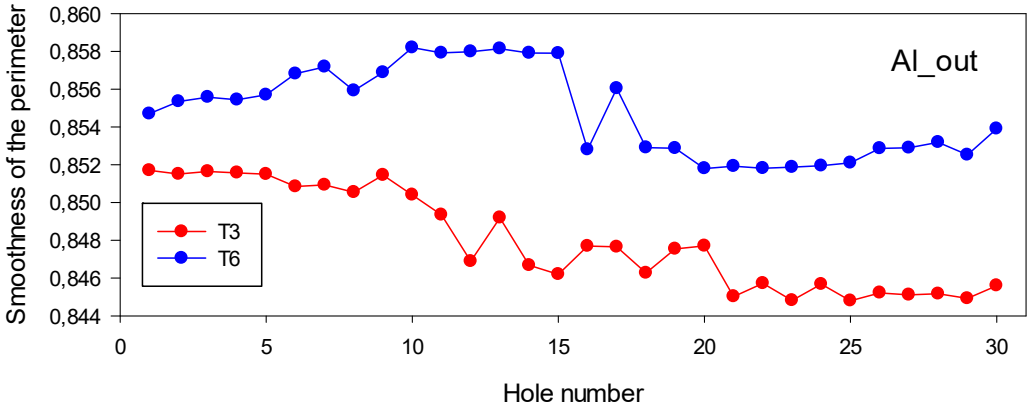

Fig. 67 T3 Vs T6 – Al_out smoothness of the perimeter.

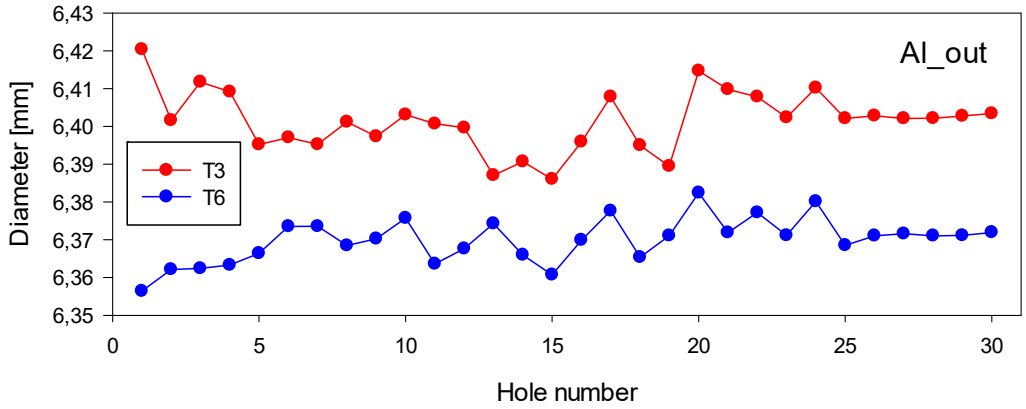

Fig. 68 T3 vs T6: Al_out hole diameter.

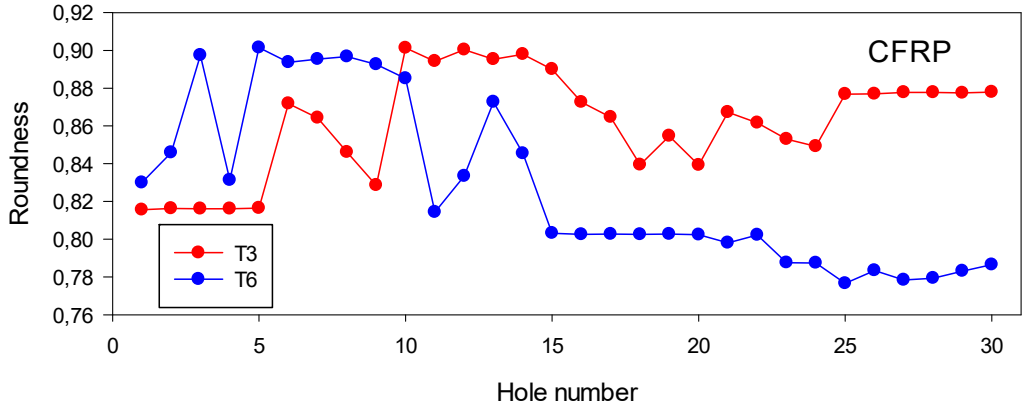

Fig. 69 T3 vs T6: CFRP roundness.

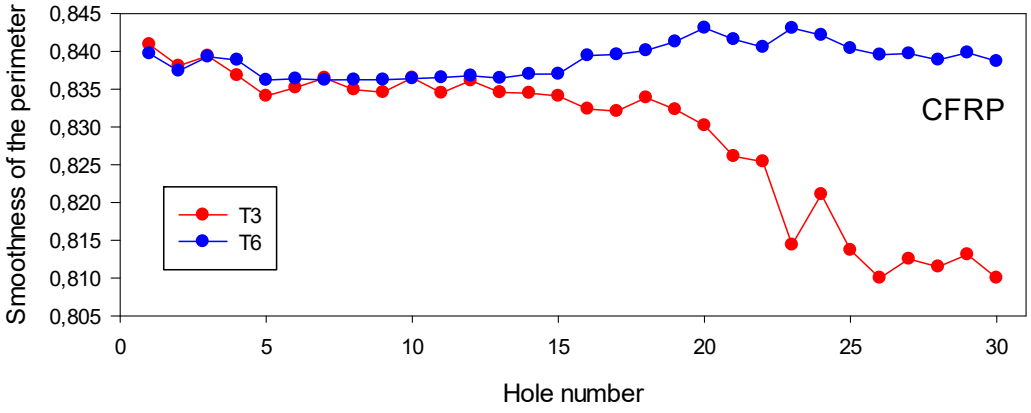

Fig. 70 T3 vs T6: CFRP smoothness of the perimeter.

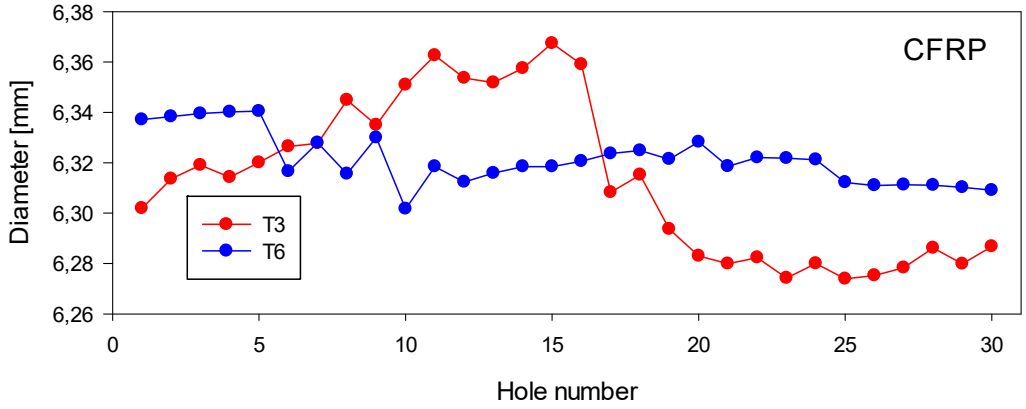

Fig. 71 T3 vs T6: CFRP hole diameter.

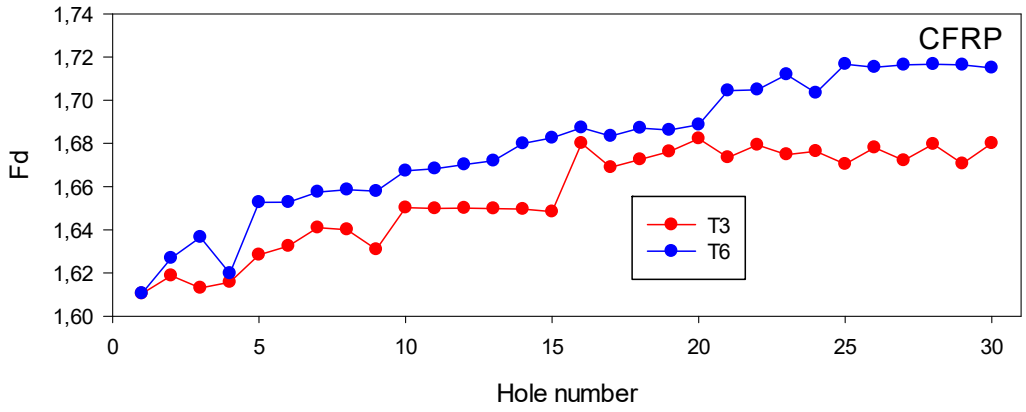

Fig. 72 T3 vs T6: CFRP delamination factor, Fd.

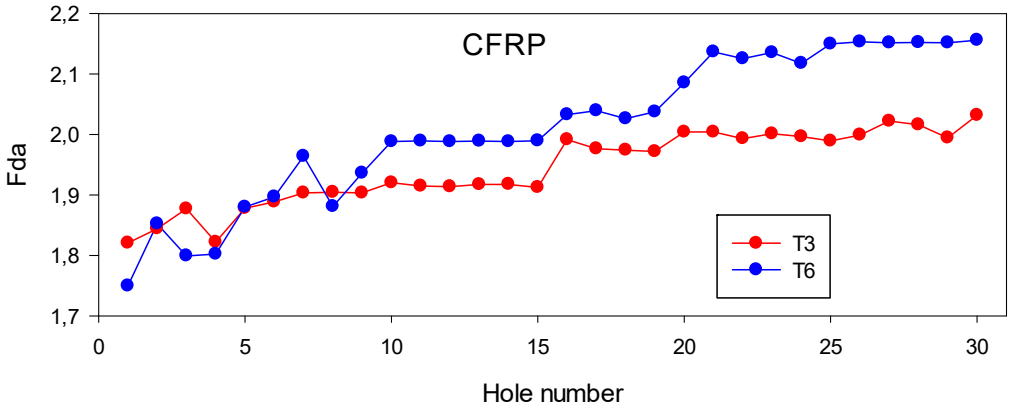

Fig. 73 T3 vs T6: CFRP adjusted delamination factor, Fda.

Best tool		
Al_in	Hole roundness	T6
	Smoothness of the perimeter	T6
	Hole diameter	T6
Al_out	Hole roundness	T3
	Smoothness of the perimeter	T6
	Hole diameter	T6
CFRP	Hole roundness	T3
	Smoothness of the perimeter	T3
	Hole diameter	T6

	Delamination factor, Fd	T3
	Adjusted delamination factor, Fda	T3

Tab. 15 Best performing Al/CFRP tools in terms of each quality parameter: T = traditional tools; 3 = 3000 rpm - 0.15 mm/rev; 6 = 4500 rpm - 0.15 mm/rev.

The traditional tool T6, working with 4500 rpm – 0.15 mm/rev (process condition 6), generally gave the best results on aluminum, whereas traditional tool T3, working with 3000 rpm – 0.15 mm/rev (process condition 3), provided the best results on CFRP. Thus, there is a need to find a compromise between them according to the needs in the simultaneous drilling of such dissimilar materials.

10. Summary and outlook

The activities of this thesis work were developed in the context of a wider project carried out at the University of Naples Federico II in collaboration with an industrial partner belonging to the aeronautical sector. In the larger project framework, the specific purpose of the presented research activities was the development of a sensor monitoring system for tool wear assessment and an in-process survey system of delamination conditions to be used during drilling of aeronautical stacks made of CFRP composite laminates and hybrid stacks made of Al alloy sheets and composite laminates. Both the objectives are highly desirable for the aeronautical industry in view of drilling process automation.

The contribution of this work consisted in the activities summarized below:

- The most significant parameters for assessing the hole quality on CFRP laminates and Al alloy sheets were identified in terms of delamination indices (Fd, Fda) and geometrical parameters (diameter, roundness, smoothness).
- The wear mechanisms of the drill bits were studied, and the flank wear (VB) was identified as the most effective parameter for the monitoring of tool wear during drilling operations.
- Drilling tests were performed on CFRP/CFRP stacks with different feed rates and spindle speeds using traditional and innovative tools in order to evaluate the optimal drilling conditions and the most suitable drill bit geometry for one-shot stack drilling.
- Drilling tests were performed on Al/CFRP stacks with different feed rates and spindle speeds with traditional tools in order to evaluate the optimal drilling conditions.
- Images of the tool flank were acquired during drilling tests after every 10 holes produced by the same tool; multiple images of each drilled hole were acquired (4 for CFRP/CFRP stacks and 3 for Al/CFRP stacks).
- An automatic procedure for image analysis was developed to estimate all the parameters related to the hole quality.
- Tool wear was measured every 10 holes produced by the same drill bit to reconstruct the tool development trend (tool wear curve).

The following conclusions can be made:

- Innovative tools, though giving a lower thrust force compared to traditional tools, proved to be less effective than the traditional tools in terms of hole quality.

- The most suitable process parameters for CFRP/CFRP stack drilling based on hole quality assessment were identified as 6000 rpm - 0.2 mm/rev and 6000 rpm - 0.15 mm/rev;
- The most suitable process parameters for Al/CFRP stack drilling were identified as 3000 rpm/ 0.15 mm/rev in terms of delamination damage and 4500 rpm/ 0.15 mm/rev in terms of geometric quality parameters;
- The study of tool wear development confirmed, in both case studies, the obtained results: tools with lower wear level produced holes with better quality.

These results pave the way for the definition of future developments of this application that can be identified in the following research directions:

- Implementation of an on-line image acquisition system for capturing drilled hole images.
- Development of an Artificial Intelligent / Machine Learning based procedure for the automatic evaluation of hole quality.

11. References

Abrão, A. M., Rubio, J. C. C., Faria, P. E., & Davim, J. P. (2008). The effect of cutting tool geometry on thrust force and delamination when drilling glass fibre reinforced plastic composite. *Materials and Design*. https://doi.org/10.1016/j.matdes.2007.01.016

Azmir, M. A., & Ahsan, A. K. (2009). A study of abrasive water jet machining process on glass/epoxy composite laminate. *Journal of Materials Processing Technology*. https://doi.org/10.1016/j.jmatprotec.2009.08.011

Brinksmeier, E., Fangmann, S., & Rentsch, R. (2011). Drilling of composites and resulting surface integrity. *CIRP Annals - Manufacturing Technology*, *60*(1), 57–60. https://doi.org/10.1016/j.cirp.2011.03.077

Caggiano, A., Centobelli, P., Nele, L., & Teti, R. (2017). Multiple Sensor Monitoring in Drilling of CFRP/CFRP Stacks for Cognitive Tool Wear Prediction and Product Quality Assessment. *Procedia CIRP*, *62*. https://doi.org/10.1016/j.procir.2017.03.047

Caggiano, Alessandra, Segreto, T., & Teti, R. (2016). Cloud Manufacturing Framework for Smart Monitoring of Machining. *Procedia CIRP*, *55*, 248–253. https://doi.org/10.1016/j.procir.2016.08.049

Campbell, F. C. (2010). *Structural composite materials*. https://books.google.it/books?hl=it&lr=&id=D3Wta8e07t0C&oi=fnd&pg=PR1&dq=composite+campbell+2010&ots=T-0kaA-4t9&sig=co2RXzoP8tchNLB5x2pyDdOH7EM#v=onepage&q=composite campbell 2010&f=false

Caprino, G., Santo, L., & Nele, L. (1996). On the origin of cutting forces in machining unidirectional composite materials. *American Society of Mechanical Engineers, Petroleum Division (Publication) PD*.

Castro, G. (2010). *Drilling Carbon Fiber Reinforced Plastic and Titanium Stacks*. *May*. https://doi.org/10.1017/CBO9781107415324.004

Darecki, M., Edelstenne, C., Enders, T., Fernandez, E., Hartman, P., Herteman, J.-P., Kerkloh, M., King, I., Ky, P., Mathieu, M., Orsi, G., Schotman, G., Smith, C., & Wörner, J.-D. (2011). Flightpath 2050. *Flightpath 2050 Europe's Vision for Aviation*, 28. https://doi.org/10.2777/50266

Dharan, C. K. H., & Won, M. S. (2000). *Machining parameters for an intelligent machining system for composite laminates*. *40*, 415–426.

Dolinšek, S., Šuštaršič, B., & Kopač, J. (2001). Wear mechanisms of cutting tools in high-speed cutting processes. *Wear*, *250–251*(1–12), 349–356. https://doi.org/10.1016/S0043-1648(01)00620-2

Durão, L. M. P., Gonçalves, D. J. S., Tavares, J. M. R. S., de Albuquerque, V. H. C., Aguiar Vieira, A., & Torres Marques, A. (2010). Drilling tool geometry evaluation for reinforced composite laminates. *Composite Structures*. https://doi.org/10.1016/j.compstruct.2009.10.035

El-Hoffy, & Abdel-Gawad, H. (2013). *Fundementals of machining processes : conventional and nonconventional processes*.

Faraz, A., Biermann, D., & Weinert, K. (2009). Cutting edge rounding: An innovative tool wear criterion in drilling CFRP composite laminates. *International Journal of Machine Tools and Manufacture*. https://doi.org/10.1016/j.ijmachtools.2009.08.002

Fernandes, M., & Cook, C. (2006). Drilling of carbon composites using a one shot drill bit. Part I: Five stage representation of drilling and factors affecting maximum force and torque. *International Journal of Machine Tools and Manufacture*. https://doi.org/10.1016/j.ijmachtools.2005.03.015

Filiz, S., & Burak Ozdoganlar, O. (2010a). A Model for Bending , Torsional , and Axial Vibrations of Micro- and Macro-Drills Including Actual Drill Geometry — Part I : Model Development and Numerical. *Journal of Manufacturing Science and Engineering, Transactions of the ASME*, *132*, 1–8. https://doi.org/10.1115/1.4001720

Filiz, S., & Burak Ozdoganlar, O. (2010b). A Model for Bending , Torsional , and Axial Vibrations of Micro- and Macro-Drills Including Actual Drill Geometry — Part II : Model Validation and Application. *Journal of Manufacturing Science and Engineering, Transactions of the ASME*, *132*. https://doi.org/10.1115/1.4001721

Fink, A., Camanho, P. P., Andrés, J. M., Pfeiffer, E., & Obst, A. (2010). Hybrid CFRP/titanium bolted joints: Performance assessment and application to a spacecraft payload adaptor. *Composites Science and Technology*, *70*(2), 305–317. https://doi.org/10.1016/j.compscitech.2009.11.002

Galloway, D. F. (1957). Some experiments on the influence of various factors on drill performance. *TRANSACTIONS OF THE ASME*.

Herzog, D., Jaeschke, P., Meier, O., & Haferkamp, H. (2008). Investigations on the thermal effect caused by laser cutting with respect to static strength of CFRP. *International Journal of Machine Tools and Manufacture*. https://doi.org/10.1016/j.ijmachtools.2008.04.007

Ho-Cheng, H., & Dharan, C. H. K. (1990a). Delamination During Drilling in Composite Laminates. *Journal of Engineering for Industry*, *112*(3), 236–239.

Ho-Cheng, H., & Dharan, C. K. H. (1990b). Delamination during drilling in composite laminates. *Journal of Manufacturing Science and Engineering, Transactions of the ASME*. https://doi.org/10.1115/1.2899580

Hocheng, H., & Tsao, C. C. (2003). Comprehensive analysis of delamination in drilling of composite materials with various drill bits. *Journal of Materials Processing Technology*. https://doi.org/10.1016/S0924-0136(03)00749-0

Hocheng, H., & Tsao, C. C. (2006). Effects of special drill bits on drilling-induced delamination of composite materials. *International Journal of Machine Tools and Manufacture*. https://doi.org/10.1016/j.ijmachtools.2005.10.004

Iliescu, D., Gehin, D., Gutierrez, M. E., & Girot, F. (2010). Modeling and tool wear in drilling of CFRP. *International Journal of Machine Tools and Manufacture*, *50*(2), 204–213. https://doi.org/10.1016/j.ijmachtools.2009.10.004

Isbilir, O., & Ghassemieh, E. (2013). Numerical investigation of the effects of drill geometry on drilling induced delamination of carbon fiber reinforced composites. *Composite Structures*, *105*, 126–133. https://doi.org/10.1016/j.compstruct.2013.04.026

Jain, S., & Yang, D. C. H. (1993). Effects of feedrate and chisel edge on delamination in composites drilling. *Journal of Manufacturing Science and Engineering, Transactions of the ASME*. https://doi.org/10.1115/1.2901782

Jain, S., & Yang, D. C. H. (1994a). Delamination-free drilling of composite laminates. *Journal of Manufacturing Science and Engineering, Transactions of the ASME*. https://doi.org/10.1115/1.2902131

Jain, S., & Yang, D. C. H. (1994b). Delamination-Free Drilling of Composite Laminates. *Journal of Engineering for Industry*, *116*(4), 475–481.

Jelinek, M., Schilp, J., & Reinhart, G. (2015). Optimised parameter sets for thermographic inspection of CFRP metal hybrid components. *Procedia CIRP*, *37*, 218–224. https://doi.org/10.1016/j.procir.2015.08.044

Karnik, S. R., Gaitonde, V. N., Rubio, J. C., Correia, A. E., Abrão, A. M., & Davim, J. P. (2008). *Delamination analysis in high speed drilling of carbon fiber reinforced plastics (CFRP) using artificial neural network model*. *29*, 1768–1776. https://doi.org/10.1016/j.matdes.2008.03.014

Karpat, Y., Bahtiyar, O., Değer, B., & Kaftanoğlu, B. (2014). A mechanistic approach to investigate drilling of UD-CFRP laminates with PCD drills. *CIRP Annals - Manufacturing Technology*. https://doi.org/10.1016/j.cirp.2014.03.077

Khashaba, U. A. (2013). Drilling of polymer matrix composites: A review. In *Journal of Composite Materials*. https://doi.org/10.1177/0021998312451609

Ko, S. L., & Chang, J. E. (2003). Development of Drill Geometry for Burr Minimization In Drilling. *CIRP Annals*, *52*(1), 45–48.

König, W., & Graß, P. (1989). Quality Definition and Assessment in Drilling of Fibre Reinforced Thermosets. *CIRP Annals - Manufacturing Technology*. https://doi.org/10.1016/S0007-8506(07)62665-1

Langella, A., Nele, L., & Maio, A. (2005). A torque and thrust prediction model for drilling of composite materials. *Composites Part A: Applied Science and Manufacturing*. https://doi.org/10.1016/S1359-835X(04)00177-0

Lazar, M. B., & Xirouchakis, P. (2011). Experimental analysis of drilling fiber reinforced composites. *International Journal of Machine Tools and Manufacture*. https://doi.org/10.1016/j.ijmachtools.2011.08.009

Lin, S. C., & Chen, I. K. (1996). Drilling carbon fiber-reinforced composite material at high speed. *Wear*. https://doi.org/10.1016/0043-1648(95)06831-7

López De Lacalle, L. N., Rivero, A., & Lamikiz, A. (2009). Mechanistic model for drills with double point-angle edges. *International Journal of Advanced Manufacturing Technology*, *40*(5–6), 447–457. https://doi.org/10.1007/s00170-007-1362-8

Lopresto, V., Caggiano, A., & Teti, R. (2016). High Performance Cutting of Fibre Reinforced Plastic Composite Materials. *Procedia CIRP*, *46*, 71–82. https://doi.org/10.1016/j.procir.2016.05.079

M'Saoubi, R., Axinte, D., Soo, S. L., Nobel, C., Attia, H., Kappmeyer, G., Engin, S., & Sim, W. M. (2015). High performance cutting of advanced aerospace alloys and composite materials. *CIRP Annals - Manufacturing Technology*, *64*(2), 557–580.

https://doi.org/10.1016/j.cirp.2015.05.002

Mathew, J., Ramakrishnan, N., & Naik, N. K. (1999). Investigations into the effect of geometry of a trepanning tool on thrust and torque during drilling of GFRP composites. *Journal of Materials Processing Technology*. https://doi.org/10.1016/S0924-0136(98)00416-6

Murphy, C., Byrne, G., & Gilchrist, M. D. (2002). The performance of coated tungsten carbide drills when machining carbon fibre-reinforced epoxy composite materials. *Proceedings of the Institution of Mechanical Engineers, Part B: Journal of Engineering Manufacture*. https://doi.org/10.1243/0954405021519735

Park, K., Beal, A., Kim, D. D., Kwon, P., & Lantrip, J. (2011). Tool wear in drilling of composite / titanium stacks using carbide and polycrystalline diamond tools. *Wear*, *271*(11–12), 2826–2835. https://doi.org/10.1016/j.wear.2011.05.038

Piquet, R., Ferret, B., Lachaud, F., & Swider, P. (2000). Experimental analysis of drilling damage in thin carbon/epoxy plate using special drills. *Composites Part A: Applied Science and Manufacturing*. https://doi.org/10.1016/S1359-835X(00)00069-5

Ramulu, M., & Spaulding, M. (2016). Drilling of hybrid titanium composite laminate (HTCL) with electrical discharge machining. *Materials*, *9*(9). https://doi.org/10.3390/ma9090746

Sheikh-Ahmad, J., & Davim, J. P. (2011). Tool wear in machining processes for composites. In *Machining Technology for Composite Materials: Principles and Practice*. https://doi.org/10.1016/B978-0-85709-030-0.50005-9

Sheikh-Ahmad, J. Y., & Davim, J. P. (2012). Cutting and Machining of Polymer Composites. In *Wiley Encyclopedia of Composites* (Second edi, pp. 648–658). John Wiley and Sons, Inc.

Shyha, I. S., Soo, S. L., Aspinwall, D. K., Bradley, S., Perry, R., Harden, P., & Dawson, S. (2011). Hole quality assessment following drilling of metallic-composite stacks. *International Journal of Machine Tools and Manufacture*, *51*(7–8), 569–578. https://doi.org/10.1016/j.ijmachtools.2011.04.007

Sousa, J. A. G., Sousa, M. N., Jackson, M. J., & Machado, Á. R. (2014). Comparison of the steel machining performance of new and reground cemented carbide drills. *Proceedings of the Institution of Mechanical Engineers, Part B: Journal of Engineering Manufacture*, *228*(3), 376–387. https://doi.org/10.1177/0954405413502199

Teti, R. (2002). Machining of composite materials. *CIRP Annals - Manufacturing Technology*.

https://doi.org/10.1016/S0007-8506(07)61703-X

Tsao, C. C., & Hocheng, H. (2004). Taguchi analysis of delamination associated with various drill bits in drilling of composite material. *International Journal of Machine Tools and Manufacture*. https://doi.org/10.1016/j.ijmachtools.2004.02.019

Tsao, C. C., & Hocheng, H. (2007). Parametric study on thrust force of core drill. *Journal of Materials Processing Technology*. https://doi.org/10.1016/j.jmatprotec.2007.04.062

Wilhelm, M., Commercial, B., & Company, A. (2001). *Aircraft Applications*. https://doi.org/10.1361/asmhba0003477

Zitoune, R., El Mansori, M., & Krishnaraj, V. (2013). Tribo-functional design of double cone drill implications in tool wear during drilling of copper mesh/CFRP/woven ply. *Wear*, *302*(1–2), 1560–1567. https://doi.org/10.1016/j.wear.2013.01.046

Zitoune, R., Krishnaraj, V., & Collombet, F. (2010). Study of drilling of composite material and aluminium stack. *Composite Structures*, *92*(5), 1246–1255. https://doi.org/10.1016/j.compstruct.2009.10.010

12. Appendix

In this appendix, the images of the traditional (T) and innovative (I) tools, acquired every 10 holes in CFRP/CFRP stacks for all process conditions (A, B, C, D, E, F) in order to evaluate the tool wear, are report. Finally, all the graphs reporting the hole quality parameters vs hole number for both the CFRP/CFRP stacks and the Al/CFRP stacks are shown.

1. Tool wear progression

Traditional tools for CFRP/CFRP stack drilling

TA tool

HOLE N. 10	HOLE N. 20	HOLE N. 30	HOLE N. 40	HOLE N. 50	HOLE N. 60
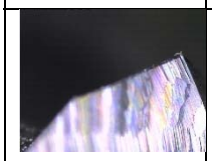	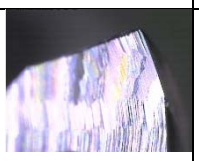	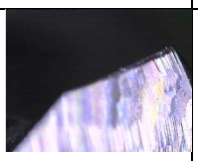	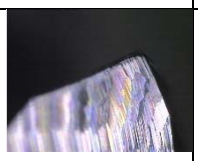		
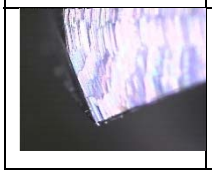	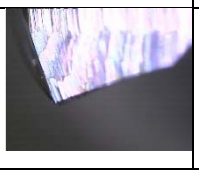	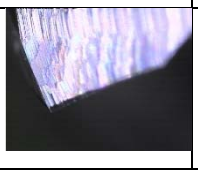	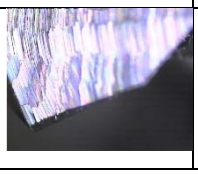	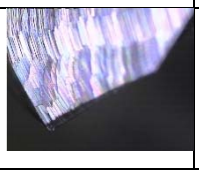	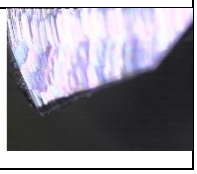

Tab. A.1 Images of tool wear progression for the TA tool (2700 rpm - 0.15 mm/rev).

TB tool

HOLE N. 10	HOLE N. 20	HOLE N. 30	HOLE N. 40	HOLE N. 50	HOLE N. 60
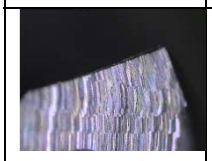	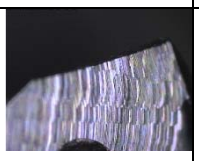	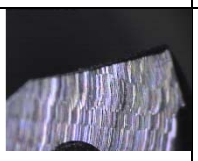	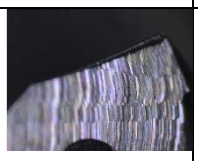	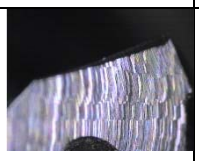	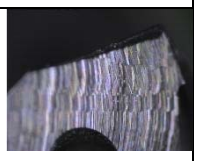
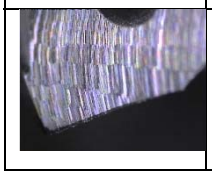	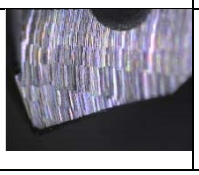	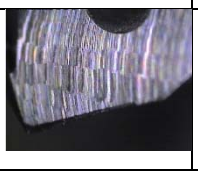	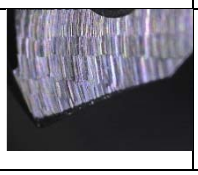	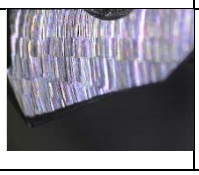	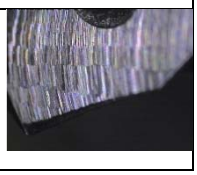

Tab. A.2 Images of tool wear progression for the TB tool (6000 rpm - 0.11 mm/rev).

TC tool

HOLE N. 10	HOLE N. 20	HOLE N. 30	HOLE N. 40	HOLE N. 50	HOLE N. 60
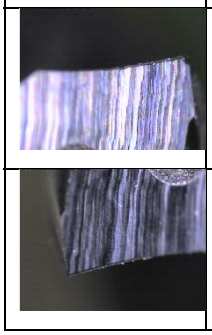	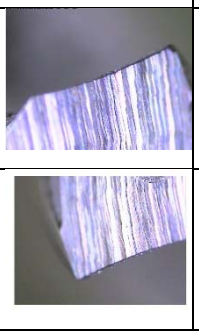	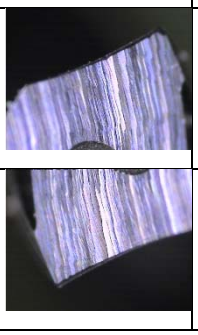	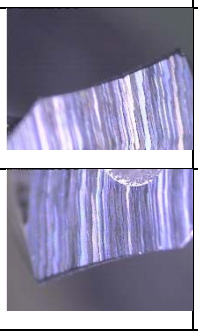	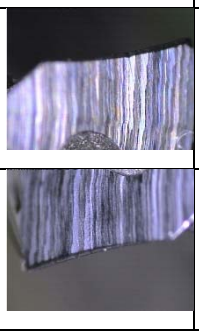	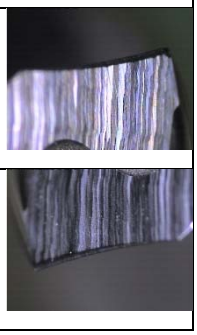

Tab. A.3 Images of tool wear progression for the TC tool (6000 rpm - 0.15 mm/rev).

TD tool

HOLE N. 10	HOLE N. 20	HOLE N. 30	HOLE N. 40	HOLE N. 50	HOLE N. 60
	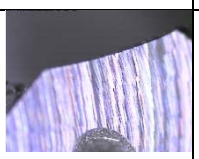	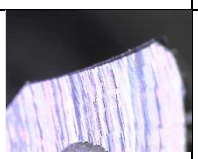	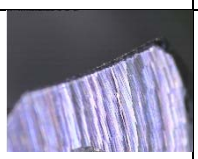	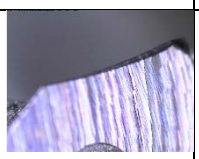	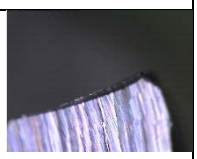
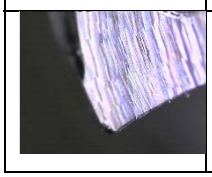	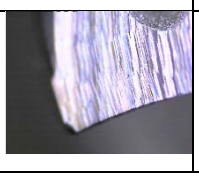	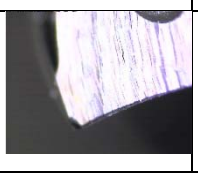	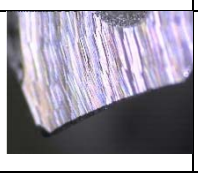	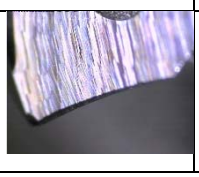	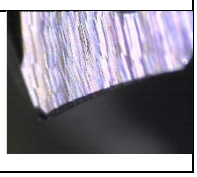

Tab. A.4 Images of tool wear progression for the TD tool (6000 rpm - 0.20 mm/rev).

TE tool

HOLE N. 10	HOLE N. 20	HOLE N. 30	HOLE N. 40	HOLE N. 50	HOLE N. 60
	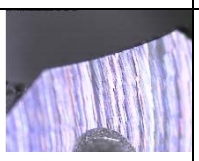	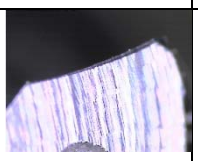	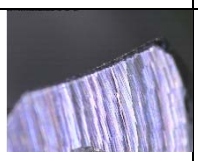	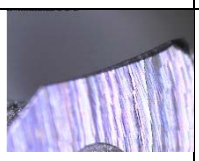	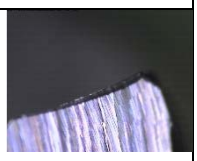
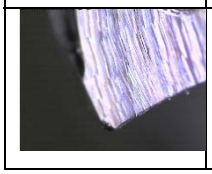	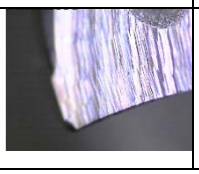	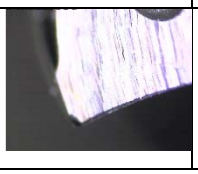	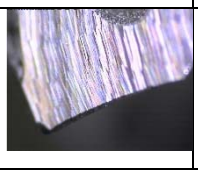	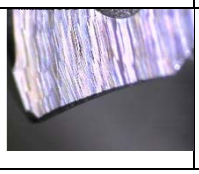	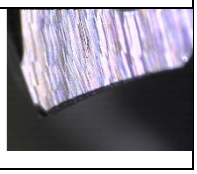

Tab. A.5 Images of tool wear progression for the TE tool (9000 rpm - 0.11 mm/rev).

TF tool

HOLE N. 10	HOLE N. 20	HOLE N. 30	HOLE N. 40	HOLE N. 50	HOLE N. 60
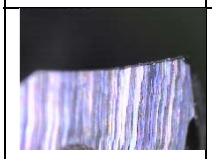	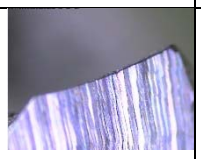	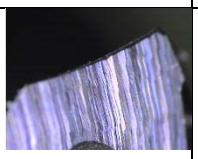	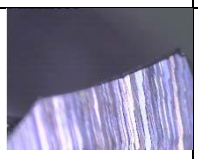	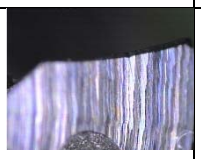	
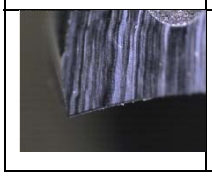	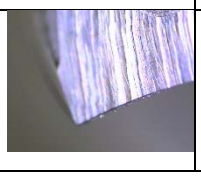		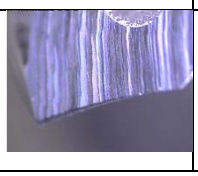	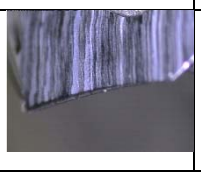	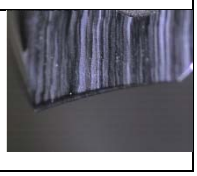

Tab. A.6 Images of tool wear progression for the TF tool (9000 rpm - 0.15 mm/rev).

Innovative tools for CFRP/CFRP stack drilling

IA tool

HOLE N. 10	HOLE N. 20	HOLE N. 30	HOLE N. 40	HOLE N. 50	HOLE N. 60
			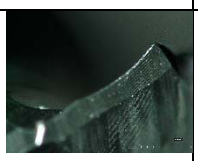	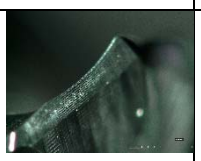	
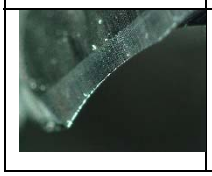	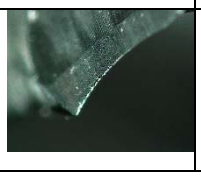	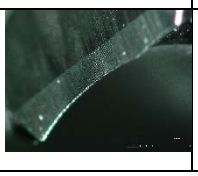	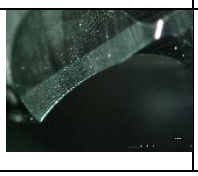	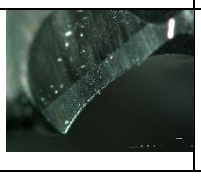	

Tab. A.7 Images of tool wear progression for the IA tool (2700 rpm - 0.15 mm/rev).

IB tool

HOLE N. 10	HOLE N. 20	HOLE N. 30	HOLE N. 40	HOLE N. 50	HOLE N. 60
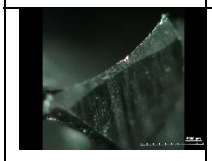	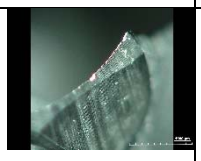	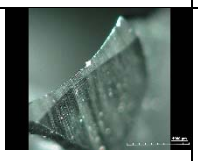	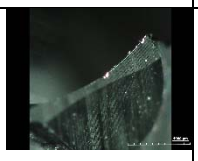	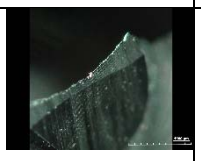	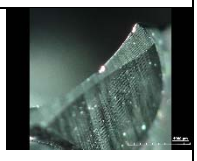
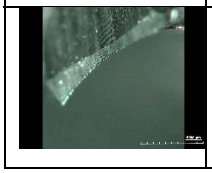			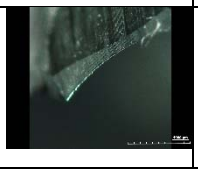		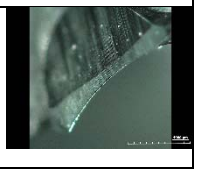

Tab. A.8 Images of tool wear progression for the IB tool (6000 rpm - 0.11 mm/rev).

IC tool

HOLE N. 10	HOLE N. 20	HOLE N. 30	HOLE N. 40	HOLE N. 50	HOLE N. 60
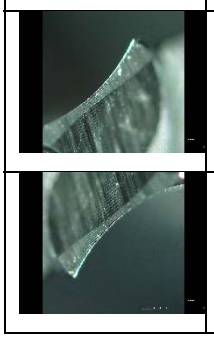	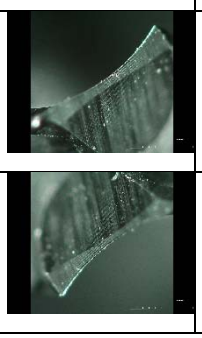	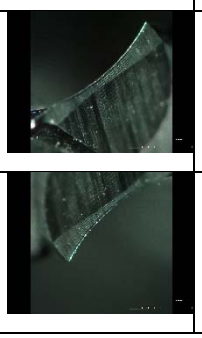	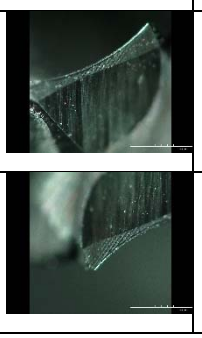	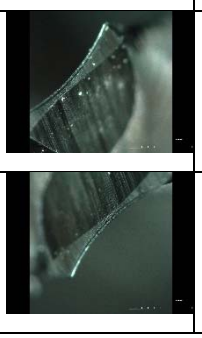	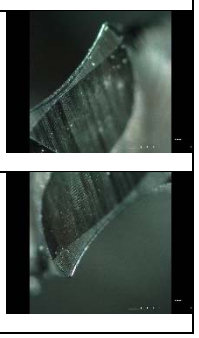

Tab. A.9 Images of tool wear progression for the IC tool (6000 rpm - 0.15 mm/rev).

ID tool

HOLE N. 10	HOLE N. 20	HOLE N. 30	HOLE N. 40	HOLE N. 50	HOLE N. 60
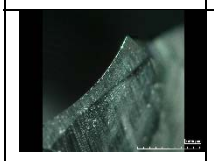		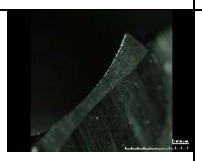		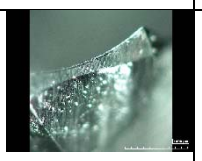	
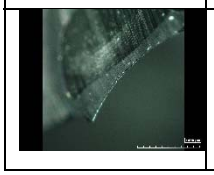	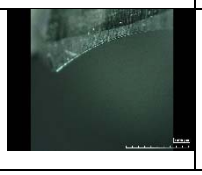		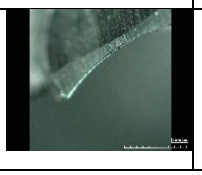	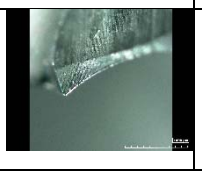	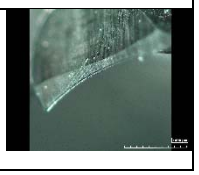

Tab. A.10 Images of tool wear progression for the ID tool (6000 rpm - 0.20 mm/rev).

IE tool

HOLE N. 10	HOLE N. 20	HOLE N. 30	HOLE N. 40	HOLE N. 50	HOLE N. 60
		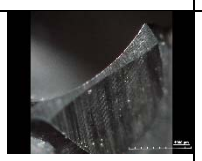	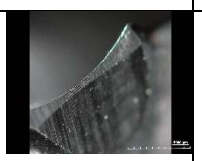		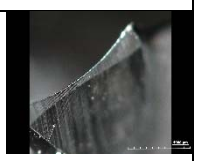
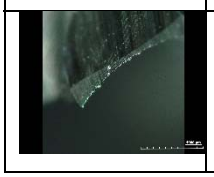	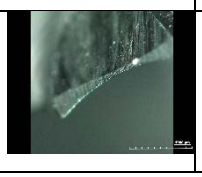				

Tab. A.11 Images of tool wear progression for the IE tool (9000 rpm - 0.11 mm/rev).

IF tool

HOLE N. 10	HOLE N. 20	HOLE N. 30	HOLE N. 40	HOLE N. 50	HOLE N. 60
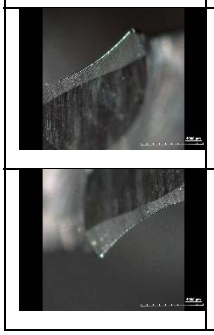	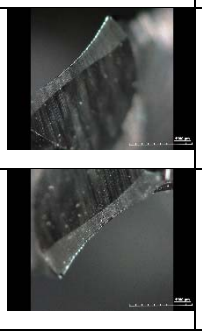	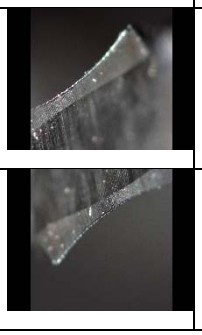	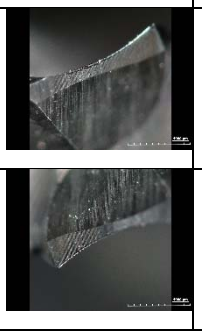	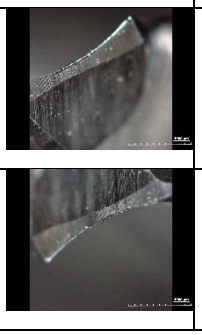	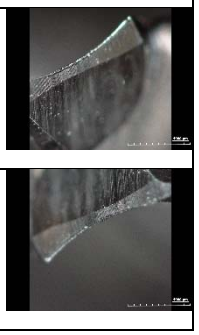

Tab. A.12 Images of tool wear progression for the IF tool (9000 rpm - 0.15 mm/rev).

Traditional tools for Al/CFRP stack drilling

T1 tool

HOLE N. 5	HOLE N. 10	HOLE N. 15	HOLE N. 20	HOLE N. 25	HOLE N. 30
	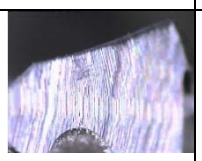	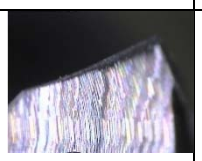	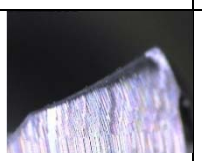		
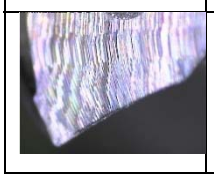	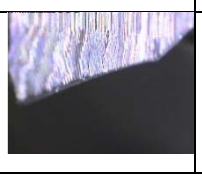	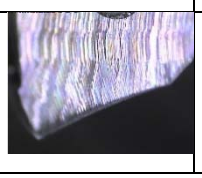	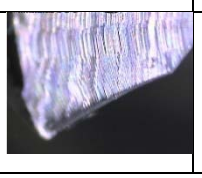	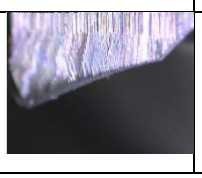	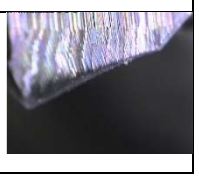

Tab. A.13 Images of tool wear progression for the T1 tool (3000 rpm - 0.05 mm/rev).

T2 tool

HOLE N. 5	HOLE N. 10	HOLE N. 15	HOLE N. 20	HOLE N. 25	HOLE N. 30
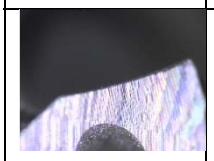		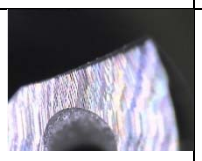	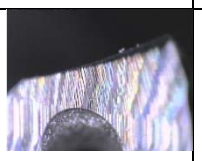	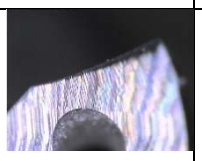	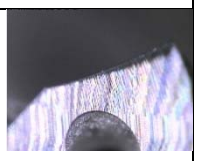
	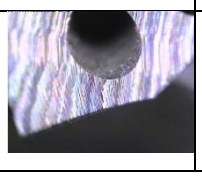	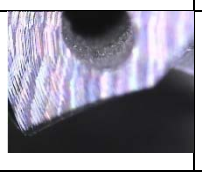	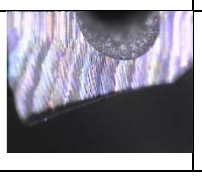	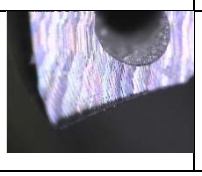	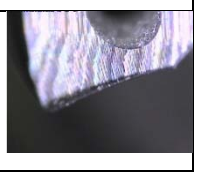

Tab. A.14 Images of tool wear progression for the T2 tool (3000 rpm - 0.10 mm/rev).

T3 tool

HOLE N. 5	HOLE N. 10	HOLE N. 15	HOLE N. 20	HOLE N. 25	HOLE N. 30
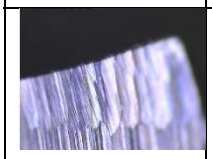	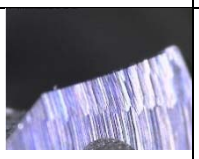		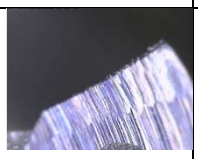		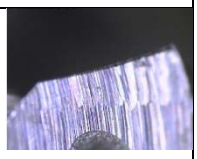
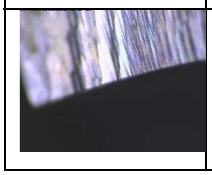	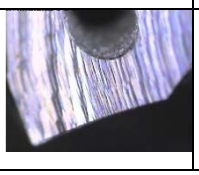	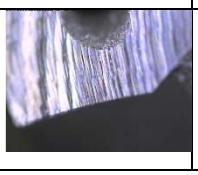	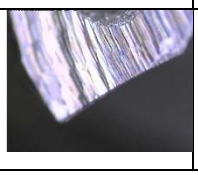	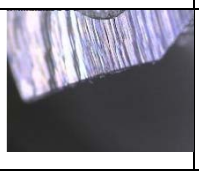	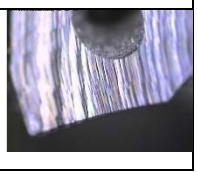

Tab. A.15 Images of tool wear progression for the T3 tool (3000 rpm - 0.15 mm/rev).

T5 tool

HOLE N. 5	HOLE N. 10	HOLE N. 15	HOLE N. 20	HOLE N. 25	HOLE N. 30
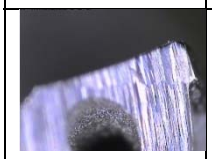	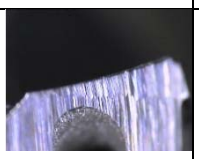	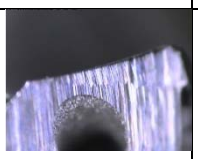	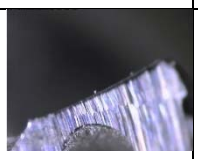		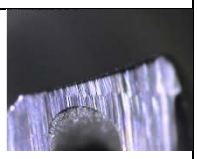
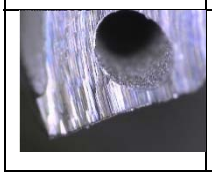	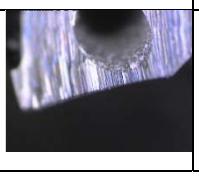	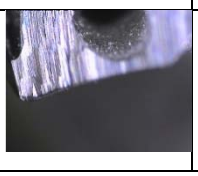	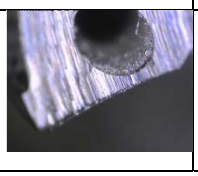	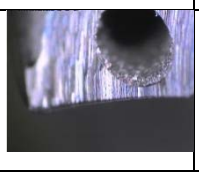	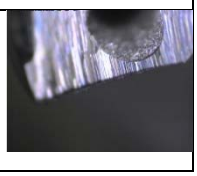

Tab. A.16 Images of tool wear progression for the T5 tool (4500 rpm - 0.10 mm/rev).

T6 tool

HOLE N. 5	HOLE N. 10	HOLE N. 15	HOLE N. 20	HOLE N. 25	HOLE N. 30
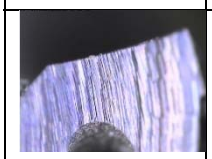				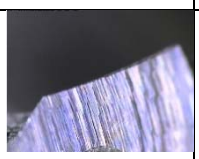	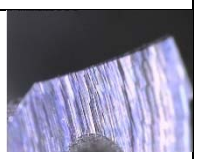
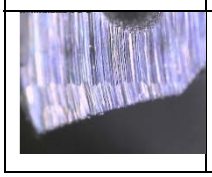	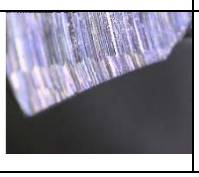	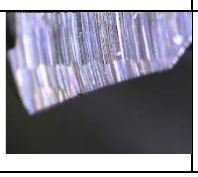	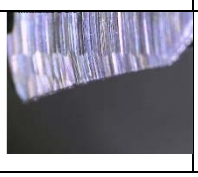	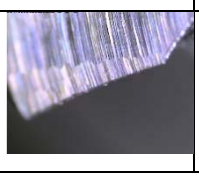	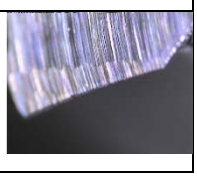

Tab. A.17 Images of tool wear progression for the T6 tool (4500 rpm - 0.15 mm/rev).

2. Results for Al/CFRP stack drilling: 3000 rpm

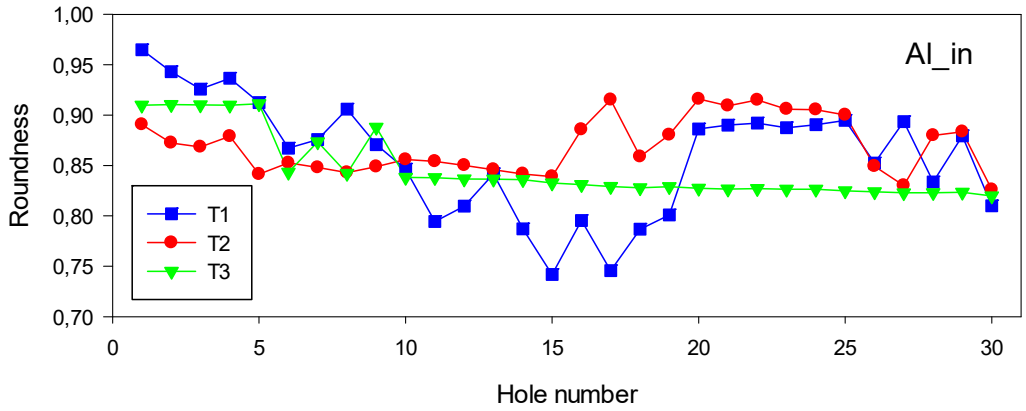

Fig. A.1 Comparison of 3000 rpm tools: Al_in – Hole roundness.

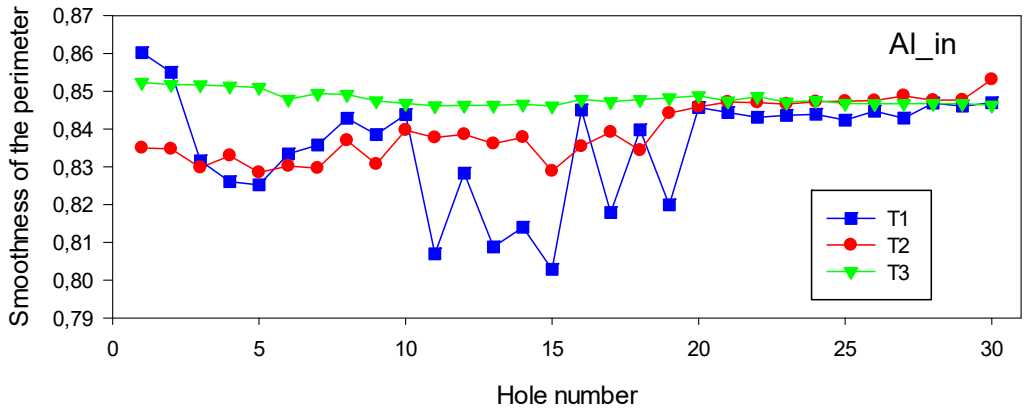

Fig. A.2 Comparison of 3000 rpm tools: Al_in - Smoothness of the perimeter.

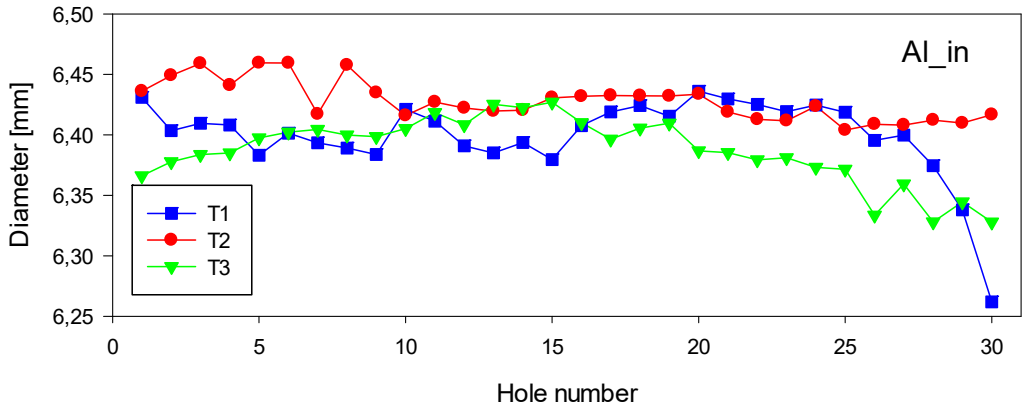

Fig. A.3 Comparison of 3000 rpm tools: Al_in – Hole diameter.

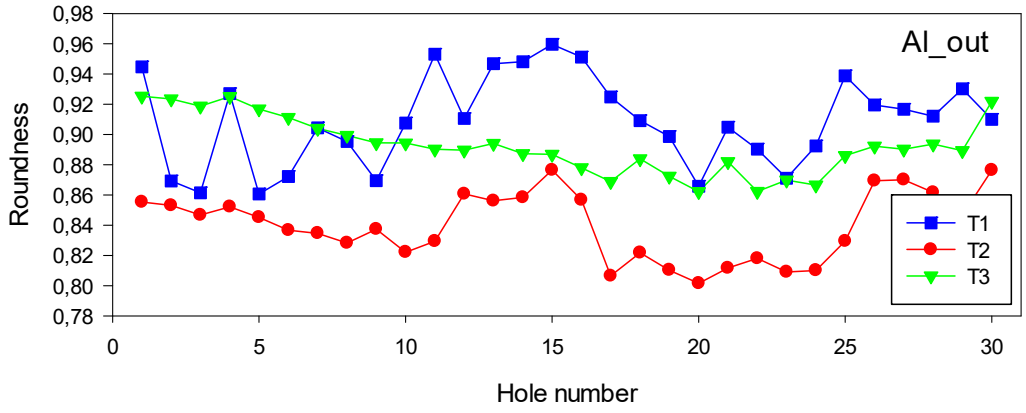

Fig. A.4 Comparison of 3000 rpm tools: Al_out – Hole roundness.

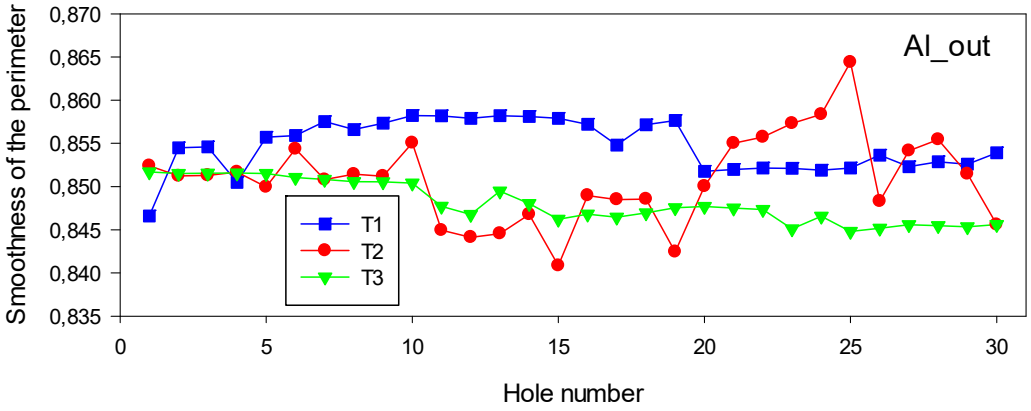

Fig. A.5 Comparison of 3000 rpm tools: Al_out - Smoothness of the perimeter.

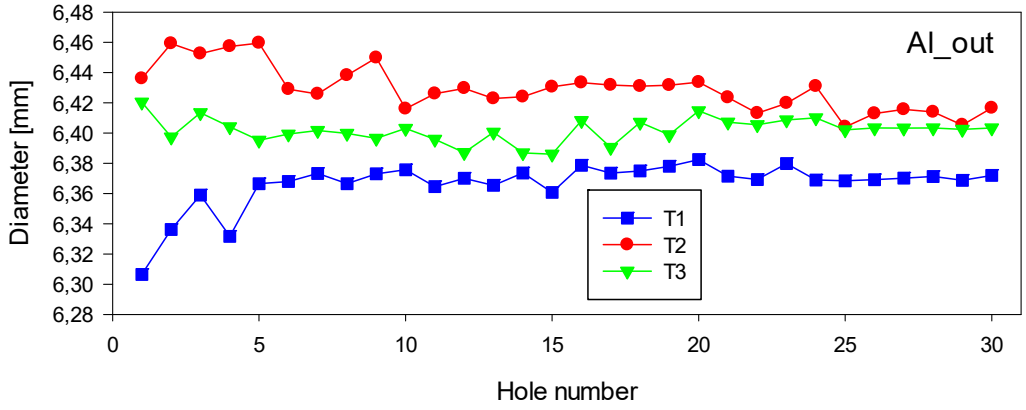

Fig.A. 6 Comparison of 3000 rpm tools: Al_out – Hole diameter.

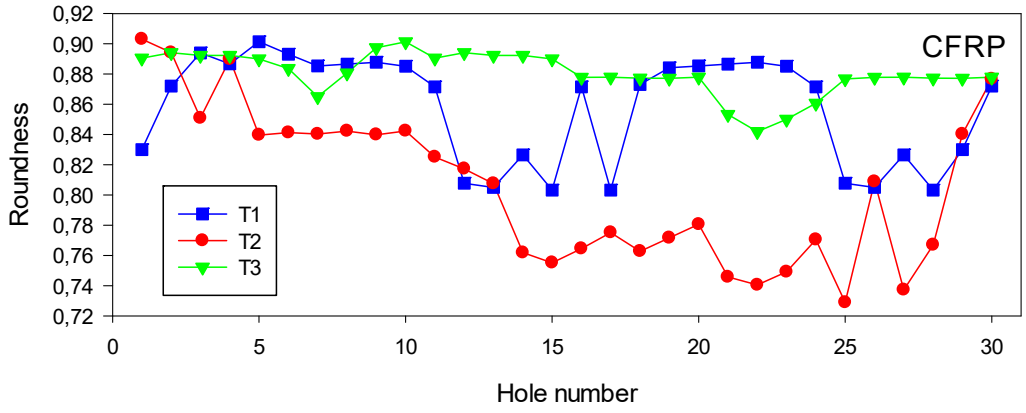

Fig. A.7 Comparison of 3000 rpm tools: CFRP – Hole roundness.

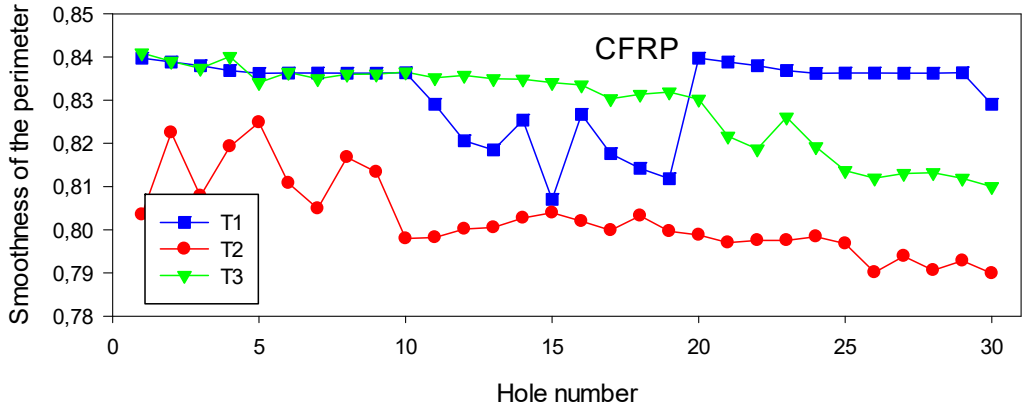

Fig. A.8 Comparison of 3000 rpm tools: CFRP - Smoothness of the perimeter.

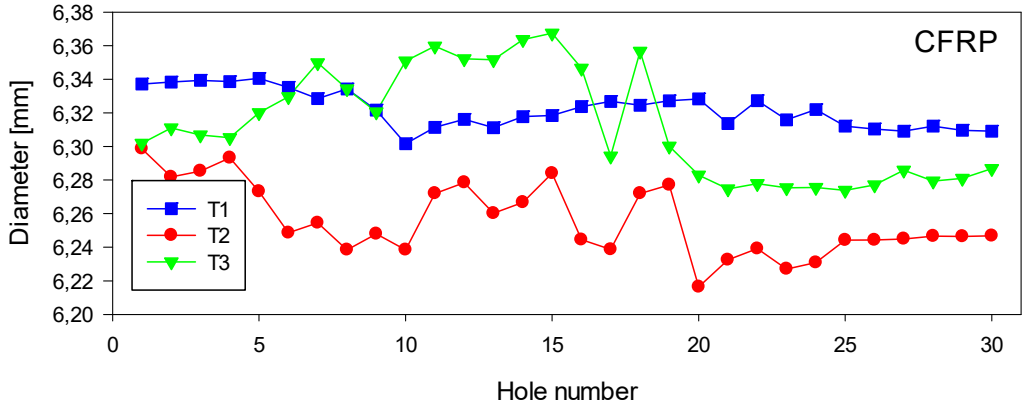

Fig. A.9 Comparison of 3000 rpm tools: CFRP – Hole diameter.

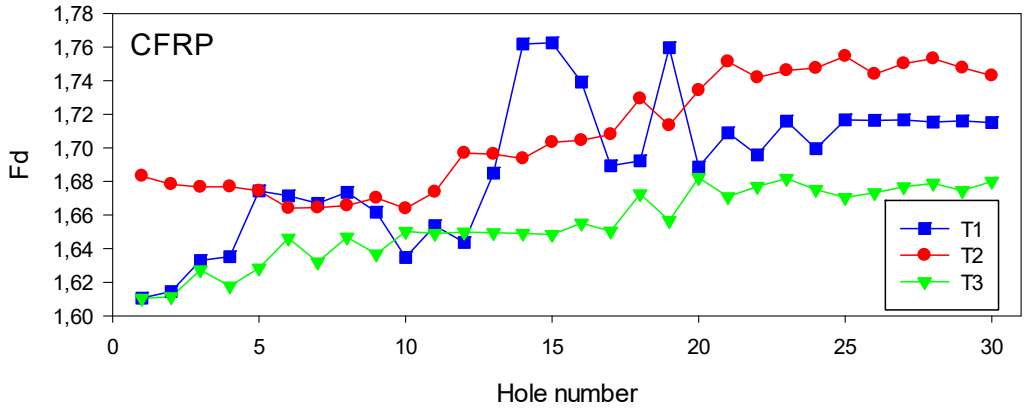

Fig.A. 10 Comparison of 3000 rpm tools - CFRP – Delamination factor Fd.

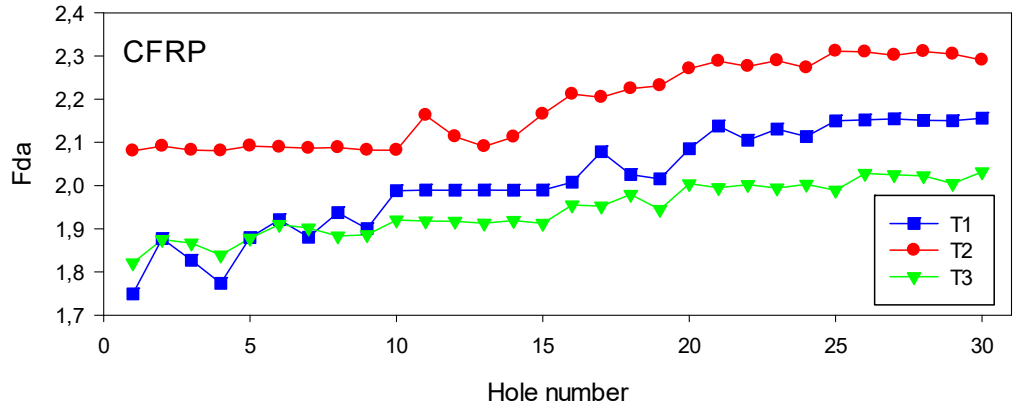

Fig.A. 11 Comparison of 3000 rpm tools: CFRP – Adjusted delamination factor Fda.

3. Results of Al/CFRP stack drilling: 4500 rpm

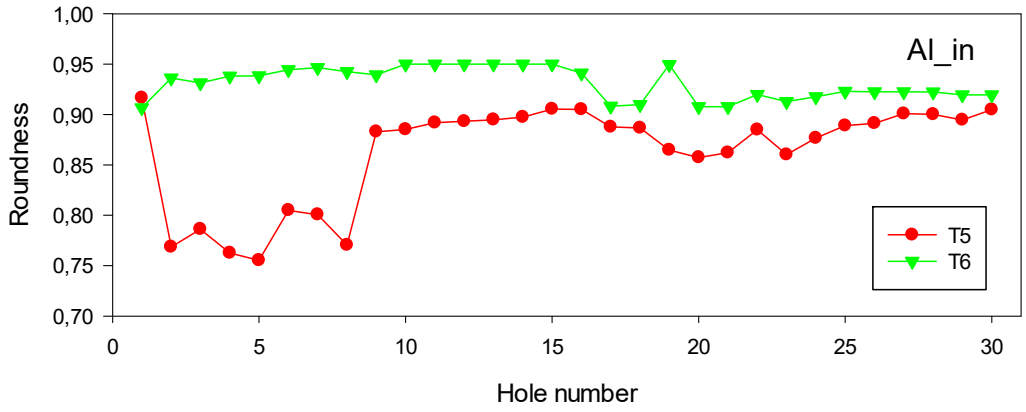

Fig. A.12 Comparison of 4500 rpm tools :Al_in – Hole roundness.

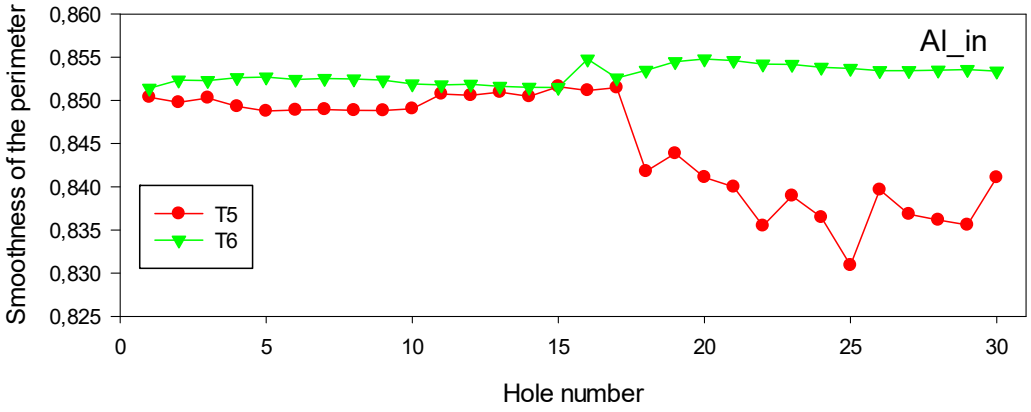

Fig. A.13 Comparison of 4500 rpm tools: Al_in - Smoothness of the perimeter.

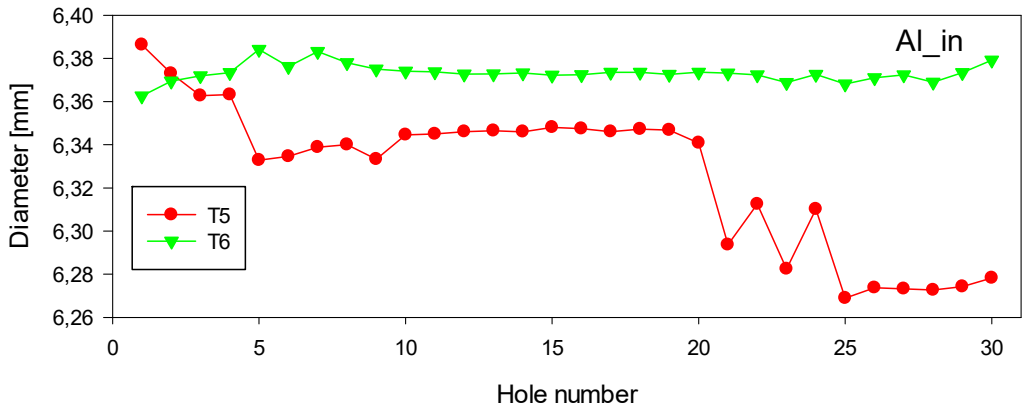

Fig. A.14 Comparison of 4500 rpm tools: Al_in – Hole diameter.

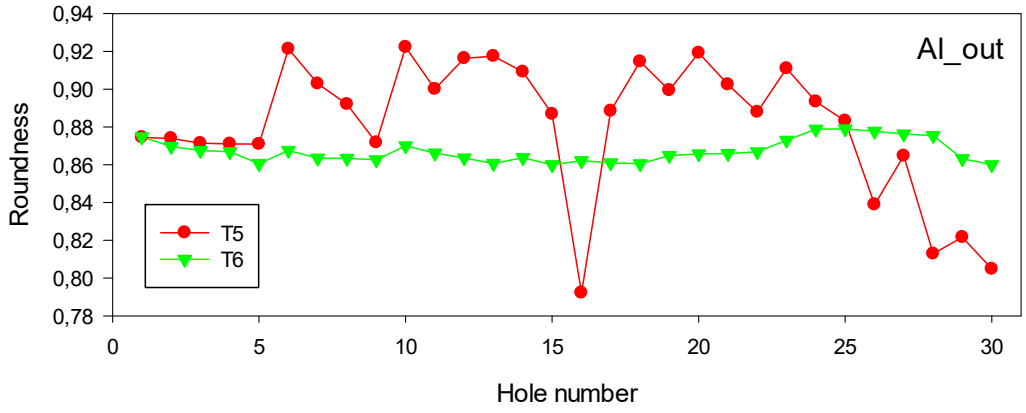

Fig. A.15 Comparison of 4500 rpm tools: Al_out – Hole roundness.

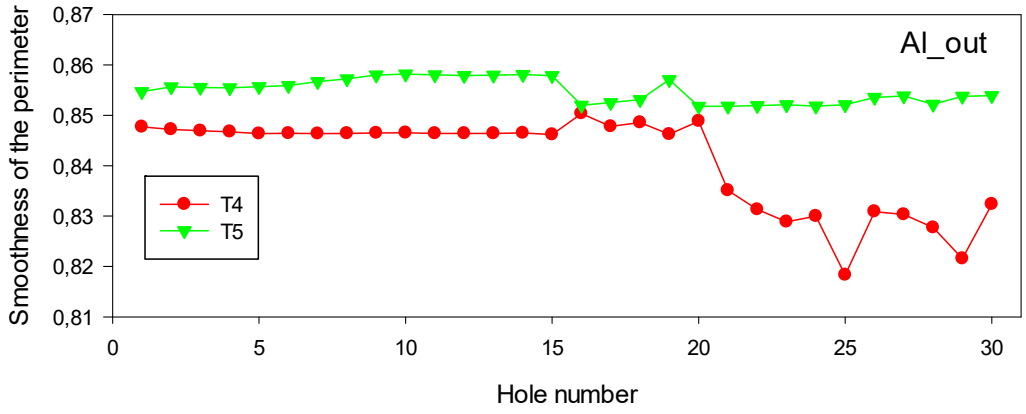

Fig. A.16 Comparison of 4500 rpm tools: Al_out - Smoothness of the perimeter.

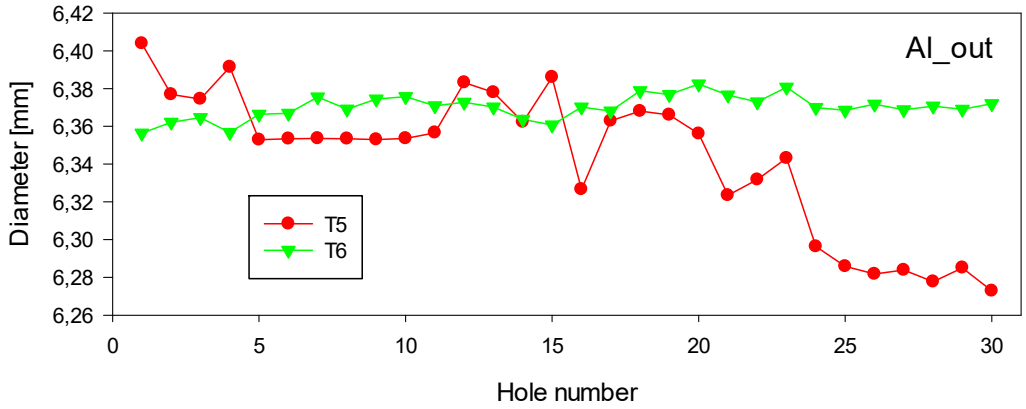

Fig. A.17 Comparison of 4500 rpm tools: Al_out – Hole diameter.

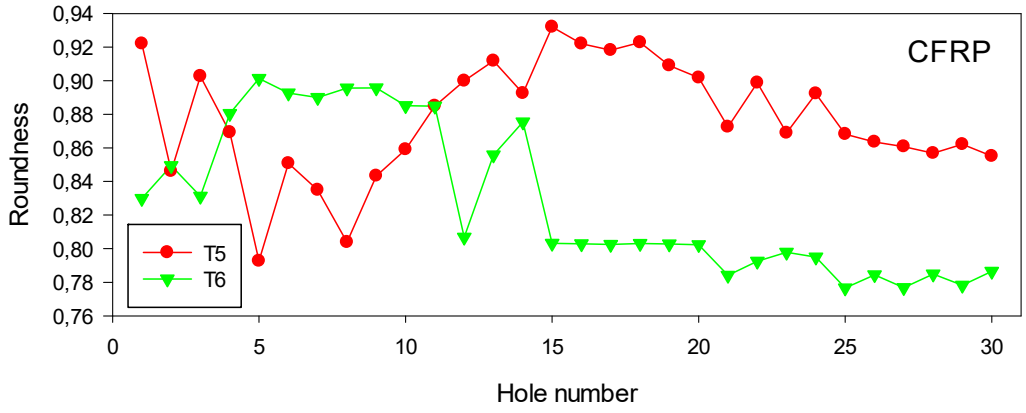

Fig. A.18 Comparison of 4500 rpm tools :CFRP – Hole roundness.

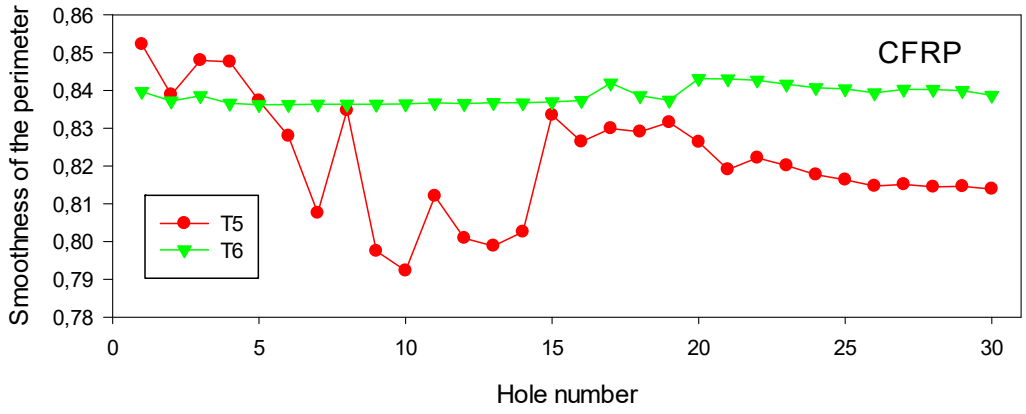

Fig. A.19 Comparison of 4500 rpm tools: CFRP - Smoothness of the perimeter.

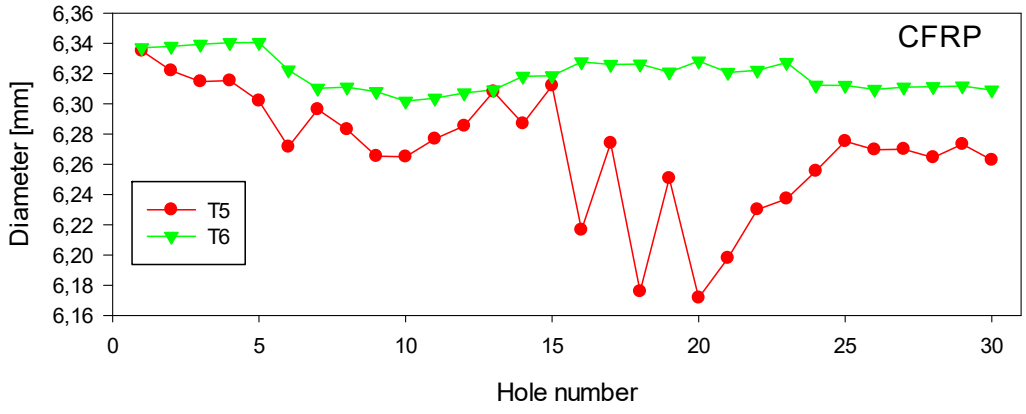

Fig. A.20 Comparison of 4500 rpm tools: CFRP – Hole diameter.

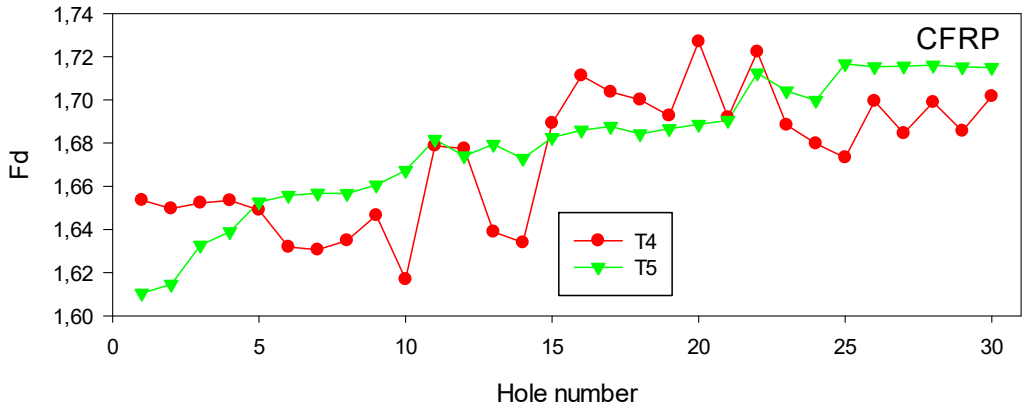

Fig. A.21 Comparison of 4500 rpm tools: CFRP – Delamination factor Fd.

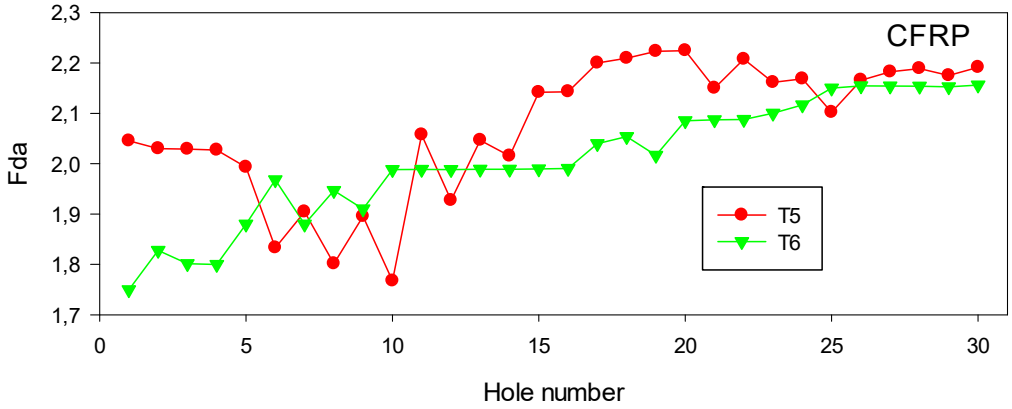

Fig. A.22 Comparison of 4500 rpm tools: CFRP – Adjusted delamination factor Fda.